UNIVERSITÀ DEGLI STUDI DI MILANO

Facoltà di Scienze Matematiche, Fisiche e Naturali
Master Degree in Physics

Effects of Isospin Symmetry-Breaking Forces on Mirror Nuclei

Supervisor: Prof. Gianluca COLÓ
Co-Supervisor: Dr. Xavier ROCA-MAZA

Giancarlo AGNELLI
Matricola n° 914079
A.A. 2018/2019

Contents

Introduction

Similarity between the neutron-neutron (*nn*), proton-proton (*pp*) and neutron-proton (*np*) nuclear forces, commonly known as their charge independence, has been well experimentally established already in 1930's. This has led to the concept of the isospin-symmetry. Since then, the isospin-symmetry has been tested and widely used in theoretical modeling of nuclei, with its explicit violation generated by the Coulomb interaction, because it distinguishes between protons and neutrons.

Within the isospin formalism, we can describe the neutron and the proton as two different states of the same particle, the *nucleon*. The isospin is a quantum number that has the same algebraic properties of the spin. Nuclei with the same total isospin are part of the so-called isospin multiplet, which is degenerate in energy (if Coulomb interaction is excluded). In the isospin-invariant description of the nuclear forces, the binding energy of the mirror nuclei (i.e. nuclei that have neutron and proton numbers interchanged) should be the same, apart Coulomb interaction. When Coulomb interaction is taken into account, we expect that the energy difference between two mirror nuclei (that is called mirror displacement energy MDE) is due to the electromagnetic interaction, which is a very evident effect of isospin symmetry-breaking (ISB).

However there is always a discrepancy between the experimental and theoretical MDEs, and a systematic study by Nolen et al. [41] has shown that MDEs can not be reproduced by using models involving the Coulomb interaction as the only source of ISB, this is called Nolen-Schiffer anomaly. In addition, there exist experimental evidences in the nucleon-nucleon NN scattering data that the nuclear interaction contains also small ISB components. These differences indicate that the *nn* interaction is about 1% stronger than the *pp* interaction and that the *np* interaction is about 2.5% stronger than the average of the *nn* and *pp* interactions [37]. These effects are called charge symmetry-breaking (CSB) and charge independence-breaking (CIB), respectively.

In order to reproduce the experimental MDEs of some pairs of mirror nuclei, we have extended the Skyrme model, which by default does not include ISB terms. In other words, we will try to reproduce MDEs through a self-consistent method, based on an effective microscopic interaction. Since the pairs of nuclei considered for this study are all open shell, it is important to take into account the effects of deformation and pairing interaction. This work is organised as follows:

Chapter 1 gives a general overview on two simple nuclear models, the liquid drop model and the shell model and in particular it is focused on the study of nuclear deformations according to these models in order to give a qualitative idea of the effects of deformation;

Chapter 2 describes the self-consistent Hartree-Fock (HF) method. It will be implemented by using the Skyrme effective interaction, which allows to more easily solve the HF problem. In order to give a theoretical description of the pairing interaction, in the end the BCS model and the Hartree-Fock-Bogolyubov (HFB) methods are described.

In chapter 3 the isospin formalism is described. The concepts of isospin invariance and isospin symmetry breaking are described. We review the studies on the effects of ISB in the literature and introduce two nuclear effective interactions that break the isospin symmetry: one is charge symmetry-breaking (CSB) and one the charge independence-breaking (CIB);

In Chapter 4 we show and discuss the numerical results performed with two FORTRAN codes (HFODD and HFBTHO) on the MDEs of some pairs of mirror nuclei, in order to try to reproduce the experimental values of the MDEs.

Chapter 1

Nuclear Ground-State Properties and Intrinsic Shapes

Calculations of nuclear binding energies and radii are very difficult to do; indeed nuclei are treated as many-body systems and the force is very complicated, also with regard to light nuclei. It is often necessary to simplify the approach and use particular nuclear models linked to simplified nuclear forces. The simplest nuclear models are the liquid drop model and the shell model; they were historically among the first models to be proposed and are based on phenomenological data. The liquid drop model describes a nucleus in a very crude way, but allows to describe well the average trends of nuclear binding energy, the nuclear deformations [44] and collective phenomena [47]. The shell model can explain many experimental results better than the liquid drop model in particular regarding spectroscopic data [30, 44]. Modern methods with the same objective as the previous ones, but more in agreement with the experimental data, are the mean-field methods. These methods concentrate on self-consistent determination of the nuclear mean-field. To this end, mean-field methods employ to the effective interactions which are linked to their primary use in mean-field calculations [11]. This chapter describes the liquid drop model and the shell model and is focused on the study of nuclear deformations according to these models.

1.1 The Liquid Drop Model

The liquid drop model (LDM) was historically the first model to be proposed as explanation of the different binding energies of the nuclei. It also explains collective behaviors, both of small amplitude like vibrations, and of great amplitude like fission [44]. The concept of treating the nucleus in terms of a liquid drop comes from considerations about the idea of a saturation density and from its substantial incompressibility. In this section the idea of the LDM is introduced [44].

1.1.1 Generalities

As already mentioned, the approximate constancy of nuclear density holds for liquids as well. This saturation property has as consequence that the total binding energy $BE(N;Z)$ grows with the number of nucleons A, in such a way that the binding energy per nucleon remains quite constant (for nuclei with $A > 12$):

$$\left.\frac{BE(N;Z)}{A}\right|_{A>12} \simeq 8{:}5 \quad \text{[MeV]}$$

In the case of atomic physics, if the binding of a many-body system comes from the interaction energy of all possible pairs combinations, the total binding energy grows as $\frac{1}{2}A(A \quad 1)$ and the binding energy per particle is proportional to A. The nuclear case is di□erent because of the saturation property of the nuclear forces: a nucleon in the nucleus can interact only with a limited number of nucleons because of the combination of the short range of the nuclear interaction. For this reason one can expect that the total binding energy rises linearly with A, as in the previous equation.

The saturation property allows also to approximate the nucleus as a sphere with constant density and a sharp surface. The surface is defined by the following radius and nuclear volume

$$R = r_0 A^{\frac{1}{3}}; \qquad V = \frac{4}{3} r_0^3 A \qquad \text{with} \qquad r_0 = 1{:}2 \quad [\text{fm}] \tag{1.1}$$

where the parameter r_0 is defined empirically. In this approximation one cane see that the density does not depend on A:

$$= \frac{A}{V} = \frac{3}{4 \ r_0^3} \quad [\text{fm}^{-3}]$$

The best formula for the binding energy per nucleon was proposed by Bethe and Weizsäcker and it is the semi-empirical mass formula:

$$\frac{BE(N;Z)}{A} = a_V + a_S A^{-\frac{1}{3}} + a_C \frac{Z^2}{A^{\frac{4}{3}}} + a_I \frac{(N \quad Z)^2}{A^2} + \quad (A) \tag{1.2}$$

where one obtains by a fit [33, 44]:

$$a_V = \quad 15{:}68; \qquad a_S = 18{:}56; \qquad a_C = 0{:}717; \qquad a_I = 28{:}1 \quad [\text{MeV}]$$

$$(A) \ ' \begin{cases} \approx \frac{12}{\sqrt{A}} & [\text{MeV}] \quad \text{for even-even nuclei} \\ 0 & \text{for odd-even nuclei} \\ \cdot + \frac{12}{\sqrt{A}} & [\text{MeV}] \quad \text{for odd-odd nuclei} \end{cases}$$

where the values of these parameters were proposed several years ago and nowadays new more precise fit give slightly di□erent values of these parameters [30, 31]. In figure 1.1 one can see that one obtains quite good overall agreement with the experimental curve with the semi-empirical mass formula (1.2).

The binding energy curve exhibits some interesting features:

For $A > 60$, the binding energy per nucleon is approximately constant around 8-9 MeV, while for small values of A it increases rapidly;

The maximum of the binding energy per nucleon is in the region of iron ($A \ ' \ 60$) and its value is approximately less than 9 MeV. It drops o□ slowly towards large A. This behaviour is crucial for the synthesis of the elements and for nuclear power production [12, 20].

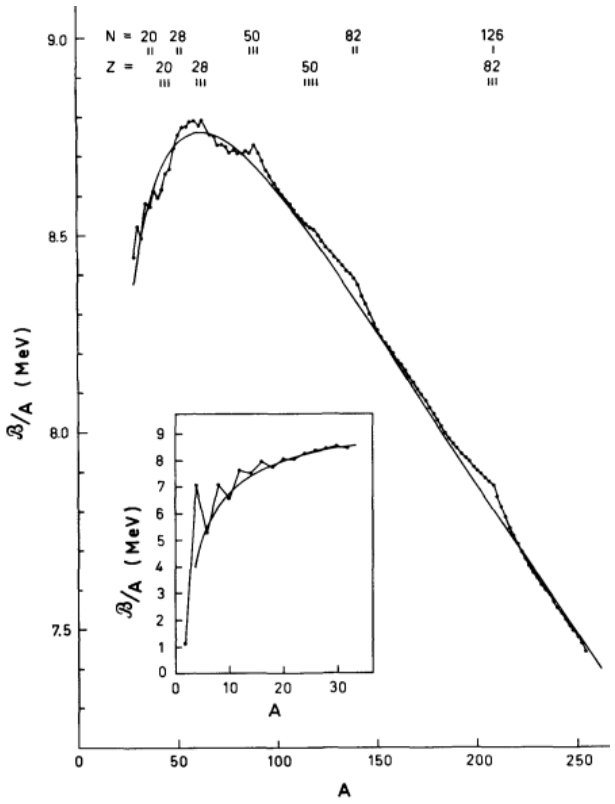

Figure 1.1: The semi-empirical mass formula (1.2) calculated with a_V = 15:56 MeV, a_S =17.23 MeV, a_C =0.69 MeV, a_I =23.28 MeV and r_0 = 1:24 fm, in comparison with experimental data [14].

The physical meaning of the five terms of (1.2) is the following:

The first term is called *volume term* because it is proportional to A. That the main term in the nuclear binding energy should be linear in A is strongly suggested by the approximate A-independence of the nuclear density;

The second term is proportional to $A^{\frac{2}{3}}$, and is therefore called *surface term*. The nucleons close to the nuclear surface are less bound than the inner nucleons because of the smaller number of nearest neighbours interactions. This term tends to decrease the binding energy. It represents, quite generally, the leading-order correction to the linear term describing the energy of a saturating system;

The third term represents the contribution due to Coulomb repulsion between protons. It is calculated by assuming that the charge is uniformly distributed within a sharp sphere. This term is proportional to Z^2 and inversely proportional to the radius. This term tends to decrease the binding energy;

The fourth term is called *symmetry energy*. This is a contribution that is not connected to the liquid drop analogy but it can be qualitatively described within the Fermi gas model [22]. Protons and neutrons, being distinct types of particles, occupy di□erent quantum states. One can think of two di□erent "pools" of states, one for protons and one for neutrons. If, for example, there are significantly more neutrons than protons in a nucleus, some of

the neutrons will be higher in energy than the available states in the proton pool. If one moves some particles from the neutron pool to the proton pool, in other words change some neutrons into protons, one significantly decreases the energy. The imbalance between the number of protons and neutrons causes the energy to be higher than it needs to be, for a given number of nucleons. The symmetry energy may be divided into a kinetic and a potential part. For given A, the kinetic energy of the nuclear Fermi gas is

$$E_{kin} = \frac{3}{5}(N\varepsilon_F^{(n)} + Z\varepsilon_F^{(p)}) \approx \frac{3}{5}A\varepsilon_F; \quad \varepsilon_F = \frac{(\hbar k_F)^2}{2m} \approx 37[\text{MeV}]; \quad k_F = \left(\frac{3\pi^2}{2}\right)^{\frac{1}{3}} \approx 1.33[\text{fm}]$$

where the equalities that refers to ε_F and k_F hold whether $N = Z$. The kinetic part of the parameter a_I can be estimated by expanding the kinetic energy (when written as the sum of protons and neutron contributions) in powers of $N - Z$. This calculation yields [14]:

$$(a_I)_{kin} = \frac{2}{3}\varepsilon_F\Big|_{N=Z} \approx 25 \quad [\text{MeV}]$$

The potential part of a_I is associated with a specific feature of the nuclear forces, which implies that the neutron-proton interaction is on the average stronger than that between like particles (see Sec. 2-5b [14]). According to the reference [14] the empirical value of a_I which is about 50 MeV, together with the previous estimate implies that the potential energy part of a_I is about 25 MeV;

The last term is called *pairing term*. Since the experimental measured binding energies exhibit a systematic variation depending on the evenness or oddness of A the semi-empirical mass formula (1.2) contains the term $\delta(A)$, which depends on evenness or oddness of A. From the Fermi gas model, one expects an odd-even difference (pairing energy) resulting from the fact that each orbit can be occupied by two protons and by two neutrons. Thus, one obtains an odd-even parameter δ that is of the order of the spacing between the one-particle energies in the neighborhood of the Fermi energy:

$$\delta(A)_{kin} \approx \frac{2}{3}\frac{\varepsilon_F}{A} \approx \frac{25}{A} \quad [\text{MeV}] \tag{1.3}$$

The odd-even mass parameter $\delta(A)$ defined above can be determined from (1.2) of a sequence of isotopes or isotones. Assuming that the masses are a smooth function of Z and N except for the pairing effect, one can define a local average of the masses of odd-A nuclei, and by comparing this value with the observed masses of the even-even nuclei, one obtains δ. Thus, for even N , one can define [14]

$$\delta_n = \frac{1}{4}[S_n(N-1;Z) - 2S_n(N;Z) + S_n(N+1;Z)]$$

$$S_n(N;Z) = BE(N;Z) - BE(N-1;Z)$$

where $S_n(N;Z)$ is the separation energy of a neutron for the nucleus $N;Z$. For odd N , the negative of this expression is taken as the neutron pairing energy. Similarly, in the same way for even Z, one can define the proton pairing energy δ_p and take the opposite sign

whether odd Z. The pairing energies $_n$ and $_p$ are plotted in figure 1.2 as a function of the number of neutrons or protons in the nucleus. It is seen that the general trend in the observed pairing energies is fit by the simple expression

$$(A) \; ' \; \frac{12}{\sqrt{A}}$$

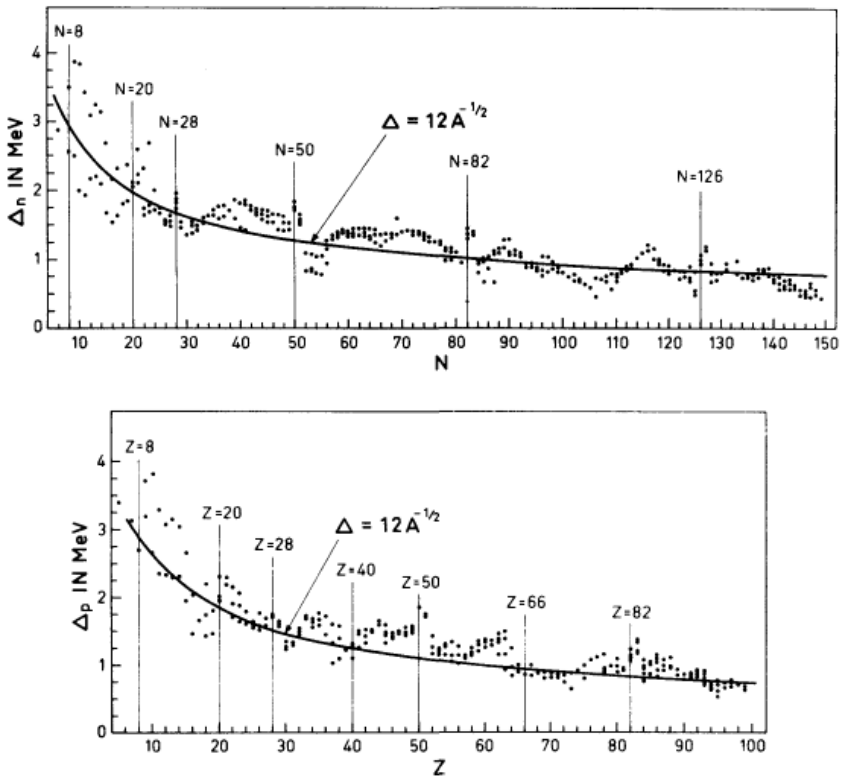

Figure 1.2: Odd-even mass di□erences for neutrons and protons [14].

The simple description of the pairing energy used in this section implies that the extra energy of an odd-odd nucleus, as compared with an even-even configuration, is 2 (A). Comparison with the observed masses of odd-odd nuclei reveals that this relation is approximately fulfilled, but that there is a systematic tendency for the odd-odd masses to be slightly lower than this estimate [14]. The pairing e□ect plays a very important role in the low-energy nuclear phenomena. The correlation e□ect is brought about by the predominantly attractive character of the nucleon-nucleon interaction; but it will be discussed in detail in the next chapter.

1.1.2 Quadrupole Deformation

Up to now, only spherical shapes of nuclei have been described within the LDM, but the nuclear surface not necessary has to be spherical. In fact it can undergo deformations, stable non-spherical shapes or surface oscillations. Experimental evidences that have led to the assumption of stable nuclear deformation are:

The existence of rotational bands: In the mass regions $A \simeq 25$ and $150 < A < 190$ (that include nuclei far from the closed shells, see next section) the nuclear excitation spectra show pronounced rotational bands with an $I(I+1)$ spectrum [15, 44];

The existence of quadrupole moments: This experimental fact is a hint about stable nuclear deformations. In the mass regions mentioned at the previous point, plots of the quadrupole moments vs the mass number A show that it is very large, while it is zero for certain values of A, corresponding to the closed shells (again, see next section) [44, 51].

Quadrupole moment, in particular, can be used to measure the deviation of a charge distribution from sphericity. The classical electric quadrupole moment is defined as

$$Q = Ze \int d^3r \; \rho(\vec{r}) r^2 (3\cos^2 \theta - 1) \tag{1.4}$$

where the charge density at point $\vec{r}$ is given by $Ze\,\rho(\vec{r})$, where $\rho(\vec{r})$ indicates the proton density. For a spherically symmetric charge density, the quadrupole moment vanishes. This section deals with how to mathematically express permanent nuclear deformations.

A way to parametrize nuclear surface when it deviates from sphericity, is by considering a multipole expansion of the radius [44]:

$$R(\theta, \varphi) = R_0 \left[1 + \sum_{lm} \alpha_{lm} Y^*_{lm}(\theta, \varphi) \right] \tag{1.5}$$

where R_0 is the radius of the sphere with the same volume, and it is defined by (1.1). α_{lm} are the coefficients of the expansion and they are complex numbers. These coefficients will be taken small in the sense that $|\alpha_{lm}|^2 \ll |\alpha_{lm}|$; in other words the region of the small deformation is considered. Equation (1.5) is widely used and useful for problems of nuclear structure. In order to make sure that $R(\theta, \varphi)$ is a real quantity, one can use the conjugation property of the spherical harmonics to show that α_{lm} must satisfy the same conjugation rule, that is:

$$\alpha^*_{lm} = (-1)^m \alpha_{l-m}; \qquad Y^*_{lm}(\theta, \varphi) = (-1)^m Y_{l-m}(\theta, \varphi)$$

The deformations described in this section do not change nuclear volume, but only the nuclear shape. In this sense the $l = 0$ term in (1.5) must be excluded because $Y^*_{00}(\theta, \varphi) = \frac{1}{\sqrt{4\pi}}$ and it is a constant function. In other words, unless the coefficient $\alpha_{00} = 0$, the volume would change because the expansion (1.5) contains the non-zero $l = 0$ term. The terms with $l = 1$ have to be excluded too, because they describe only a rigid translation of the whole system. The parameters α_{1m} can be fixed by the condition that the origin of the frame system coincides with the center of mass:

$$0 = \int_V \vec{r}\, d^3r \tag{1.6}$$

So equation (1.5) starts from $l = 2$. One can easily demonstrate that for an expansion of the radius starting from $l = 2$, the request of volume conservation is fulfilled. The volume of the system can be calculated as

$$\begin{aligned} V &= \int d\Omega \int_0^{R(\theta,\varphi)} dR R^2 = \int d\Omega \, \frac{R_0^3}{3} \left[1 + \sum_{l \geq 2; m} \alpha_{lm} Y^*_{lm}(\theta, \varphi) \right]^3 \\ &\simeq \frac{4}{3} \pi R_0^3 \left(1 + 3 \sum_{l \geq 2; m} |\alpha_{lm}|^2 \right) \end{aligned} \tag{1.7}$$

where indicates a contract notation for the solid angle and in the last step the expansion of the cube has been stopped at the second order, the term in $^{*}_{lm}\ _{lm}$ has been interpreted as a coe□cient $_{00}$ and the orthonormality property of the spherical harmonics has been used

$$\int d\ Y^{*}_{lm}(\ ;\ ')Y_{l^0m^0}(\ ;\ ') = \ _{ll^0}\ _{mm^0} \tag{1.8}$$

The result of (1.7) explains that if the parameters $j\ _{lm}j^2$ are negligible as mentioned above, the volume of the system is unchanged.

The shapes of nuclear surface associated to the lowest multipolarity in equation (1.5) are displayed in figure 1.3. The deformations corresponding to $l = 2$ have ellipsoidal shapes. At higher levels of multipolarity or combined low levels of multipolarity, the nuclear shape becomes more complicated.

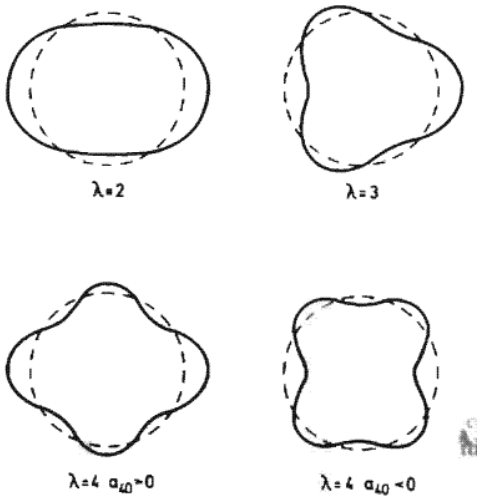

Figure 1.3: Nuclear shapes with quadrupole = 2, octupole = 3 and hexadecupole = 4 deformations [44]

The most widespread shape in the isotope chart is the static ellipsoidal shape, or the static quadrupole deformation. It can be represented by stopping (1.5) to the $l = 2$ term. In this way the radius becomes

$$R(\ ;\ ') = R_0\ \left[1 + \sum_{m=-2}^{m=2}\ _{2m}Y^{*}_{2m}(\ ;\ ')\right] \tag{1.9}$$

Equation (1.9) can be written, in principle, in terms of the Cartesian coordinates:

$$R(\ ;\ ') = R_0\ \left[1 + \ _{xx}\frac{x^2}{r^2} + \quad + \ _{xz}\frac{xz}{r^2} + :::\right] \tag{1.10}$$

It is possible by using the expressions which describes the spherical harmonics in Cartesian coordinates:

$$Y_2^{\pm2}(\ ;\ ') = \frac{1}{4}\sqrt{\frac{15}{2}}\sin^2\ e^{\pm2i\ '} = \frac{1}{4}\sqrt{\frac{15}{2}}\frac{x^2\quad y^2\quad 2ixy}{r^2}$$

$$Y_2^{\pm1}(\ ;\ ') = \frac{1}{2}\sqrt{\frac{15}{2}}\sin\ \cos\ e^{\pm i\ '} = \frac{1}{2}\sqrt{\frac{15}{2}}\frac{xz\quad iz}{r^2}$$

$$Y_2^{\pm 2}(\ ;\ ') = \frac{1}{4}\ \overline{5}(3\cos^2 \qquad 1) = \frac{1}{4}\ \overline{5}\frac{2z^2 \quad x^2 \quad y^2}{r^2}$$

In this way, one can find the correspondence between the coe□cients $_{2m}$ of equation (1.9) and the coe□cients $_{ij}$ (with $i;j = x;y;z$) of the expansion (1.10):

$$\begin{aligned} {}_{2\pm 2} &= \frac{2}{15}\,(\ _{xx} \qquad _{yy} \quad 2i\ _{xy}) \\ {}_{2\pm 1} &= \quad 2\ \frac{2}{15}\,(\ _{xz} \quad i\ _{yz}) \\ {}_{20} &= \frac{2}{3}\ \overline{5}\,(\ _{zz} \qquad _{xx} \qquad _{yy}) \end{aligned} \tag{1.11}$$

The radius of a pure quadrupole deformation (1.9) has five deformation parameters, the coe□cients $_{2l}$, but they do not give a clear or direct idea about the deformation of the liquid drop. In order to study better the nuclear deformations, it is useful to introduce another coordinate system, in addition to the laboratory system. The new system is solidal to the nucleus and its axes are identifiable as those with respect to which the tensor of inertia is diagonal and it is called *intrinsic frame*. The components of the tensor of inertia are proportional to the coe□cients $_{ij}$ of the expansion (1.10). In this work the laboratory system will be indicated with O, while the intrinsic frame with O'. The intrinsic frame O' is rotated respect to O, but they are linked through the Euler angles $= f\ ;\ ;\ g$ and the following transformations between the two systems holds:

$$Y_{lm}(\ ';\ '') = \sum_{mm'} D^{(l)}_{mm'}(\ )Y^*_{lm'}(\ ;\ ') \tag{1.12}$$

In the last equation the right side refers to the laboratory frame, while the left side to the intrinsic frame. $D^{(l)}_{mm'}(\ )$ are the Wigner functions and they are unitary matrices which describe rotations in the space, in this case, they describe rotations about the Euler angles. Because of (1.12), the expansion for the radius in (1.9) has a valid expression also in the intrinsic frame. In particular, if the coe□cients $_{2m}$ in the intrinsic frame are labelled as a_{2m}, one obtains that

$$a_{21} = 0 \qquad \text{and} \qquad a_{22} = a_{2-2} \tag{1.13}$$

This fact is due to the tensor of inertia that is diagonal, in this way all the "mixed" coe□cients (like $_{xy}$) in (1.11) are null. It is more useful to introduce two new deformation parameters and and to express a_{20} and a_{22} in such a way that

$$a_{20} = \quad \cos\ ; \qquad a_{22} = \frac{}{\sqrt{2}}\sin \qquad ! \qquad \sum_m j\ _{2m}j^2 = \ ^2 = a_{20}^2 + 2a_{22}^2 \tag{1.14}$$

In this way five degrees of freedom in the intrinsic frame have been defined and they are equivalent to the five coe□cients $_{2m}$ of the expansion (1.9). The Euler angles are three of these degrees of freedom in the intrinsic frame and represent the orientation of the system in the space. The last two degrees of freedom are the parameters and ; they are closely related to the nuclear shape. In particular, as it will be showed below, represents the variation of the radius from sphericity, namely how long or narrow is in the three principal axes (if they are all equal,

the shape is spherical); while is related to the "global shape" of the nucleus, or it explains whether the nucleus is *axially deformed* or *triaxial*. These considerations will be clarified below. Equation (1.9) in the intrinsic frame becomes:

$$\begin{aligned} R(\ ;\ ') &= R_0 \,\Big[1 + a_{20}Y^*_{20}(\ ;\ ') + a_{22}Y^*_{22}(\ ;\ ') + a_{2-2}Y^*_{2-2}(\ ;\ ') \\ &= R_0\ \ 1 + \sqrt{\frac{5}{16}}\ \cos\ \ (3\cos^2\ \ \ 1) + \sqrt{3}\sin\ \ \sin^2\ \ \cos(2\ ') \Big] \end{aligned} \tag{1.15}$$

where in the last step the fact that $a_{22} = a_{2-2}$ and the conjugation property of the spherical harmonics $Y^*_{lm}(\ ;\ ') = (\ 1)^m Y_{l-m}(\ ;\ ')$ have been used. Furthermore, the specific increments of the three semi-axes with respect to R_0 in the intrinsic frame as functions of and read:

$$\begin{aligned} R_x &= R\ \ \tfrac{}{2};0 \quad\ R_0 = R_0\ \ \sqrt{\frac{5}{4}}\cos\ \ \ \frac{2}{3} \\ R_y &= R\ \ \tfrac{}{2};\tfrac{}{2} \quad\ R_0 = R_0\ \ \sqrt{\frac{5}{4}}\cos\ \ + \frac{2}{3} \\ R_z &= R\,(0;0) \quad R_0 = R_0\ \ \sqrt{\frac{5}{4}}\cos \end{aligned} \tag{1.16}$$

In the figure 1.4 the $l = 2$ shapes are represented with respect to the coordinates ; . It is important to notice that [44]:

If = 0, one finds that $R_x = R_y < 0$ while $R_z > 0$. In this case the nucleus is called as *axially deformed* with z axis as symmetry axis under rotation and *prolate*, i.e. it is elongated along the z axis and shrunk on the perpendicular axes (a "cigar" shape);

If = $\tfrac{}{3}$, one finds that $R_x = R_z > 0$ while $R_y < 0$. In this case the nucleus is still *axially deformed* with y axis as symmetry axis under rotation but it is *oblate*, i.e. the nucleus is shrunk around the symmetry axis and enlarged on the perpendicular plan (a "pancake" shape);

If $0 <$ $< \tfrac{}{3}$, a single symmetry axis can not be identified under rotation, so it has a complicated shape called *triaxial shape*;

Values of outside the interval $0;\tfrac{}{3}$ produce the same shapes described above, but with the other symmetry axes.

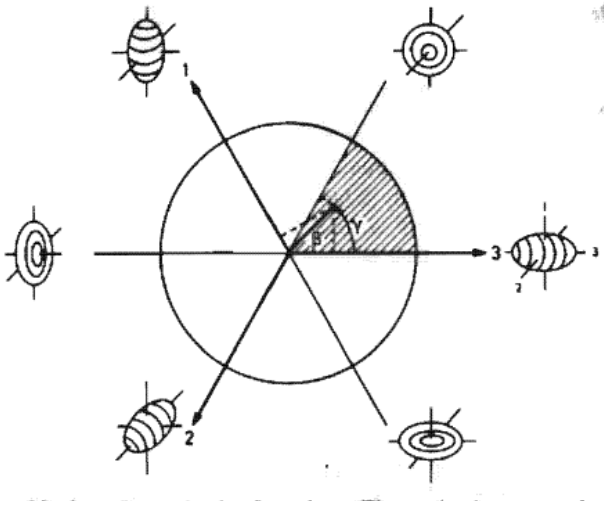

Figure 1.4: Quadrupole nuclear shapes in the plane [44].

In conclusion, the parameters and together with (1.9) can only describe exactly ellipsoidal shapes in the limit of the small deformations, or small values.

1.2 The Shell Model

The liquid drop model accounts for gross nuclear features, but it can not explain specific properties of excited nuclear states. According to the shell model many nuclear properties seem to be describable in terms of the idea that the nucleons in a nucleus are to be considered as independent particles moving on almost stationary single particle orbits. The reason for that is mainly due to the action of the Pauli principle, according to which the nucleus is not a very dense system. The nucleon-nucleon interaction is composed also by a component for which at very short range (r ' 0:4 fm [44]) the interaction is repulsive and by an attractive component which dominates at higher ranges. This aspect of the nuclear force is, in a certain way, "reduced" by the fact that the nucleons are, on the average, quite far apart. In other words, they feel mainly the attractive part of the interaction, so the system can be described, to a first approximation, in terms of single-particle motion. If the idea of independent particles is accepted, it is quite natural to expect that this single particle motion is governed by some average potential created by all the nucleons in the nucleus. The occurrence of the so-called *magic numbers*:

$$2; 8; 20; 28; 50; 82; 126$$

has been the strongest motivation for the formulation of a nuclear shell model. In fact from an experimental point of view [31, 44], nuclides with either N or Z equal to a magic number turn out to be particularly stable. A similar feature is observable in the trends of binding energies in atomic physics, when a particular number of electrons "closes" the shell. In this section the nuclear shell model will be discussed.

1.2.1 The Average Potential of the Nucleus

As already mentioned, the magic numbers reveal the analogy between electrons and nucleons about the e□ect of the closed shell. For the electrons the mean potential is imposed from the

outside, i.e. by the Coulomb interaction with the positive charge contained in the nucleus, which furthermore imposes also a spherical distribution of the electrons. In the nuclear case, the nuclear interaction is not *a priori* a central field and one can imagine such a potential as being built up by the action of all the nucleons. A model which describes the dynamics of the nucleons only with such an average potential treats the nucleons as completely independent of one another.

Experiments show that the density within the nucleus is approximately constant and in principle it does not depend on the mass number A [44]. By this consideration one can expect that at the edge of the nucleus the density decreases and the attractive potential decreases as well. In a more formal way, a nucleon close to the center of the nucleus will feel nuclear forces uniformly, so it will not feel a net force:

$$\left.\frac{@V(r)}{@r}\right|_{r=0} = 0$$

The nuclear binding forces get stronger going from the surface ($r = R_0$) towards the center of the nucleus, that is:

$$\left.\frac{@V(r)}{@r}\right|_{r<R_0} > 0; \qquad V(r) \; ' \; 0; \qquad r > R_0$$

Because of the finite range of the nuclear forces, outside of the nucleus the attractive interaction must be zero. An empirical potential that reproduces the nuclear phenomena and the conditions above quite well is a "Fermi distribution-like" function, or the the *Woods-Saxon potential* (WS). In the case of spherical nuclei, this reads:

$$V_{WS}(r) = V_0 \left[1 + e^{\frac{r - R_0}{a}}\right]^{-1} \tag{1.17}$$

and it has the form a central potential. As previously said, the density profile (that can be extracted by electron scattering) is consistent to a similar shape:

$$(r) = {}_0 \left[1 + e^{\frac{r - R_0}{a}}\right]^{-1} \tag{1.18}$$

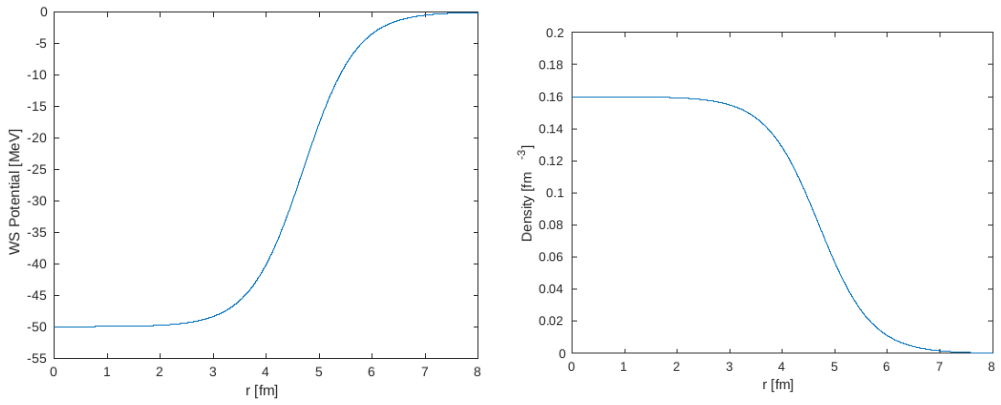

(a) (b)

Figure 1.5: Shapes of the Woods-Saxon potential (a) and the saturation density (b) for $A = 60$.

In the equations (1.17) and (1.18) $V_0 \simeq 50$ MeV is the potential depth, R_0 is given by (1.1), $_0 = 0{:}16$ fm^{-3} is the saturation density within the nuclear volume and $a \simeq 0{:}5$ is a parameter that defines the nuclear surface.

In order to understand the shell structure created by the WS potential (1.17), one should solve numerically the Schrödinger equation associated with it. Since the WS potential is a central potential, one can solve the Schrödinger equation with the eigenfunctions written as:

$$_{njlms}(r;\ ;\ ';\ ) = \frac{u_n(r)}{r}\ Y_l^m(\ ;\ ')\quad {}_{\frac{1}{2}}(\ )\ _{jm} \tag{1.19}$$

where $u(r)$ is a solution of the reduced or radial Schrödinger equation

$$\frac{h^2}{2m}\frac{d^2}{dr^2}u_n(r) + \frac{h^2 l(l+1)}{2mr^2}u_n(r) + V_{\text{ws}}(r)u_n(r) = "_n u_n(r) \tag{1.20}$$

where $"_n$ are the eigenvalues. In order to more easily calculate the eigenfunctions of the potential (1.17), one can use use the approximation of the harmonic oscillator (HO) potential for qualitative considerations, that means

$$V(r) = \frac{1}{2}m!(r \quad R_0)^2 \tag{1.21}$$

or the square well:

$$V(r) = \begin{cases} V_0 & \text{for} \quad r \quad R_0 \\ +1 & \text{for} \quad r > R_0 \end{cases} \tag{1.22}$$

Since the harmonic potential (1.21) is central-type, one can solve the equation (1.20) with such potential and the HO eigenvalues are given by

$$"_{nl} = h!\quad N + \frac{3}{2}\quad = h!\quad 2n + l\quad \frac{1}{2} \tag{1.23}$$

where $h!$ is the typical HO quantum. One can easily demonstrate that approximately the HO level are equally spaced by

$$h! \simeq 41A^{-\frac{1}{3}} \tag{1.24}$$

N is called the principal quantum number and in the last step one has rewritten $N = 2(n \quad 1) + l$. n represents the number on nodes of the radial wave function and can assume values $n = 1; 2; : : :$ up o N; l can assume only positive values ($l \quad 0$) up to N and gives the parity of each N th level, which is $(\ 1)^l$. Taking into account the Pauli principle and spin, the HO energy levels have a large degeneracy, which is given by $(N + 1)(N + 2)$. Each HO level have a large degree of degeneracy, that can be written in terms of l:

$$(N + 1)(N + 2) = \sum_l 2(2l + 1) \tag{1.25}$$

The group of degenerate HO levels related to a specific N is called oscillator shell. Table 1.1 gives the lower HO energy states and HO magic numbers which satisfy what have been said.

N	n	l	Parity	$(N+1)(N+2)$	HO magic numbers	Orbitals
0	1	0	+	2	2	$1s$
1	1	1	-	6	8	$1p$
2	1,2	0,2	+	12	20	$2s$,$1d$
3	1,2	1,3	-	20	40	$2p$,$1f$
4	1,2,3	0,2,4	+	30	70	$3s$,$2d$,$1g$
5	1,2,3	1,3,5	-	42	112	$3p$,$2f$,$1h$

Table 1.1: Magic number and orbitals within the HO approximation

1.2.2 Spin-Orbit Coupling

Only the first three magic numbers in the table 1.1 are correct, by comparing with experimental results. However, up to now the spin of the nucleons has not been taken into account yet (apart from a factor 2 in determining the magic numbers). A nucleon with orbital angular momentum l and spin s can have total angular momentum given by $j = l + s = l \quad \frac{1}{2}$. For example a nucleon in the HO shell $N = 1$ stays in the orbital $1p$, but it can have total angular momentum either $j = \frac{3}{2}$ or $j = \frac{1}{2}$.

The nucleon-nucleon force has a spin-orbit component [12, 44], and one can expect that the average single-particle potential also has a spin-orbit part with strength compatible with the original nucleon-nucleon force. If $f(r)$ indicates the intensity of the spin-orbit strength, in such a way that the spin-orbit potential has the form

$$V_{ls} = f(r)\hat{l}\ \hat{s}$$

one can show that $f(r)$ is peaked at the nuclear surface [33]. By the analogy with the electronic case [44], one often chooses $f(r)$ related to the spin independent part of the average potential in the following way

$$f(r) = \frac{1}{r}\frac{dV}{dr}; \qquad ' \quad 0{:}5 \quad [\mathrm{fm}^2] \tag{1.26}$$

Let's see what happens if a generic spin-orbit potential is added to the Schrödinger equation (1.20). It has the form [30]:

$$V_{ls} = f(r)\ \hat{l}\ \hat{s} \qquad \hat{j} = \hat{l} + \hat{s} \tag{1.27}$$

$f(r)$ is a scalar coe□cient for the potential and in principle it depends on $l; s$ and it represents the spin-orbit strength. The e□ect of this potential on a generic state $jjlsi$ is given by

$$\hat{j}^2 = \ \hat{l} + \hat{s}\ ^2 \qquad =) \qquad \hat{l}\ \hat{s}\ = \frac{1}{2}\ j^2 \quad l^2 \quad s^2$$

$$\hat{l}\ \hat{s}\ \ jjlsi = \frac{1}{2}[j(j+1) \quad l(l+1) \quad s(s+1)]\,jjlsi \tag{1.28}$$

The e□ect of the spin-orbit coupling is di□erent depending on the z projection of the nucleon spin. In other words for fixed l and $j = l \quad \frac{1}{2}$ one obtains

$$\hat{l}\ \hat{s}\ \ jjlsi = \begin{cases} \frac{1}{2}ljjlsi & \text{for} \quad j = l + \frac{1}{2} \\ \frac{1}{2}(l+1)jjlsi & \text{for} \quad j = l \quad \frac{1}{2} \end{cases} \tag{1.29}$$

This is a confimation that in the shell model breaks the degeneracy of the levels. The displacement energy E_{ls} of the splitting in (1.29) is

$$E_{ls} \quad l + \frac{1}{2}$$

The difference between two levels with the same orbital angular momentum increases with increasing l. Furthermore one should expect that the effect of the spin-orbit coupling increases with increasing mass number A, because massive nuclei usually have high angular momentum, so this effect becomes very important.

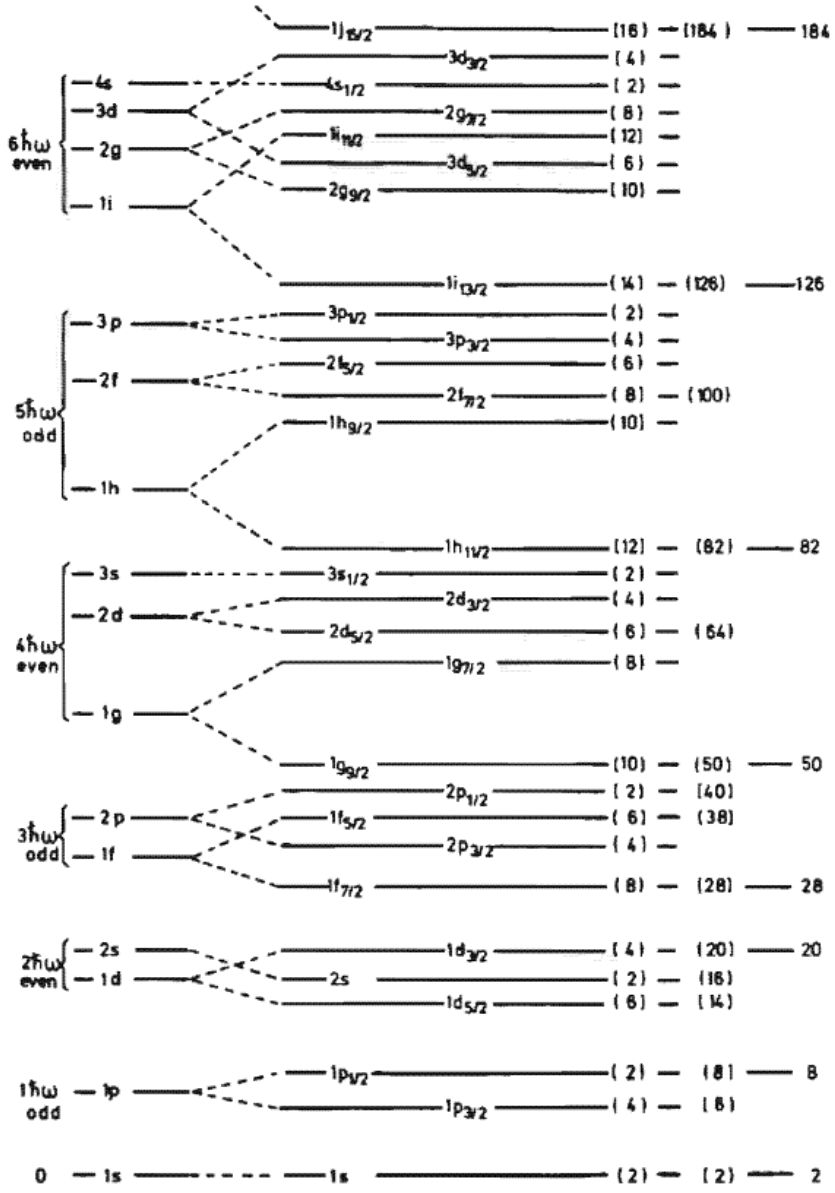

Figure 1.6: Schematic nuclear levels of the shell model within the spin-orbit coupling [44].

Let's consider the figure 1.6:

The spin-orbit coupling shifts the levels $j = l + \frac{1}{2}$ downward while it shifts the levels $j = l - \frac{1}{2}$ upward. In other words the parallel coupling of l and s is more attractive than the anti-parallel coupling;

The nucleons are disposed on the levels from the bottom up and the degeneration of each level is given by $2j + 1$;

At high values of l the spin-orbit splitting becomes so strong intense that the HO shell structure is modified. Examples are the level $1f_{\frac{7}{2}}$ which opens a new shell and adds the magic number 28; the level $1g_{\frac{9}{2}}$ which is so low that adds the level to the lower shell, making the magic number 40 become 50.

1.2.3 An Outline to Deformed Shell Model

What has been said up to now is true for nuclei with closed or nearly closed shells and for such nuclei the spherical shell model is very successful. Far from the closed shells, that is for the mass numbers $A \simeq 25$, $150 < A < 190$ and $A > 220$ one should assume a deformed particle potential, that is slightly different from the WS potential (1.17). In the spherical case the WS potential represents a quite good average potential. It is quite natural, in the deformed case, to generalize it to a deformed case [44]:

$$V(r;\ ;\ ') = V_0 \left[1 + \exp\left(\frac{r - R(\ ;\ ')}{a(\ ;\ ')}\right)\right]^{-1} \tag{1.30}$$

where in this situation the parameter a is slightly dependent on the angles. By following the reasoning of the previous section, one should now approximate (1.30) with a deformed harmonic oscillator potential. A deformed HO Hamiltonian has the form

$$H_{HO} = \left(\frac{h^2}{2m}\right) r^2 + \frac{1}{2}m\left(!_x^2 x^2 + !_y^2 y^2 + !_z^2 z^2\right) \tag{1.31}$$

In other words one separates the Hamiltonian in the three directions. The eigenstates related to (1.31) are separable in the three directions as well:

$$E_{HO} = h!_x\left(n_x + \frac{1}{2}\right) + h!_y\left(n_y + \frac{1}{2}\right) + h!_z\left(n_z + \frac{1}{2}\right) \tag{1.32}$$

In the case of axially symmetric deformation, by choosing z-axis as the symmetry axis, one should introduce the deformation parameter $"$ in such a way that [44]

$$!_z = !_0\left(1 - \frac{2}{3}"\right)\ ; \qquad !_\perp = !_x = !_y = !_0\left(1 + \frac{1}{3}"\right)\ ; \qquad \text{where} \quad h!_0 = 41A^{-\frac{1}{3}} \tag{1.33}$$

By neglecting the quadratic values of $"$ (limit of the small deformations) the volume conservation $!_z !_\perp^2 = !_0^3$ holds. In this way, by inserting the (1.33) in a spherical HO hamiltonian, the deformed HO Hamiltonian can be written as

$$\begin{aligned} H &= \left(\frac{h^2}{2M}\right) r^2 + \frac{1}{2}M!_0 r^2 - \frac{1}{3}"\sqrt{\frac{16}{5}}M!_0^2 r^2 Y_{20} \\ &= H_0 + "H_1 \end{aligned} \tag{1.34}$$

If ε is a small parameter, the effect of the deformation, that means εH_1 in (1.34) can be treated within the first order of the perturbation theory. The degenerate levels in the spherical case undergo a splitting, that is

$$\begin{aligned} E &= \langle nljmj|\varepsilon H_1|nljmj\rangle = \\ &= \frac{\varepsilon}{6} M\omega_0 \frac{3m^2 - j(j+1)}{j(j+1)} \int dr r^2 u_{nlj}^2(r) \end{aligned} \tag{1.35}$$

In the last step of (1.35) a standard wave function like (1.19) has been used. The latter expression explains that states remains degenerate, but the states with maximum projection $m = \pm j$ are shifted up, while the states with minimum projection $m = \pm \frac{1}{2}$ are shifted down.

The equipotential surfaces are ellipsoids. At the first order in the deformation ε they can be represented by the equation (1.5) [44]

$$r \quad (1 + \quad Y_{20}(\ ;\ ')) \qquad \text{with} \qquad = \frac{1}{3}\varepsilon \sqrt{\frac{16}{5}} + \ldots \tag{1.36}$$

The deformation parameter ε of equation (1.33) is roughly equal to introduced in the equations (1.14). In the case of axial symmetry, it is convenient to put in cylinder coordinates [28, 44]. The eigenstates are characterised by new quantum numbers n_z, n and m_l where m_l is the projection of the orbital angular momentum on the symmetry axis. The relation with the cartesian numbers is $N = n_x + n_y + n_z = n_z + 2n + m_l$. The energy eigenvalues are rewritten as [44]

$$\begin{aligned} E_{HO} &= \hbar\omega_z \left(n_z + \frac{1}{2}\right) + \hbar\omega_\perp (2n + m_l + 1) \\ &\simeq \hbar\omega_0 \left(N + \frac{3}{2}\right) + \varepsilon \left(\frac{N}{3} - n_z\right) \end{aligned} \tag{1.37}$$

The axial symmetry makes m_l a good quantum number, and the same holds for the third spin component and s_z and the j_z component of the total angular momentum which has eigenvalue $= m_l + m_s = m_l \pm \frac{1}{2}$. The quantum numbers in the cylindrical coordinates are usually grouped in the so called "Nilsson quantum numbers" in the notation $[Nn_z m_l]$, where indicates the parity of the states. For example, for $N = 3$, the energy eigenvalues (1.37) become

$$E_{HO}^{N=3} \simeq \hbar\omega_0 \left(\frac{9}{2} + \varepsilon(1 - n_z)\right) \tag{1.38}$$

According to the relations between all the quantum numbers in cylindrical coordinates, all the possible combinations for the quantum numbers are listed in the following table.

n_z	m_l	n		Degeneracy
0	1 3	1 0	$\frac{1}{2}$ $\frac{3}{2}$ $\frac{5}{2}$ $\frac{7}{2}$	4-fold
1	0 2	1 0	$\frac{1}{2}$ $\frac{3}{2}$ $\frac{5}{2}$	3-fold
2	1	0	$\frac{1}{2}$ $\frac{3}{2}$	2-fold
3	0	0	$\frac{1}{2}$	1-fold

Table 1.2: Construction of the Nilsson quantum numbers for $N = 3$ [44].

In order to agree with the experimental results, a spin-orbit potential has to be added to the Hamiltonian (1.34); it this way the right magic numbers can be reproduced. Nilsson added two terms to (1.34) [44]:

$$H = \frac{h^2}{2M} + \frac{1}{2}M\,!_{\perp}^{2}(x^2 + y^2) + !_z z^2 + C\hbar\, s + D\hbar^2 \qquad (1.39)$$

The constants C and D are usually given in the form

$$C = 2h!_0\ ; \qquad D = h!_0$$

where C gives the strength of the spin-orbit force and $D\hbar^2$ shifts downward the levels with high l. In general and values are di erent depending on the shells, they are adjusted for the nucleus $(N;Z)$ on which one is interested in, see [44] for more details on Nilsson model.

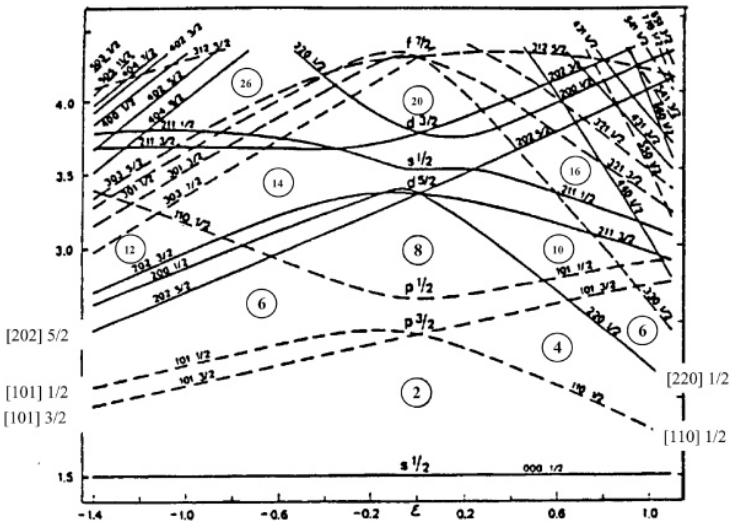

Figure 1.7: Level diagram in the Nilsson model [29].

The typical energy diagram within the Nillson model for small mass numbers A is shown in figure 1.7. For zero deformation the levels agree with the ones shown in figure 1.6. In this limit ($" = 0$) the states are $(2j + 1)$-fold degenerate. The deformation lifts the degeneracy. For instance in figure 1.7 the state $1p_{\frac{3}{2}}$ splits into two states and the state $1d_{\frac{5}{2}}$ splits into three levels, as predicted by (1.35). A nucleon with total angular momentum j in the spherical case gives rise to $\frac{1}{2}(2j + 1)$ di erent energy levels. The factor $\frac{1}{2}$ describes a remainig twofold degeneracy which is due to the symmetry of the nucleus about the xy plane: the states m and m have the same energy.

Chapter 2

Microscopic Mean-Field Models for Nuclear Structure

The problem of nuclear structure is a many-body problem. Since it is a complicated problem, as already mentioned, a possible approach to the problem is the use of mean-field models. In this approach, the totality of the interactions acting on a nucleon in an "average potential" is approximated. In such average potential a nucleon moves independently from the other constituents of the system. These models concentrate on self-consistent determination of the nuclear mean field. For this purpose e□ective interactions are employed and are strictly connected to their primary use in mean-field calculations. This concept is closely related to energy-density-functional (EDF) theory in electronic systems [11, 44]. There exists a theory which allows one to calculate the shell model potential microscopically. This theory is the Hartree-Fock method and its generalisations (HF Bogolyubov). This chapter starts with the Hartree-Fock self consistent method, supported by the Skyrme-type e□ective interaction. It is followed by two its extensions which are the BCS theory and the Hartree-Fock-Bogolyubov method. In the middle of this chapter it will be shown that modern calculations of this type give quite good and detailed agreement of the binding energies over the whole mass region.

2.1 The Nuclear Hartree-Fock Method

The idea that nucleons move independently in an average potential produced by the nucleon themselves comes from the successful results of the shell model of the nucleus. According to this model, nucleons can move in a average potential independently from each other; so the problem of the Hartree-Fock method is how to extract a single-particle potential out of the sum of two-body interactions:

$$V(1;:::;A) = \frac{1}{2}\sum_{i\neq j} v(r_i;r_j) \; ' \sum_{i=1} v(r_i)$$

without losing generality on the physical system. It will be shown that the single-particle potential can be derived by a variational principle using the Slater determinants as wave functions [44].

The variational principle solves in approximated way the eigenvalue problem of the exact Schrödinger equation [44]

$$\hat{H}j\ i = Ej\ i \tag{2.1}$$

This approach is useful for solving many-body problems, in which it is very difficult to divide the Hamiltonian into two parts as one wants to use perturbative theory. This method is used not only in Hartree-Fock method, but also in other impotant theories in nuclear physics like the Bardeen-Cooper-Schrieffer (BCS) theory, for pairing interaction.

2.1.1 Hartree-Fock Equations

As already mentioned, Hartree-Fock theory tries to give a microscopic explanation to the existence of a nuclear mean-field. It starts from a many-body Hamiltonian with a two-body interaction between nucleons:

$$\hat{H} = \hat{T} + V = \frac{\hbar^2}{2m} \sum_i \nabla_i^2 + \frac{1}{2} \sum_{i \neq j} v(i,j) \tag{2.2}$$

The purpose of the Hartree-Fock method is resolving an eigenvalue problem in which the total wave function has the form of the totally anti-symmetric product of single-particle wave functions ψ_i (these are the trial wave functions); this total wave function is in general unknown. A totally anti-symmetric product of single-particle wave function is determined by the Slater determinant:

$$\Phi(\mathbf{r}_1, \ldots, \mathbf{r}_A) = \frac{1}{\sqrt{A!}} \begin{vmatrix} \psi_1(\mathbf{r}_1) & \cdots & \psi_1(\mathbf{r}_A) \\ \cdots & \cdots & \cdots \\ \psi_A(\mathbf{r}_1) & \cdots & \psi_A(\mathbf{r}_A) \end{vmatrix} \tag{2.3}$$

In order to find the minimum of the energy functional, now the variational principle to the eigenvalue problem (2.1) has to be applied, where the Hamiltonian is expressed in (2.2). Before applying the variational principle it is important to add a Lagrange multiplier to ensure the orthonormality of the wave functions. In other words, the variational principle that has to be calculated is the following:

$$\delta E \int d^3r \, \psi_i^*(\mathbf{r}) \psi_i(\mathbf{r}) = 0 \tag{2.4}$$

The expectation values of kinetic and potential operators reads

$$\langle i | \hat{T} | i \rangle = \frac{\hbar^2}{2m} \sum_{i=1}^{A} \int d^3r \, \psi_i^*(\mathbf{r}) \nabla^2 \psi_i(\mathbf{r})$$

$$\langle i | V | i \rangle = \frac{1}{2} \sum_{i \neq j} \int d^3r \int d^3r' \, \psi_i^*(\mathbf{r}) \psi_j^*(\mathbf{r}') v(\mathbf{r}, \mathbf{r}') \left[\psi_i(\mathbf{r}) \psi_j(\mathbf{r}') - \psi_j(\mathbf{r}) \psi_i(\mathbf{r}') \right]$$

Then, by making the variation on the orbitals ψ_i^*, one obtains the following set of equations for each orbital:

$$\frac{\hbar^2}{2m} \nabla_i^2(\mathbf{r}) \psi_i(\mathbf{r}) + \frac{1}{2} \sum_{j=1}^{A} \int d^3r' \left[\psi_j^*(\mathbf{r}') v(\mathbf{r}, \mathbf{r}') \left[\psi_i(\mathbf{r}) \psi_j(\mathbf{r}') - \psi_j(\mathbf{r}) \psi_i(\mathbf{r}') \right] = \varepsilon_i \psi_i(\mathbf{r}) \right. \tag{2.5}$$

In equation (2.5) the Lagrangian multiplier has assumed the meaning of eigenvalues of the Scrödinger equations (single-particle energies), which are properly the structure of (2.5). These are the *Hartree-Fock equations*. In this equation the first term represent the kinetic component

and the second term the local density-depending potential, called Hartree term; it should represent the local mean-field potential. The third term represents a non-local contribution to energy, which is related to the fermionic nature of the nucleons; it is also called Fock term. In (2.5) one can note that both the local and non-local potentials depend on the single-particle wave functions, and we can call these *self-consistent* equations. The solution of the Hartree-Fock equations must be found in a iterative way: one starts by choosing a specific potential (like a Saxon-Woods potential or the harmonic oscillator one) to be applied to the equations (2.5) and finds a wave function. Then this first wave function has to be put again in the equations (2.5) and a new potential will be obtained. The Hartree-Fock equations can be solved by repeating several times this procedure until convergence.

By remembering the density definition based on single-particle wave functions:

$$(\mathbf{r}) = \sum_{i=1}^{A} \psi_i^*(\mathbf{r})\,\psi_i(\mathbf{r}) = \sum_{i=1}^{A} |\psi_i(\mathbf{r})|^2$$

The Hartree term in (2.5) can be rewritten as follows:

$$\sum_{j=1}^{A} \int d^3r'\,\psi_j^*(\mathbf{r}')v(\mathbf{r};\mathbf{r}')\,\psi_i(\mathbf{r})\,\psi_j(\mathbf{r}') = \int d^3r' v(\mathbf{r};\mathbf{r}')\ (\mathbf{r}')\ \psi_i(\mathbf{r}) \qquad (2.6)$$

Written in these terms, the Hartree term (2.6) represents the potential which influences the state of a nucleon in an environment in which all the other nucleons are distributed with density distribution $(\mathbf{r})$. This term corresponds to a multiplicative factor to the single-particle wave function and it does not affect the structure of the equation. Unfortunately the Fock term can not be rewritten as a multiplicative factor to the single-particle wave functions and it makes the Hartree-Fock equations (2.5) a set of integro-differential equations.

The binding energy of the nucleus, within the Hartree-Fock model, is given by adding the expectation values of the kinetic and potential parts:

$$E = \sum_{i} \langle ij|\hat{T}|ji\rangle + \frac{1}{2}\sum_{i\neq j} \langle ij|V|ji\rangle_{AS} \qquad (2.7)$$

where the single matrix elements are expressed more clearly (remember that the potential matrix element is anti-symmetrized):

$$\langle ij|\hat{T}|ji\rangle = \frac{\hbar^2}{2m}\int d^3r\,\psi_i^*(\mathbf{r})\,\nabla^2\psi_i(\mathbf{r})$$

$$\langle ij|V|ji\rangle_{AS} = \int d^3r \int d^3r'\,\psi_i^*(\mathbf{r})\,\psi_j^*(\mathbf{r}')v(\mathbf{r};\mathbf{r}')\ \psi_i(\mathbf{r})\,\psi_j(\mathbf{r}') - \psi_j(\mathbf{r})\,\psi_i(\mathbf{r}')$$

The potential expectation value contains a direct and an exchange term; it is a consequence of the fact that the Slater determinant is a totally anti-symmetric product. The Hartee-Fock equations can be easily solved whether an effective potential can be defined *ad hoc*, whose parameters are fitted to describe well the ground states of nuclei in the Hartree-Fock approximation. It is the case of a Skyrme-type force or a Gogny-type one. In order to generalise the Hartree-Fock equations, the single-particle wave function can be generealised by making they depending on spin and isospin coordinates: $\psi_i(\mathbf{r}) \to \psi_i(\mathbf{r};\sigma_i;q_i)$, where q stays for the nucleon charge.

2.1.2 The Skyrme Interaction

In this work the HF equations are solved by using a Skyrme interaction [52, 58]. It is an effective interaction proportional to the delta function $(\vec{r}_1 - \vec{r}_2)$; in this way the Fock term in (2.5) is no-longer non-local and the HF equations become consequently only differential and no longer integro-differential. The orginal Skyrme force is composed by a two-body interaction and a three-body interaction [19, 52, 58]:

$$V_{Skyrme} = \sum_{i<j} v_{ij}^{(2)} + \sum_{i<j<k} v_{ijk}^{(3)} \tag{2.8}$$

The two-body force is written as

$$\begin{aligned} v_{ij}(1;2) = {} & t_0(1 + x_0 P^{12})\ (\vec{r}_1 - \vec{r}_2) + \frac{1}{2} t_1 (1 + x_1 P^{12})\ (\vec{r}_1 - \vec{r}_2)\ k^2 + k'^2 \\ & + t_2\ 1 + x_2 P^{12}\ (\vec{k}\ \tilde{k}')\ (\vec{r}_1 - \vec{r}_2) + iW_0 (\sigma_1 + \sigma_2)\ (\vec{k}\ \tilde{k}')\ (\vec{r}_1 - \vec{r}_2) \end{aligned} \tag{2.9}$$

where t_i, x_i and W_0 are free parameters that can be fixed by fitting to experimental data. In the equation (2.9) some symbols are here specified:

$$P^{12} = \frac{1}{2}(1 + \sigma_1 \sigma_2); \qquad \vec{k} = \frac{1}{2i}(\nabla_1 - \nabla_2)$$

where the vector $\tilde{k}'$ is the complex conjugated of $\vec{k}$ and it acts on the left and P_{12} is the spin exchange operator. The first term in equation (2.9) is the central one because it depends on the only difference of the positions $\vec{r}_1 - \vec{r}_2$. The second and the third ones depends on the relative momentum $\vec{k}$. The fourth term is the spin-orbit component of the interaction. Effective Skyrme interaction, though proportional to a delta, mimics the finite but short range of the NN interaction via the terms dependent on k [44, 52]. As regards the three-body term in the equation (2.8) can be written in terms of a zero-range force as well:

$$v_{ijk}(1;2;3) = t_3\ (\vec{r}_1 - \vec{r}_2)\ (\vec{r}_2 - \vec{r}_3) \tag{2.10}$$

It can be rewritten, in terms of a two-body force, the prove is shown in [58]:

$$v_{ij}(1;2) = \frac{1}{6} t_3 (1 + x_3 P^{12}) \quad \frac{\vec{r}_1 + \vec{r}_2}{2} \qquad (\vec{r}_1 - \vec{r}_2) \tag{2.11}$$

The equivalence between the three-body term and the two-body force holds only if one considers the ground-state of even-even nuclei and = 1 [58]. Such a term provides a simple phenomenological representation of many nucleon interactions in an effective way, and describes the way in which the interaction between two nucleons is influenced by the presence of the others. The latter interaction that has to be included before calculating the expectation value of the total energy, the Coulomb interaction. Unlike the Skyrme force, the Coulomb interaction has a non-zero range; so, one should add a component that is an approximation, in order to keep the Coulomb term local. This approximation was made by Slater [53], and he added the *exchange term* to Coulomb interaction, which now it is composed by a direct and an exchange term. It can be written as:

$$V_c(\vec{r}) = \quad e^2 \quad \frac{3}{\pi} \quad {}_p(\vec{r}) \quad {}^{\frac{1}{3}} + \int d^3 r' \ {}_p(\vec{r}') \frac{e^2}{|\vec{r} - \vec{r}'|} \tag{2.12}$$

where $_p(\mathbf{r})$ is the proton density, and the first term refers to the exchange term while the second to the direct one. By using (2.7) the expectation value of the total energy can be calculated as

$$\begin{aligned} E &= h \; j\hat{T} + V j \; i = \\ &= \sum_{Z^i} \frac{h^2}{2m} h i j \, r_i^2 j i i + \frac{1}{2} \sum_{i \neq j} h i j j v_{ij}(1;2) j i j \, i_{AS} \\ &= \; d^3 r H(\mathbf{r}) \end{aligned} \tag{2.13}$$

where in (2.13) the potential term $v_{ij}(1;2)$ includes the two-body force (2.9), the three-body term converted to a two-body one (2.11).

For the Skyrme interaction the energy density $H(\mathbf{r})$ depends locally on the nucleon density, the kinetic energy and the spin density, respectively listed below:

$$\begin{aligned} _q(\mathbf{r}) &= \sum_{i;} j \, '_i(\mathbf{r};\;;q) j^2 \\ K_q(\mathbf{r}) &= \sum_{i;} j \tau \, '_i(\mathbf{r};\;;q) j^2 \\ J_q &= (\; i) \sum_{i;\;;\;0} \, '^{*}_i(\mathbf{r};\;;q) \; \tau \, '_i(\mathbf{r};\;';q) \quad h \; 'j \sim j \; i \end{aligned} \tag{2.14}$$

where the q to the subscript indicates the charge of the single particle $'_i$, that is whether the density refers to protons ($q \quad p$) or neutrons ($q \quad n$). These quantities depend on the single particle states defining the Slater determinant. The kinetic energy density $K_q(\mathbf{r})$ is usually marked by the symbol $_q(\mathbf{r})$. Since the symbol in this work indicated the isospin operators (see next chapter); so, in order to avoid overlapping in the notation, for kinetic energy density $K_q(\mathbf{r})$ has been used. The sums is equations (2.14) are taken over all occupied single-particle states. The expression for $H(\mathbf{r})$ is explicitly derived in the appendix of [58] for the case of even-even nuclei, which has the advantage of the fact that if a single particle state is occupied, also its time-reversed state is occupied, and as a consequence the expectation value of operators as $\sim_1 \; \sim$ is zero. The density functional $H(\mathbf{r})$ can be split into the sum of terms associated to the different part of the force [19]:

$$H = K + H_0 + H_3 + H_{eff} + H_{fin} + H_{so} + H_{sg} + H_c \tag{2.15}$$

where K is the kinetic term, H_0 is the central term, H_3 is the three-body term, H_{eff} is an effective mass term, H_{fin} is a finite range term, H_{so} is the spin-orbit term, H_{sg} is a term due to the tensor coupling with spin and gradient and H_c is the Coulomb term. Some of the terms in (2.15) are specified below to give to the reader an idea of how their shape is:

$$H_0(\mathbf{r}) = \frac{1}{4} t_0 \;\; (2 + x_0) \;\; ^2(\mathbf{r}) \quad\; (2x_0 + 1) \quad _n^2(\mathbf{r}) + \; _p^2(\mathbf{r})$$

$$H_3(\mathbf{r}) = \frac{1}{24} t_3 \quad (\mathbf{r}) \;\; (2 + x_3) \;\; ^2(\mathbf{r}) \quad\; (2x_3 + 1) \quad _n^2(\mathbf{r}) + \; _p^2(\mathbf{r})$$

$$H_c(\mathbf{r}) = \frac{1}{2} \int d^3 r V_c(\mathbf{r}) \;\; _p(\mathbf{r})$$

all the other terms of (2.15) are listed in [19]. Total density is defined as $(\mathbf{r}) = {}_p(\mathbf{r}) + {}_n(\mathbf{r})$, where ${}_p(\mathbf{r})$ and ${}_n(\mathbf{r})$ are respectively the proton and the neutron densities in (2.14), and the same as regards kinetic energy and spin density.

In order to solve the HF equations, one has to apply the variational principle (2.4). Using the explicit expression (2.15) for $H(\mathbf{r})$, one obtains that the single-particle wave functions and their corresponding energies has to satisfy the following self-consistent equation [19, 58]:

$$\hat{T} \quad \frac{h^2}{2m_q^*(\mathbf{r})}\hat{T} + U_q(\mathbf{r}) + \hat{W}_q(\mathbf{r}) \quad (\quad i)(\hat{T} \quad \sim) \quad '_i(\mathbf{r}) = e_i '_i(\mathbf{r}) \tag{2.16}$$

where the q stands for the charge of the single-particle state, that means $q \quad p$ for protons and $q \quad n$ for neutrons. The equation (2.16) has the form of a local Schrödinger equation and its prove can be found in the appendix of [58]. The effective mass $m_q^*(\mathbf{r})$ is part of the energy density functional and depends on the density only [19, 58]. $U_q(\mathbf{r})$ represent the nuclear mean potential and it depends on the density and the kinetic energy density. $\hat{W}_q(\mathbf{r})$ is the spin-orbit potential. In reference to the dependence of H on these quantities and densities, their definition is given by the following variations on $H(\mathbf{r})$ [11, 58]:

$$\frac{h^2}{2m_q^*(\mathbf{r})} = \frac{H(\mathbf{r})}{\mathrm{K}_q(\mathbf{r})}; \qquad U_q(\mathbf{r}) = \frac{H(\mathbf{r})}{{}_q(\mathbf{r})}; \qquad \hat{W}_q(\mathbf{r}) = \frac{H(\mathbf{r})}{\mathfrak{J}(\mathbf{r})} \tag{2.17}$$

In this way the contribution of the "density-depending" terms of the energy density to the mean fields can be analytically calculated. The exchange term in (2.5) is now local and is included in the mean-field potential $U_q(\mathbf{r})$, so that equation (2.16) is a pure differential equation.

In conclusion the Hartree-Fock method provides a tool for calculating the average potential from an effective nucleon interaction. It becomes very important to use density effective interaction to get quantitative agreement with experimental results [11, 44]. In this case the method is able to reproduce very well the ground-state binding energies and the charge radii of spherical nuclei. Vautherin and Brink [58] in 1972 solved the HF equation (2.16) for the spherical closed shell nuclei ^{16}O, ^{40}Ca, ^{48}Ca, ^{90}Zr and ^{208}Pb and were able to adjust six parameters t_0, t_1, t_2, t_3, x_0 and W_0 in equations (2.9) and (2.11). In order to reproduce the ground-state binding energies and radii of these nuclei, they presented two sets of coefficients, that they grouped in the forces Skyrme I and Skyme II) which gave a good description of these closed shell nuclei [58]. These set of parameters have large values of t_3, which means a strong density dependence. Later, in 1975, Beiner et al. [9] proposed two other sets of force parameters (Skyrme III and Skyrme IV), with slightly different values of t_3. Skyrme III [9, 44] gives reasonable values for binding energies per nucleon and a little less reasonable as regards charge radii; it's all summed up in table 2.1.

Nuclide	Experiment E=A [44]	Skyrme III E=A [9]	Experiment r_{ch} [44]	Skyrme III r_{ch} [9]
^{16}O	-7.98	-7.96	2.73	2.69
^{40}Ca	-8.55	-8.54	3.49	3.48
^{48}Ca	-8.67	-8.71	3.48	3.53
^{90}Zr	-8.71	-8.71	4.23	4.32
^{208}Pb	-7.87	-7.87	5.50	5.57

Table 2.1: Experimental and calculated binding energies per nucleon (in [MeV]) and root mean square charge radii (in [fm]).

Up to now, many other set of parameters for an effective Skyrme force has been proposed. Their analytical simplicity allows a determination of their parameters which incorporates basic physical properties such as the saturation of infinite nuclear matter, binding energies of some nuclei and other simple nuclear experimental results or informations [18, 19]. The measurements of the giant monopole resonances gave the foundations for the proposal of the set SkM, an example of a Skyrme interaction tailored to account for these resonances [34]. However, large deformations were not correctly reproduced with SkM. From SkM, with a slight adjustment of the parameters which was intended to improve the surface tension SkM, Bartel et. al. proposed SkM* [8]. Chabanat et. al. [18, 19] proposed other set of Skyrme parameters, that are SLy4, SLy5, SLy6, SLy7. Sly4 for example, was proposed as a good candidate to describe spectroscopic properties of nuclei from the stability line to the drip lines. The other sets were proposed to be used when the spin-gradients, the two-body center of mass correction term, or both are included in the Skyrme functional [18, 19].

A modern Skyrme set parameters that has been recently proposed is SAMi [45]. SAMi is a non relativistic functional of the Skyrme type that includes the central tensor terms (J^2 term) and two spin-orbit parameters. The new functional is as accurate as previous Skyrme models in the description of uniform nuclear matter properties around saturation and of masses and charge radii of doubly magic nuclei. It is also precise in the description of the giant monopole resonance (GMR) and giant dipole resonance (GDR) in ^{208}Pb, and the GTR, isobaric analog resonance (IAR), and spin dipole resonance (SDR) in medium and heavy mass nuclei [45].

2.2 Pairing Correlations and Models

The last section has concluded that Hartree-Fock theory, supported by an appropriate effective interaction, is a good way to reproduce well the binding energies of nuclear ground-state. However, this is true only for magic isotopes. Up to now, in the HF method, one has to consider the short-range part of the of the force which causes particle-particle correlations [44]. These particle-particle (or pairing) correlations allow to understand some effects which can not be explained within a pure HF picture.

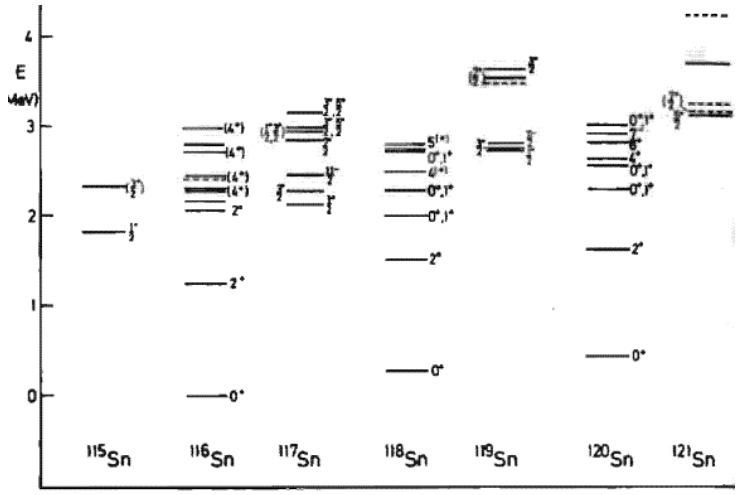

Figure 2.1: Excitation spectra of the $_{50}$Sn isotopes [44].

The main experimental evidences which lead to the idea of pairing correlations are scheduled below:

The trend of the binding energies The last term of the semi-empirical mass formula (1.2) includes a pairing term that is negative for even-even nuclei, null for odd nuclei and odd-odd nuclei. This fact should introduce the idea that nucleons of the same species tend to form pairs;

Odd-even effect The total binding energy of a odd-even nucleus is found to be smaller that the arithmetic mean of the binding energies related to its neighbour nuclei $A-1$ and $A+1$, that is [44]:

$$BE(A_{odd}) < \frac{BE(A-1) + BE(A+1)}{2}$$

The energy gap In reference to the figure 2.1, the excitation spectrum of even-even open-shell nuclei shows a gap of about 1-2 MeV between the ground state and the first excited state. For odd nuclei the spectrum is different: it shows many excited states in the same energy interval;

The moments of inertia of deformed nuclei can be measured from the level structure of rotational bands. Calculations based on the pure HF single-particle model deviate from the experimental values. If pairing is included, theory predictions and experiment results are in much better agreement.

Given the existence of all these experimental evidences, it can be understood that the pairing correlations are important and therefore the pairing term was added to the mass semi-empirical formula (1.2).

Göpper and Mayer [14, 38] proved that for short-ranged, attractive and two-body forces the coupling of two nucleons in a shell of given total angular momentum j in a pair with total angular momentum zero ($J = 0$) is energetically favored over all the other possible couplings. Two nucleons can make a pair the same shell when the relative third components of angular momentum have opposite sign. Without considering spin, a $J = 0$ couple can be formed and can be mathematically expressed as:

$$\begin{aligned} |J=0; M=0\rangle &= \sum_{m_1 m_2} \langle jm_1 jm_2 | j0 0 | jm_1 ij jm_2 i = \\ &= \sum_{m} \langle jmj \quad mj0 0 | jj m ij j \quad mi \end{aligned} \tag{2.18}$$

where the first term in (2.18) are the Clebsch-Gordan coefficients [16], which vanish if $m_1 + m_2 \neq M$ ($M = 0$ in this case). Because of the behaviour of angular momentum under the effect of the time-reversal operator, the two states m and $-m$ can be considered time-reversed states, that reads:

$$\hat{T}|jmi = (-1)^{j+m}|j \quad mi = |j-mi$$

where in the last equation $\hat{T}$ indicates the time-reversal operator.

For even-even nuclei between closed shells, the energetically most favored configuration is the one in which all the nucleons are coupled. In order to excite these nuclei to the first excited state, one has to break at least the last pair and the binding energy of a pair is about 1-2 MeV. In the case of odd nuclei, all the nucleon are coupled except the last one and in order to excite them, it

is sufficient to excite this last nucleon and the needed energy is less than 1-2 MeV. So in this way qualitatively one can explain the level scheme in figure 2.1.

Furthermore the presence of $J = 0$ pairs favors a spherical nuclear intrinsic shape. Nuclei in the neighbourhood of closed shell have still spherical symmetry, since the influence of the pairing force overcomes the tendency to deform [44].

2.2.1 The BCS Theory

The pairing gap in the excitation spectrum is similar to that happens in the semiconductors. Consequently the same BCS theory that describes the features of the semiconductors can be used in atomic nuclei. In this sense, since the pairing involves either protons and neutrons, one can speak of nuclear superfluidity. This theory make use of the second quantisation formalism.

The BCS theory starts defining the ground-state wave function. It makes an ansatz in which the terms of the wave functions correspond to pairs of nucleons in time-reversed states, that is

$$|BCS\rangle = \prod_{k>0} u_k + v_k a_k^\dagger a_{\bar{k}}^\dagger \; |\rangle \tag{2.19}$$

where k, replaces $|jm\rangle$ in a contract form, $k > 0$ labels the states with positive projection of the total angular momentum , u_k and v_k are variational parameters and the $a_k^\dagger$ are creation parameters acting on the vacuum state $|\rangle$. One can note that the BCS state (2.19) generalises the pure HF state. The state HF of even-even nuclei corresponds to filled orbitals with both m and $\bar{m}$ up to the Fermi energy. It is obtained by setting in (2.19) $v_k = 1$ and $u_k = 0$, vice-versa otherwise.

The Hamiltonian in second quantisation is written as

$$H = \sum_{k_1 k_2} \langle k_1|\hat{t}|k_2\rangle a_{k_1}^\dagger a_{k_2} + \frac{1}{4} \sum_{k_1 k_2 k_3 k_4} \langle k_1 k_2|\hat{v}|k_3 k_4\rangle a_{k_1}^\dagger a_{k_2}^\dagger a_{k_4} a_{k_4} = T + V \tag{2.20}$$

The BCS equations are derived from the variational principle. Since the BCS wave functions mix states with different particle number, in order to ascertain that such number be conserved, one should impose the variational principle to the following quantity:

$$\langle BCS|H \quad N|BCS\rangle = 0; \qquad \text{where} \qquad = \frac{@}{@N}\langle BCS|H|BCS\rangle \tag{2.21}$$

and v_k is the parameter that will be varied. In (2.21) represents the Fermi energy, or the energy that is necessary to add or remove a particle. First of all, in order to be sure that the BCS state are normalised. For this purpose one must require that $u_k^2 + v_k^2 = 1$ and this is valid for each k. Under these considerations u_k is the probability amplitude that the state k is empty, while v_k that it is filled. In other words v_k^2 is the BCS occupation probability of the state k. Now one has to calculate the expectation values before doing the minimisation (2.21):

$$\begin{aligned}\langle BCS|T + V \quad N|BCS\rangle = & \sum_k (t_{kk} \quad) v_k^2 \\ & + \frac{1}{2}\sum_{kk'} \hat{v}_{kk'kk'} v_k^2 v_{k'}^2 + \sum_{kk'>0} \hat{v}_{k\bar{k}k'\bar{k}'} u_k v_k u_{k'} v_{k'}\end{aligned} \tag{2.22}$$

where in (2.22) the definition of number operator has been used: $\hat{N} = \sum_k a_k^\dagger a_k$ and a contracted notation for the matrix elements has been used ($\langle k_1|\hat{t}|k_2\rangle = t_{kk}$) and from now on this notation will

be used, until the end of this section. Once done the minimisation (2.21) by using as variational paramiter v_k and taking care that $u_k = \sqrt{1 - v_k^2}$, one can build a closed system of six equations, composed by (for the details about the calculations see [44]):

$$N = \sum_k v_k^2 = 2 \sum_{k>0} v_k^2 \tag{2.23}$$

$$\tilde{\varepsilon}_k = \frac{1}{2}\left[(t_{kk} + t_{\bar{k}\bar{k}}) - 2\lambda + \sum_{k'} (\tilde{v}_{kk'kk'} + \tilde{v}_{\bar{k}k'\bar{k}k'}) v_{k'}^2\right] \tag{2.24}$$

$$E_k = \sqrt{\tilde{\varepsilon}_k^2 + \Delta_k^2} \tag{2.25}$$

$$v_k^2 = \frac{1}{2}\left(1 - \frac{\tilde{\varepsilon}_k}{2E_k}\right) \tag{2.26}$$

$$u_k^2 = \frac{1}{2}\left(1 + \frac{\tilde{\varepsilon}_k}{2E_k}\right) \tag{2.27}$$

$$\Delta_k = \sum_{k'>0} \frac{\Delta_{k'}}{2E_{k'}} \tilde{v}_{k\bar{k}k'\bar{k}'} \tag{2.28}$$

An interpretation of the quantities introduced in the equations from (2.23) to (2.28) is reported below:

The number equation (2.23) expresses the fact that in average, the particle number is conserved;

Equation (2.24) expresses the single-particle energy less the Fermi energy;

The quasi-particle energy (2.25) in the HF limit ($\Delta_k = 0$) reduces to $\tilde{\varepsilon}_k$. In a most general case, in order to add a nucleon to the system the minimum energy needed is greater than Δ_k. This is the situation as regards even nuclei, which present a gap the spectrum that is Δ_k. The case of a odd nucleus is different: the last nucleon is added on the top of the wave function, but it can't make a pair. So its energy can be very small respect to the Fermi level, and the odd system does not display any gap.

The gap equation (2.28) establishes whether the system has a simple solution (pure HF), or a super fluid solution, that is a solution that involves a non null gap $\Delta_k = 0$.

Let us consider a state close to the Fermi level and see what's the behaviour of the relative gap Δ_k [44]. In this case the contributions to the sum in (2.28) come from the states near the Fermi level. This is due to the fact that the term $\frac{\Delta_{k'}}{2E_{k'}} \simeq 1$ because $\tilde{\varepsilon}_{k'} \simeq 0$ and the matrix elements $\tilde{v}_{k\bar{k}k'\bar{k}'}$ for $k \simeq k'$ are larger than the other matrix elements because k and k' belong to similar quantum numbers. In the opposite situation, when one considers a state far from the Fermi level, all the terms in (2.28) are small. More precisely, the matrix elements of the potential with $k \simeq k'$ are large, but now the factor $\frac{\Delta_{k'}}{2E_{k'}} \simeq 0$ because $\tilde{\varepsilon}^2_{k'} \gg \Delta^2_{k'}$. The effect of the pairing force is therefore restricted to the neighborhood of the Fermi level, that is only when $\Delta_k \neq 0$.

2.2.2 The Hartree-Fock-Bogolyubov Method

The Hartree-Fock-Bogolyubov (HFB) theory [44] generalises and uni es the simple HF method and the BCS model. Within this theory the wave functions related to independently moving quasi-particles will be calculated. The base of this method is still the variational principle and it takes into account as many correlations as possible within a single-particle picture. It turns out that, in this approximation, the Hamiltonian reduces to two average potentials: a self consistent eld, which is known from the pure HF theory and the additional pairing potential, known from the BCS model.

The basic idea of any quasi-particle concept is to represent the ground-state of a nucleus as a vacuum with respect to quasi-particles, which are de ned by the low-lying excitations of neighboring nuclei. This is what Landau and Migdal, who de ned in their works [35] the vacuum and the quasi-particles in terms of exact eigenstates of many-body systems. A quasi-particle operator is a linear trasformation from the creation and annihilation $c_l^y; c_l$ to $_k^y$, $_k$:

$$_k^y = \sum_l U_{lk} c_l^y + V_{lk} c_l \tag{2.29}$$

where the indices $k; l = 1; : : : ; M$ run over the whole con guration space. The hermitian conjugate of (2.29) gives the operator $_k$ and U_{lk} and V_{lk} are two transofrmation matrices. The two transformations are writable as a matrix product

$$_y = \begin{pmatrix} U^y & V^y \\ V^T & U^T \end{pmatrix} \begin{pmatrix} c \\ c^y \end{pmatrix} = W^y \begin{pmatrix} c \\ c^y \end{pmatrix}; \qquad W = \begin{pmatrix} U & V \\ V & U \end{pmatrix} \tag{2.30}$$

where the standard notation on the matrices has been used, that is U^T indicates the transposed matrix, U indicates the complex conjugated matrix and U^y indicates the combination of the rst two operations. The coe cients $U; V$ are not completely arbitrary; in fact the operators $_k^y$, $_k$ must anti-commutate. This restricts W to be unitary.

The ground-state of a many-body system $j\ i$ with respect to the quasi-particles, that is for each $k = 1; : : : ; M$:

$$_k j\ i = 0 \tag{2.31}$$

Wave functions which satisfy the previous condition for a corresponding set of quasi-particle operators (2.29) and will, in the following will be called the HFB wave functions. One can show that this de nition of wave function is always possible and unique [44]. In this discussion the HFB wave function (2.31) can be written as [5, 44]

$$j\ i = \prod_i a_i^y \prod_p u_p + v_p a_p^y a_{\bar{p}}^y\ j\ i \tag{2.32}$$

Depending on whether the number of occupied levels is is odd or even, the wave function (2.32) is a superposition of states with odd or even particle number. In this situation i is called number parity and a wave function $j\ i$ with even i will describe only system with even particle number and vice-versa. Dependent on the coe cients U and V in the Bogolyubov transformations (2.29), which completely de ne the wave function, one gets even or odd parity number. These coe cients are determined by a variation of the energy expectation value, according to the HFB equations de ned below. They are non-linear equations and the solution with the lowest energy provides the coe cients $U; V$ with which the corresponding vacuum $j\ i$ describes the ground-state.

Before describing the HFB equations, two new de nitions are here introduced. Their usefulness is to uniquely determine the wave funtion $|\Psi\rangle$, once introduced in the HFB equations. They are the normal density and the abnormal density, respectively:

$$\begin{aligned} \rho_{\mu\mu'} &= \langle\Psi|c^{\dagger}_{\mu'}c_{\mu}|\Psi\rangle; & \kappa_{\mu\mu'} &= \langle\Psi|c_{\mu'}c_{\mu}|\Psi\rangle \\ &= V^{*}V^{T}; & &= V^{*}U^{T} = -UV^{\dagger} \end{aligned} \tag{2.33}$$

ρ is herimitian $\rho = \rho^{\dagger}$, while κ is anti-symmetric $\kappa^{T} = -\kappa$, and these matrix can be Bloch-Messiah decomposed [13]. By following the unitary rules of the $\mathcal{R}_k$ and (2.33), one can demonstrate that ρ and κ are linked by these relations:

$$\rho^{2} = \rho^{\dagger}; \qquad \rho = 1 - \rho^{*} \tag{2.34}$$

By assuming that $|\Psi\rangle$ is an approximation for the exact ground-state of the Hamiltonian [44]:

$$H = \sum_{\mu_1\mu_2} t_{\mu_1\mu_2} c^{\dagger}_{\mu_1} c_{\mu_2} + \frac{1}{4} \sum_{\mu_1\mu_2\mu_3\mu_4} \bar{v}_{\mu_1\mu_2\mu_3\mu_4} c^{\dagger}_{\mu_1} c^{\dagger}_{\mu_2} c_{\mu_4} c_{\mu_3} \tag{2.35}$$

that is similar to (2.20), but in this situation the trial wave functions are the set of generalised product states $|\Psi\rangle$ of the HFB type. As in the BCS model, the HFB wave function violate the symmetry connected to the particle number; so one has to impose a constraint on the particle number and vary the new Hamiltonian $H' = H - \lambda N$. Since one has to investigate small variations $|\delta\Psi\rangle$ neighbor to the solution $|\Psi\rangle$, one can use the theorem of Thouless [57] to express the wave function $|\Psi'\rangle = |\Psi\rangle + |\delta\Psi\rangle$ as [44, 57]

$$|\Psi'\rangle = \exp\left(\sum_{k<k'} Z_{kk'} \, \beta^{\dagger}_{k} \beta^{\dagger}_{k'} \right) |\Psi\rangle \tag{2.36}$$

Written in these terms, $|\Psi'\rangle$ is not orthogonal to $|\Psi\rangle$. The solution $|\Psi\rangle$ of a variational equation

$$\frac{\langle\Psi|H|\Psi\rangle}{\langle\Psi|\Psi\rangle} = 0 \tag{2.37}$$

with the Hamiltonian given by (2.35), corresponds to $Z_{kk'} = 0$. After the variation with respect to $Z_{kk'}$ yields [10, 44]

$$\frac{\partial}{\partial Z_{kk'}} \frac{\langle\Psi'|H|\Psi'\rangle}{\langle\Psi'|\Psi'\rangle}_{Z=0} = 0 \tag{2.38}$$

and many considerations listed in [44], one obtains the so called HFB equations [6, 7, 44]:

$$\begin{pmatrix} h & \Delta \\ -\Delta & -h \end{pmatrix} \begin{pmatrix} U_k \\ V_k \end{pmatrix} = \begin{pmatrix} U_k \\ V_k \end{pmatrix} E_k \tag{2.39}$$

where the columns U_k and V_k of the matrices U and V determine the quasi-particle operators (2.29); and the terms in equation (2.39) are here explained [44]:

$$h = t + \Gamma; \qquad \Gamma_{\mu\mu'} = \sum_{\nu\nu'} \bar{v}_{\mu\nu\mu'\nu'} \rho_{\nu\nu'}; \qquad \Delta_{\mu\mu'} = \frac{1}{2} \sum_{\nu\nu'} \bar{v}_{\mu\mu'\nu\nu'} \kappa_{\nu\nu'} \tag{2.40}$$

represents the self consistent potential while represents the pairing eld. is the Fermi energy and it is determined by the particle number Tr = N .

The HFB equations (2.39) are a 2M dimensional set of non-linear equations and can be solved for protons and neutrons separately. These equations contain the Fermi energy which has to be determined by the particle number and allow to constrain the variational equation. The HFB equations contain two potentials and ; in particualar corresponds to the HF potential, which describes the sharp of the nucleus (spherical or deformed), whereas determines the pairing correlations. Unlike the BCS case, in equation (2.40) is no longer given by a number $_k$ as in equation (2.28), but it is now a matrix which mixes di erent levels. If the solution corresponds to the absolute minimum in the surface energy (see section 7.3.3 in [44]), it depends on how one solves these equations, and in particular on the initial conditions of the iterative solution. The HFB equations in principle can be used for the self-consistent approximation of all eigenstates of H whose wave functions have the structure of generalised products. In an actual solution by iterative diagonalisation of (2.39), one encounters that the equations have 2M -dimensional eigenvalues and eigenvectors. In order to construct a set of quasi-particle operators (2.29) and for the calculations of and in (2.33), one chooses M of them. However, to each eigenvector $\begin{matrix} U_k \\ V_k \end{matrix}$ with eigenvalue E_k there corresponds an eigenvector $\begin{matrix} U_k \\ V_k \end{matrix}$ with eigenvalue E_k. It is not possible to choose both E_k and E_k at the same time, otherwise it is impossible to ful ll the commutation rules for the quasi-particle operators. Therefore, one has to decide for each k whether one takes the eigenvalue E_k with its eigenvector or E_k with its eigenvector [44].

Chapter 3

Isospin Symmetry in Nuclei

An important characteristic of nuclear structure is associated with the presence of the two-kinds of nucleons, the neutron and the proton. The near equality of the mass of these two particle should suggest a deep similarity, and the more detailed study of their role in nuclear processes has revealed a basic symmetry between neutrons and protons in all nuclear interactions. The existence of a general symmetry betweenmp, nn and pp interactions is born out by the comparison of the spectra of di erent isobars [14]. The only explicit violation of this symmetry is the Coulomb interaction, but in principle, isobaric nuclei have the same energy. Charge independence of nuclear forces leads to the introduction of a new conserved quantum number, isospin. There also exist experimental evidences in the nucleon-nucleonNN scattering data [2, 14] that prove that the nuclear forces contain not only isospin-invariant terms; but also small isospin symmetry-breaking (ISB) components [39, 40]. In this chapter the concepts of isospin and charge-dependent forces are introduced. In particular it will be seen how the e ect of the ISB forces has been studied in literature and how will be studied in this work.

3.1 Isospin Formalism

3.1.1 Generalities on Isospin

Up to now protons and neutrons have been always considered separately. Apart from the electromagnetic interaction, protons and neutrons have practically the same physical properties. The NN interaction are in general independent of whether one considers protons or neutrons. As long as one neglects the in uence of the Coulomb interaction, the proton and the neutron can be considered as just two di erent manifestations of the same particle. This concept is very similar to the spin. Instead of a quantum number indicating whether a nucleon is up or down, this new quantum number indicates whether the nucleon is a proton or a neutron and it is called*isospin*. The operator related to this quantum number $\hat{t}$ has the same features of spin operators, but it doesn't act either on ordinary coordinate space or in spin space. This quantum number, usually indicated as$t$, assumes only the two possible value related to the state that mean neutron or proton. In general for a single nucleon$t = \frac{1}{2}$ but its third component assumes the values of $\frac{1}{2}$:

$$\hat{t}_z|n\rangle = +\frac{1}{2}|n\rangle \qquad \hat{t}_z|p\rangle = -\frac{1}{2}|p\rangle \tag{3.1}$$

Like ordinary spin, the isospin vector operator is formed out of its three cartesian components $\hat{\vec{t}} = (\hat{t}_x, \hat{t}_y, \hat{t}_z)$. One can also express the operators related to isospin in terms of the Pauli matrices:

$$\hat{\tau}_x = \begin{matrix} 0 & 1 \\ 1 & 0 \end{matrix} \qquad \hat{\tau}_y = \begin{matrix} 0 & -i \\ i & 0 \end{matrix} \qquad \hat{\tau}_z = \begin{matrix} 1 & 0 \\ 0 & -1 \end{matrix} \tag{3.2}$$

together with the commutation rule $[\hat{\tau}_i, \hat{\tau}_j] = 2i\varepsilon_{ijk}\hat{\tau}_k$, one has $\hat{\tau}_i = 2\hat{t}_i$. The isospin operators $\hat{t}^2$ and $\hat{t}_z$ obey to the eigenvalue equations

$$\hat{t}^2 |t, t_z\rangle = t(t+1)|t, t_z\rangle \qquad \hat{t}_z |t, t_z\rangle = t_z |t, t_z\rangle$$

The charge of the nucleon represented by the state $|t, t_z\rangle$ is then given by

$$q = e\left(\frac{1}{2} - t_z\right) \tag{3.3}$$

The allowed values of t and t_z are the same as for spin eigenvalues; i.e. t can assume either integer or half-integer value, while t_z can assume $(2t+1)$ values between $-t$ to t. In this notation of isospin formalism, the components t_x and t_y are not directly connected to physical observables. However, their linear combinations

$$\hat{t}_\pm = \hat{t}_x \pm i\hat{t}_y$$

have a physical meaning: applied to the state $|t, t_z\rangle$, $\hat{t}_+$ raises and $\hat{t}_-$ lowers the value of the third component by a unity. The operation follows this rule (for a $t = \frac{1}{2}$ particle) [30]:

$$\hat{t}_- |t, t_z\rangle = \sqrt{(t - t_z)(t - t_z + 1)}\; |t, t_z - 1\rangle \tag{3.4}$$

In summary the lowering and the raising operators $\hat{t}_\pm$ change a the neutron into a proton and vice versa.

3.1.2 Isospin in Nuclei

A nucleus with A nucleons, Z protons and N neutrons has total charge Ze, that can be written as

$$Ze = \sum_{i=1}^{A} q_i = e\left(\frac{A}{2} - T_z\right) \tag{3.5}$$

where the third component of the total isospin is obtained by summing over all the single third components of isospin of the nucleons; the same thing for total isospin $\vec{T}$ holds:

$$\vec{T} = \sum_{i=1}^{A} \vec{t}_i; \qquad \hat{T}_z = \sum_{i=1}^{A} \hat{t}_{z;i}; \qquad T_z = \frac{N - Z}{2} \tag{3.6}$$

Since T_z is a component of $\vec{T}$, the values of T must satisfy the interval

$$\frac{|N - Z|}{2} \leq T \leq \frac{A}{2}$$

The previous equation shows that T is integer if A is even, otherwise it is half-integer. The isospin state are $(2T+1)$-fold degenerate.

Isospin Invariance

At the dawn of nuclear physics the similarity between the neutron-neutron (nn), proton-proton (pp) and neutron-proton (np) nuclear forces, commonly known as their charge independence, has lead to the concept of the isospin symmetry. In this overall picture the NN interaction do not distinguish between proton and neutron. As long as only the NN interaction is present, the isospin vector $\vec{T}$ can point in any direction. In other words there exists rotational invariance in the isospin space [30]:

$$[H_{NN}, \vec{T}] = 0 \tag{3.7}$$

where H_{NN} is the pure NN Hamiltonian (Coulomb interaction excluded). In this situation, as already mentioned the $(2T + 1)$ states of a multiplet with different values T_z are degenerate and have the same total energy. It is important to stress that $\vec{T}$ is a vector in the isospin space, not in ordinary space. The electromagnetic interaction breaks the isotropy of the isospin space:

$$[H_{NN} + H_{em}, \vec{T}] \neq 0 \tag{3.8}$$

where H_{em} is the Hamiltonian related to the electromagnetic interaction. In any case a quantity that is always conserved is the electric charge, and it depends on T_z because of (3.5). In this sense the third component of isospin is conserved in the presence of electromagnetic interaction [30]:

$$[H_h + H_{em}, \hat{T}_z] = 0 \tag{3.9}$$

In conclusion, since electromagnetic interaction, Coulomb interaction in particular, distinguishes between protons and neutrons; so it is a source of isospin symmetry-breaking [30, 62]. In general, Coulomb interaction is treated on the mean-field level, in nuclear density functional theory (DFT), see next sections for details.

Isobaric Analogue States

All the members of an isospin multiplet are expected to have the same quantum numbers, apart form T_z and the electric charge. In other words, by excluding electromagnetic interactions, all the nuclei of the same multiplet have the same binding energy. If the electromagnetic interaction is switched on, the degeneracy of the $(2T + 1)$-state is broken, as indicated in figure 3.1. Each of the substates is characterized by a unique value of T_z.

The strong interaction is, with good approximation, charge-symmetric and charge-independent [36]. Charge-symmetric means that the interaction between two protons is identical to that between neutrons ($V_{pp} = V_{nn}$), while charge-independent means $V_{pp} + V_{nn} = 2V_{np}$. Without considering the electromagnetic interaction, the concepts of charge symmetry and independence can result in identical behavior of two nuclei with the same total number of nucleons (isobaric nuclei), but with different numbers of neutrons and protons. Of course, the Pauli Principle puts obvious constraints on the available configurations and hence on the range of the symmetries observed. Isospin thus becomes a good quantum number to characterize analogue states in isobaric multiplets [61]. These states are termed *isobaric analogue states* (IAS) [30, 62, 61]. Energy differences between IAS are due to isospin non-conserving forces.

(a) (b)

Figure 3.1: Effect of electromagnetic interaction on the isospin multiplet T (in both the figures indicated as I, whereas T_z is indicated as I_3.). Panel (a) shows how electromagnetic interaction breaks the $(2T+1)$-fold degenerate state. Panel (b) reports the specific example of the effect of electromagnetic interaction on the $A = 7$ isospin doublet. It lifts and breaks the degenerate state into two sub-states [30].

An interesting couple of the constituents of the same isospin multiplet are the *mirror nuclei*, which consist in nuclei with the same mass number A, but Z and N are interchanged, that means ${}^{A}_{Z}X^{N} \$ {}^{A}_{N}Y^{Z}$. These nuclei are also characterised by the opposite sign of third component of total isospin: $T_z = \ T$. Examples of mirror nuclei are ${}^{30}_{14}Si^{16}$-${}^{30}_{16}S^{14}$ or ${}^{34}_{16}S^{18}$-${}^{34}_{18}Ar^{16}$. The electromagnetic force produces an energy difference between members of an isospin multiplet, that is for isobars $(A;Z)$ and $(A;Z+1)$

$$E = E(A;Z+1) \quad E(A;Z) ' \quad E_{Coul} \quad (m_n \quad m_p) \tag{3.10}$$

The energies refers to the neutral atoms and include the electrons; it is graphically showed in figure 3.1 panel(b). The simplest way to estimate the Coulomb energy, as already mentioned, is by assuming that the charge Ze has a spherical distribution.

Let us consider some example. Isospin singlets $(T = 0)$ can appear only in nuclides with $N = Z$. Examples are ${}^{2}H$, ${}^{2}He$, ${}^{6}Li$, ${}^{8}Be$, ${}^{12}Ca$, ${}^{14}N$ and all have ground-state characterised by $T = 0$ [30, 14]. Isospin doublets are found in mirror nuclides with odd A for which $Z = \frac{A\ 1}{2}$. An example of mirror doublet is the pair ${}^{7}Li$ and ${}^{7}Be$; they have ground-state and the first-excited state with $T = \frac{1}{2}$ [30]. A total isospin $T = 1$ can have three projection on $T_z = 0;\ \ 1$ and these three states make up a isospin triplet.

The easiest way to study the isospin multiplets is by considering a very simple system. It consists of a system formed by two nucleons: nn, pp and np. In this case, T_z can be $0;\ \ 1$ and so the value of T is restricted to 0 and 1. For the charge-independence of the NN interaction, any state that can be constructed in the pp or nn system must also exist in the np system. However, the inverse statement cannot be made. That is, there are some states in the np system that are forbidden by the Pauli principle in the pp and nn system composed by identical particles. The ground state of the deuteron np with $J = 1^+$ is such a state and, therefore, must have $T = 0$ as the isospin projection is limited only to $T_z = 0$. Similarly, any state in the nn system (and its equivalent state in pp) must have $T = 1$ as the projection is (1 for pp). However, as a $T = 1$ state can have a $T_z = 0$ projection, this state must also exist in the np system. Thus, there are three identically-constructed $T = 1$ states which can be found in the nn, np and pp systems (i.e. with $T_z = 0;\ \ 1$ respectively). These states form an isospin triplet, and the lowest $J = 0^+$ states

in these three two-nucleon systems form such a triplet. All three of these states are unbound. This argument can be extended to states in many-particle systems, where it is also useful to remember that, in general, the lowest energy states (e.g. the ground state) of a nucleus will have the lowest available value of isospin.

Figure 3.2: Level structure in the $A = 22$ isospin triplet [36].

Figure 3.2 shows the isobaric triplet of mass $A = 22$ formed by the odd-odd $N = Z$ nucleus ^{22}Na and the two mirrors ^{22}Mg ($Z = 12$) and ^{22}Ne ($Z = 10$). The ground state of ^{22}Na is a $T = 0$ state, but the spin and parity are $J = 3^+$. The first $T = 1$, $J = 0^+$ state lies at 693 keV excitation energy and is the isobaric analogue state of the ground states of ^{22}Mg and ^{22}Ne. Due to the Pauli Principle, isospin symmetry breaking in mirror nuclei the $N = Z$ nucleus has more excited states than the other members of the triplet. The small differences between the excited states are a consequence of the effect of the isospin breaking-terms of the interaction such as the Coulomb force. Once this effects are taken into account, the size of remaining differences constitutes a test of the charge independence of the nuclear interaction.

3.2 Isospin Symmetry-Breaking

Nucleon-nucleon (NN) scattering experiments has revealed that the NN interaction includes isospin-symmetry-breaking (ISB) components [37]. There were found that nn interaction V_{nn} is about 1% stronger than the pp interaction V_{pp}, and that the np interaction, V_{np}, is about 2.5% stronger than the average between V_{nn} and V_{pp}. These effects are called charge-symmetry breaking (CSB) and charge-independence breking (CIB), respectively [37, 40], as mentioned above.

3.2.1 Classification of Charge-Dependent NN Forces

On a fundamental level, the isospin symmetry is broken due to: (i) different masses and electromagnetic interactions of u and d quarks (the strong and electromagnetic interactions among these quarks give rise to a mass splitting among the baryonic and mesonic multiplets [3, 4]), (ii) meson mixing (in particular the ^{0} ! mixing [40]), and (iii) irreducible meson-photon exchanges [39]. The CSB force originates from the differences in mass between protons and neutrons, leading to different kinetic energies and in uencing the boson or two-boson exchange. The major cause of the CIB force is the pion mass splitting. For more details see [37, 39].

The isospin formalism o ers the following classi cation of di erent components of the nuclear forces between two nuleons by dividing them into four classes [39]:

Class I : These are isoscalar forces, they are invariant under rotations in the isospin-space, i.e. satisfy (3.7). These forces doesn't break either charge symmetry or charge independence. In general they have form

$$V_I = a + b(\tau_1 + \tau_2) \tag{3.11}$$

where a and b are isospin independent operators and 1 and 2 label two nucleons;

Class II : These are isotensor forces that break charge independence but preserve charge symmetry. They have form

$$V_{II} = c \quad {}^z_1 \, {}^z_2 \quad \frac{1}{3}\tau_1 \quad \tau_2 \tag{3.12}$$

Class III : These are isovector forces that breaks both the charge independence and are symmetric under exchange of the two interacting particles. A Class III force di erentiates between nn and pp systems, but vanishes in a np system. They have form:

$$V_{III} = d[\,{}^z_1 + \,{}^z_2] \tag{3.13}$$

Class IV : These forces break both charge independence and charge symmetry and they are anti-symmetric under exchange of the two interacting particles:

$$V_{IV} = e[\tau_1 \quad \tau_2] \quad \Gamma[\,{}^z_1 \quad {}^z_2] + f\,[\tau_1 \quad \tau_2] \quad \Gamma[\tau_1 \quad \tau_2]^z \tag{3.14}$$

In this work the e ects of the class II and III forces will be studied; in particular their e ects on total energy and charge radii will be discussed.

3.2.2 Studies on ISB E ects in Literature

Based on what has been said so far, isospin symmetry and independence lead to the conclusion that binding energy di erences between IAS are due only to electromagnetic e ects or other isospin breaking terms. In the previous section the concept of the binding energies two nuclei of the same isospin multiplet di er of a quantity roughly estimated by equation (3.10). Furthermore, experimental results [30, 39, 41] have shown that there is a di erence in energy between two contiguous isobaric analogue states. This di erence is called Coulomb Displacement Energy (CDE). In 1969 Nolen and Schi er [41] proved that by considering the only electromagnetic interaction is not su cient to describe the CDE, in fact calculations show that Coulomb energy usually contributes with about 90% to CDE. This is known as Nolen-Schi er anomaly. In order to obtain better agreement between theory and experimental results one has to include in the calculations not only Coulomb interaction but also other sources of ISB, like the forces listed above. The classi cation explained in the previous section was originally proposed by Henley and Miller [39, 40] and subsequently used in framework of potential models based on boson-exchange formalism, like Machleidt in 2000 (CD-Bonn) [37] and Wiringa et al. [63] in 2013, who applied this formalism to the study of isospin mixing in ^{8}Be. The CSB and CIB were also studied in chiral e ective eld theory [59]. The Henley and Miller's classi cation has been used within the Density Functional Theory (DFT) for example in [17, 55]. In particular in the work of Suzuki et

al. [55] in 1993 used CSB and CIB within DFT to explain the discrepancies between the CDE experimental results and theoretical ones of IAS of some magic nuclei like ^{48}Ca, ^{90}Zn and ^{208}Pb.

The most evident manifestations of the ISB is in the mirror displacement energy (MDE) de ned as the di erence between the binding energies of mirror nuclei [2]:

$$MDE = BE(T; T_z = \quad T) \quad BE(T; T_z = T) \tag{3.15}$$

The study of Nolen and Schi er [41] has showed that MDEs can not be reproduced by considering Coulomb interaction as the only source of ISB. Another source of informations about ISB e ects is the triplet displacement energy(TDE) [2]:

$$TDE = BE(T = 1; T_z = \quad 1) + BE(T = 1; T_z = 1) \quad 2BE(T = 1; T_z = 0) \tag{3.16}$$

TDE measures the binding energy curvature within the isospin triplets. In above de nitions of MDE and TDE, the binding energies are negative, and neutron and protons have the isospin projection de ned by (3.1). Baczyk et al. [2, 3, 4] has systematically studied MDE and TDE of several IAS for several mass nembers A. To this aim, in all the listed works, Baczyk's group has used a conventional mean- eld model with "generalized" Skyrme interaction (described above) which includes CSB and CIB terms and derived the corresponding energy density functional. In [3] and [4], they have been able to reproduce the experimental values of MDE and TDE for some $A = 4n$ or $A = 4n + 2$ IASs. The discrepance between experimental values and theory is, on average, 100 keV. In particular in the work [3] they focused on the numerical optimisation on the code HFODD [23, 24, 25, 50] that they have used for the calculations, that is the same used for the calculations of this work. In the study [2] they have systematically reproduced observed MDEs and TDEs of $T = \frac{1}{2}$ and $T = 1$ multiplets. They based the study [2] on the introduction of a single class II ISB term within the pn-mixed DFT [43, 48]. They showed that the characteristic staggering patterns of MDEs are related to the standard Coulomb e ects [41] which require the presence of class II ISB terms, whereas those of TDEs require that the class III ISB terms is included. Baczyk et al. [2] performed their calculation with the code HFODD, the same of this work. In summary they have shown that CSB and CIB term can be included in a Skyrme e ective force within a general DFT to reproduce well experimental data for MDEs and TDEs.

Given the scienti c literature on the e ects of ISB on binding energies, almost all the studies carried out so far have focused on quantities related to binding energies and few on charge radii. Thus, this study is focused on the study of the e ects of ISB on binding energies of some mirror nuclei and their charge radii. Given the successful results by Baczyc et al [2], [3, 4], a similar approach will be used. In particular, the mirror nuclei on which this work has focused on are ^{30}Si-^{30}S, ^{34}S-^{34}Ar, ^{50}Ti-^{50}Ni and ^{52}Cr-^{52}Ni. In this work the binding energies and radii of these pairs of nuclei is calculated with the help of the code HFODD. Since all these nuclei are open shells nuclei, the pairing e ect is included by solving the HFB equations and this is permitted by the code. Other HFB calculations have been made in the past with a Gogny e ective interaction [32]. This is the "AMEDEE" database showing the results of Hartree-Fock-Bogoliubov calculations based on a Gogny e ective nucleon-nucleon interaction. This databese considers more than 1700 nuclei within the drip lines.

3.3 Isospin Symmetry-Breaking in Hartree-Fock

The aim of this work is to study the e ect of the ISB on the nuclear masses within the nuclear DFT. To this end one builds some ISB local forces and add its terms on a complete Skyrme e ective interaction. In this work there have been used only a CSB force, that is a class III force, and the CIB force, that is a class II force. They are written as a two-body potential and are, respectively:

$$\begin{aligned} v_{CSB}(1;2) = (\ ^z_1 + \ ^z_2)\ \ (\mathbf{r}_1 \quad \mathbf{r}_2)\ \ s_0\ \ 1 + y_0 P^{12} \\ + \frac{1}{2} s_1\ \ 1 + y_1 P^{12}\ \ \ k^2 + k'^2\ \ + s_2\ \ 1 + y_2 P^{12}\ \ (\mathbf{k}'\ \ \mathbf{k}) \end{aligned} \tag{3.17}$$

$$\begin{aligned} v_{CIB}(1;2) = (\ ^z_1\ ^z_2)\ \ (\mathbf{r}_1 \quad \mathbf{r}_2)\ \ u_0\ \ 1 + z_0 P^{12} \\ + \frac{1}{2} u_1\ \ 1 + z_1 P^{12}\ \ \ k^2 + k'^2\ \ + u_2\ \ 1 + z_2 P^{12}\ \ (\mathbf{k}'\ \ \mathbf{k}) \end{aligned} \tag{3.18}$$

where $s_{0;1;2}$, $y_{0;1;2}$, $u_{0;1;2}$ and $z_{0;1;2}$ are free parameters, which one can nd by tting to experimental data. In (3.18) the component $\sim_1\ \sim_2$ has been neglected. The reason of this choice is due to the fact that the contribution of this class II force to the energy density functional depend explicitly on the pn-mixed densities and then requires the use of pn-mixed DFT [48]. As it will be mentioned in the next chapter, the code HFODD permits calculations that include pn-mixed densities only if the pairing is not included. The pairs of mirror nuclei on which the ISB e ect is studied, are all open shell and therefore the pairing e ect is not negligible. This makes also the calculation of the CIB contribution easier.

As already mentioned in the previous chapter $_z$ has a di erent values depending on its acting on a neutron ($\frac{1}{2}$) or a proton ($\ \frac{1}{2}$). The calculation of the expectation value of the potentials (3.17) and (3.18) follows the same way of (2.7) and it is explicitly shown in appendix A. The calculation of these terms is very similar to the calculation explained in the appendix of [58]. The energy densities of the two potential are printed below:

$$\begin{aligned} H_{CSB}(\mathbf{r}) = \ & \frac{s_0(1 \quad y_0)}{2}\ \ \ ^2_n(\mathbf{r})\ \ \ \ ^2_p(\mathbf{r}) \\ & + \frac{s_1(1 \quad y_1)}{8}\ \ \ \frac{3}{2}\ _n(\mathbf{r})r\ ^2\ _n(\mathbf{r}) + \frac{3}{2}\ _p(\mathbf{r})r\ ^2\ _p(\mathbf{r}) \\ & + 2\ _n(\mathbf{r})K_n(\mathbf{r})\ \ \ 2\ _p(\mathbf{r})K_p(\mathbf{r}) + \ J_n^2(\mathbf{r})\ \ \ J_p^2(\mathbf{r}) \\ & + \frac{s_2(1 + y_2)}{8}\ \ 6K_n(\mathbf{r})\ _n(\mathbf{r})\ \ \ 6K_p(\mathbf{r})\ _p(\mathbf{r}) \\ & + \frac{3}{2}\ _n(\mathbf{r})r\ ^2\ _n(\mathbf{r})\ \ \ \frac{3}{2}\ _p(\mathbf{r})r\ ^2\ _p(\mathbf{r})\ \ \ \ J_n^2(\mathbf{r})\ \ \ J_p^2(\mathbf{r}) \end{aligned} \tag{3.19}$$

$$
\begin{aligned}
H_{CIB}(\vec{r}) = {} & \frac{u_0(1 - z_0)}{4}\left[\rho_n^2(\vec{r}) + \rho_p^2(\vec{r})\right] - u_0\left[1 + \frac{z_0}{2}\right]\rho_n(\vec{r})\,\rho_p(\vec{r}) \\
& + \frac{u_1}{16}\,2(1 - z_1)\left[-\frac{3}{2}\rho_n(\vec{r})\nabla^2\rho_n(\vec{r}) - \frac{3}{2}\rho_p(\vec{r})\nabla^2\rho_p(\vec{r}) + K_n(\vec{r})\,\rho_n(\vec{r}) + K_p(\vec{r})\,\rho_p(\vec{r})\right] \\
& + 2(2 + z_1)\left[-\frac{3}{2}\rho_n(\vec{r})\nabla^2\rho_p(\vec{r}) + \frac{3}{2}\rho_p(\vec{r})\nabla^2\rho_n(\vec{r}) - K_p(\vec{r})\,\rho_n(\vec{r}) - K_p(\vec{r})\,\rho_n(\vec{r})\right] \\
& + (-z_1 - 1)\left(J_n^2(\vec{r}) + J_p^2(\vec{r})\right) - 2z_1\vec{J}_n(\vec{r})\cdot\vec{J}_p(\vec{r}) \\
& + \frac{3u_2(1 + y_2)}{8}\left[K_n(\vec{r})\,\rho_n(\vec{r}) + K_p(\vec{r})\,\rho_p(\vec{r}) + \frac{1}{4}\left[\rho_n(\vec{r})\nabla^2\rho_n(\vec{r}) + \rho_n(\vec{r})\nabla^2\rho_n(\vec{r})\right]\right] \\
& - \frac{u_2(2 + z_2)}{8}\left[-\frac{1}{4}\left[\rho_n(\vec{r})\nabla^2\rho_p(\vec{r}) + \rho_p(\vec{r})\nabla^2\rho_n(\vec{r})\right] + \left(K_n(\vec{r})\,\rho_p(\vec{r}) + K_p(\vec{r})\,\rho_n(\vec{r})\right)\right] \\
& - \frac{u_2}{16}(1 + z_2)\left[J_n^2(\vec{r}) + J_p^2(\vec{r})\right] - 2z_2\vec{J}_n(\vec{r})\cdot\vec{J}_p(\vec{r})
\end{aligned}
\tag{3.20}
$$

By using the de nitions (2.17), one can calculate the contribution of the CSB and CIB terms to the mean- eld, e ective mass and spin potential.

As already discussed, CSB and CIB e ects have been widely discussed in literature in the previous section. Although it is known that CSB and CIB forces have to be taken into account to reproduce the Nolen-Schi er anomaly [41], the information on these forces in nuclear medium is not generous. In this context, SAMi-ISB [46] has been recently proposed. Roca-Maza et. al. [46] used the same tting protocols of SAMi [45] but including CSB and CIB interactions. SAMi-ISB is a new (2018) parametrization of Skyrme-like EDF. It reconcile standard nuclear properties (saturation density, binding energies and charge radii of nite nuclei) with the density behaviour of the symmetry energy and the reproduction of the IAS energy of ^{208}Pb [46]. The SAMi-ISB parameter set is showed in the next table [46]:

Parameter	Value ( )
t_0 [MeV fm^3]	-2098.3 (149.3)
t_1 [MeV fm^5]	394.7 (15.8)
t_2 [MeV fm^5]	-136.4 (10.8)
t_3 [MeV fm^{3+3}]	11995 (686)
x_0	0.242 (9)
x_1	-0.17 (33)
x_2	-0.470 (4)
x_3	0.32 (21)
W_0	294. (6)
	0.223 (31)

Table 3.1: SAMi-ISB parameter set. The statistical errors ( ) are given in parenthesis. See [46] for the details on the t.

SAMi-ISB is the set of Skyrme parameters used in this work for the calculations whose results are showed and discussed in the next chapter.

Chapter 4

Results and Discussion

In this chapter the results of the calculations made for the mirror nuclei ^{30}Si-^{30}S, ^{34}S-^{34}Ar, ^{50}Ti-^{50}Ni and ^{52}Cr-^{52}Ni are presented and discussed. The aim of this work is to describe the effects of the ISB interaction, and the energy density functionals related to them have been calculated in the previous chapter. The aim of this work is to try to reproduce the experimental MDEs grouped in this table (experimental values taken from [60]):

	^{30}Si-^{30}S	^{34}S-^{34}Ar	^{50}Ti-^{50}Ni	^{52}Cr-^{52}Ni
MDE_{Exp} [MeV]	11.937	13.118	51.985	36.243

Table 4.1: Experimental Mirror Displacement Energies for each pair. Binding energies from [60].

In order to reproduce these experimental MDE, the calculation of the binding energies for the mirror nuclei has been made by solving the Skyrme-HFB equations for them. Similar calculations have been made by using a Gogny effective interaction [32]. The calculations have been performed by the code HFODD [23, 24, 25, 50] with SAMi-ISB as effective Skyrme interaction whose set parameters are listed in table 3.1.

HFODD is one of the most sophisticated Hartree-Fock-Bogolyubov codes for simulations in nuclear structure (120.000 lines), its programming language is FORTRAN90 and the update to its latest version took place recently [50]. In its first version (1997) HFODD solves only Skyrme-Hartree-Fock problem by using a deformed Cartesian harmonic oscillator basis. HFODD solves the HF equations by expanding the single-particle wave functions onto the deformed harmonic oscillator (HO) wave functions in the Cartesian coordinates. The complete list of expressions required to calculate local densities, total energies, self-consistent fields and the implementation of the self-consistent symmetries is discussed in [23]. In the same reference formulas to calculate matrix elements in the Cartesian harmonic oscillator basis are derived for nuclear and Coulomb interactions. The user of HFODD has the possibility of choosing among various symmetries of the nuclear HF problem for rotating or non-rotating nuclei; they vary from the spherical nuclear shapes, through those also breaking the intrinsic parity, towards the most complicated shapes. The program uses the Cartesian HO to expand single-particle wave functions of neutrons and protons interacting by means of Skyrme effective interaction. The expansion coefficients are determined by the iterative diagonalization of the mean-field Hamiltonian which depends on the local proton or neutron densities. Details on calculation times and the description of the input and the output are explained in [24]. Pairing can be taken into account because the code can solve the BCS equations(2.23)-(2.28) separately for protons and neutrons. A newer version of the code (IV,

2004) [25] is able to solve either the Skyrme-Hartree-Fock or Skyrme-Hartree-Fock-Bogolyubov problem, by using the Cartesian harmonic oscillator basis. This code has been tested with both the options, HF+BCS for numerical test and HFB to study the mirror nuclei listed above. In the newest version of the code (VIII, 2017) [50] many features and methods have been added respect to the first version, but the most useful for this work is the possibility to include ISB terms in a Skyrme-Hartree-Fock caluculation. The details on these terms are explained in the next section. In order to test the performances of the code HFODD has been tested on two simple nuclei, and the results are shown in appendix B.

The results are compared with those calculated with another code, HFBTHO [42]. This code solves the self-consistent HFB equations by using the axial transformed harmonic oscillator (THO) basis, which allows for a correct treatment of the single-quasiparticle wave function asymptotics. The calculation performed with HFBTHO have been independently made by a person other than the author of this thesis. In order to compare the two codes, a systematic of deformed nuclei have been made in [26] and the two codes give results in agreement with each other.

4.1 Results

In the latest version of the code HFODD [50], the strong-force ISB terms have been added as effective, two-body, zero range corrections to the conventional isospin-invariant Skyrme interaction. Contributions of class II (CIB) and class III (CSB) [39], have been implemented as follows [50]:

$$\begin{aligned} v^{II}(1;2) &= t_0^{II}\,(1+x_0^{II}P^{12})\,[3-\tau_{z1}-\tau_{z2}-\tau_1\cdot\tau_2] \\ v^{III}(1;2) &= t_0^{III}\,(1+x_0^{III}P^{12})\,[\tau_{z1}+\tau_{z2}] \end{aligned} \tag{4.1}$$

where the labels 1,2 indicated two nucleons, $t_0^{II,III}$ and $x_0^{II,III}$ are coupling constants, P^{12} is the spin-exchange operator, and $\tau = (\tau_x;\tau_y;\tau_z)$ are the isospin Pauli matrices. Both forces are charge-dependent, but only class III breaks charge symmetry. The corresponding energy densities read, in the code [50]

$$\begin{aligned} H^{II} &= \frac{1}{2}t_0^{II}\,(1+x_0^{II})\Big[\rho_n^2+\rho_p^2-2\rho_n\rho_p-2\rho_{np}\rho_{pn}-\vec{J}_n^2-\vec{J}_p^2+2\vec{J}_n\cdot\vec{J}_p+2\vec{J}_{np}\cdot\vec{J}_{pn}\Big] \\ H^{III} &= \frac{1}{2}t_0^{III}\,(1-x_0^{III})\,\rho_n^2-\rho_p^2-\vec{J}_n^2+\vec{J}_p^2 \end{aligned} \tag{4.2}$$

The formulas indicated above indicate that parameters $x_0^{II,III}$ are redundant and can be set to zero, that is what is done hereafter. Note that the contribution due to the class III force depends entirely on the standard nn and pp densities; in other words it can be taken into account within the conventional pn-separable DFT approach. The contribution due to the class II force, instead, depends explicitly on the pn-mixed scalar and vector densities which are defined as [48].

$$\begin{aligned} \rho_{np} &= \frac{1}{2}(\rho_1+i\rho_2); & \rho_{pn} &= \frac{1}{2}(\rho_1-i\rho_2) \\ \vec{J}_{np} &= \frac{1}{2}(\vec{J}_1+i\vec{J}_2) & \vec{J}_{pn} &= \frac{1}{2}(\vec{J}_1-i\vec{J}_2) \end{aligned} \tag{4.3}$$

where $\vec{J}_{1;2}$ and $\vec{J}_{1;2}$ are the particle and spin densities related to the particle 1 or 2 [50, 48]. Therefore, such forces can only be used within the mean-field formalism involving pn-mixing [48].

The last version of the code HFODD does not allow calculations involving at the same time pairing effects and pn-mixing, for this reason the class II force has not been included in the calculations for the mirror nuclei that the the object of this study.

4.1.1 Preliminary Tests

There are some systematic studies reported in the references [43, 3] in which the effects of the class II and class III forces are tested on several couples of mirror nuclei. Baczyk et al. in [4] have also tested these effects on the $A = 30$ isospin triplet, that is $^{30}_{14}$Si-$^{30}_{15}$P-$^{30}_{16}$S ($T_z = 1; 0; -1$ respectively). In order to understand how these ISB effects behave in the code, the same test has been reproduced in this work. In order to investigate the influence of the (4.2) terms on the ground-state binding energies for the isospin triplet $A = 30$, the test calculation has been performed without pairing and without Coulomb interaction. The calculation has been performed by controlling the isospin degrees of freedom with the isocranking method, see [49]. The technique is analogous to the well known cranking method (see [44]) in real space and allows to calculate the entire isospin multiplet T by starting from the isospin aligned state $|T; T_z = T\rangle$ and isocranking it by an angle ω around the z axis in the isospace.

(a) (b)

Figure 4.1: Calculated ground-state energies of the A=30 isospin-triplet nuclei. Calculations were performed with Skyrme parameter set SV [44] and without Coulomb interaction and without pairing. Full red squares in the (a) and (b) panels show the results obtained by adding only the class II and the class III forces, respectively. The dashed green line indicates the ground state energy without any ISB terms included. The parameters t_0 and x_0 has been set with the values $t_0^{II} = 20$ MeV fm^3, $t_0^{III} = -8$ MeV fm^3, $x_0^{II} = x_0^{III} = 0$, as indicated in [4]

More precisely, it is realised by adding the isocrenking term to the mean-field Hamiltonian $\hat{h}$ [4, 50]:

$$\hat{h}' = \hat{h} - \vec{\omega} \cdot \hat{t} \tag{4.4}$$

where the single-nucleon isospin operator $\hat{t} = \frac{1}{2}\vec{\tau}$ are expressed by means of the Pauli matrices in isospace. By adjusting the isocranking frequences $\vec{\omega}$, one can control both the length and direction of the isospin vector. In HFODD $\vec{\omega}$ can be parametrized as follows

$$\vec{\omega} = (\omega_x, \omega_y, \omega_z) = (\omega_0 \sin\theta_0 \cos\varphi_0, \omega_0 \sin\theta_0 \sin\varphi_0, \omega_0 \cos\theta_0 + \omega_{off}) \tag{4.5}$$

For $_{off} = 0$, it corresponds to the standard spherical coordinate-type parametrization. O set frequency $_{off}$ is introduced to facilitate calculations with the Coulomb interaction. The procedure has been made by following the indications reported in [48], in which a "recipe" about how to use the isocranking method is explained. By adding to the isospin-invariant Skyrme interaction either the class II or class III forces and without considering the Coulomb interaction the in uence of ISB forces on the binding energies. The results are reported in gure 4.1. The results are in very good agreement with what was published in [4]. This test allows to understand how these ISB e ect can in uence the MDE in a mirror nuclei pair. In gure 4.1 panel (a) one can note that a class II force (that means a CIB force) has the same e ect in the state with $T_z = 1$ and it does not in uence in a evident way the value of the calculated MDE. Panel (b), instead, shows that a class III force (that means CSB force) in uences the binding energie of the $T = 1$ state in the opposite way: the $T = 1$ binding energy is shifted up while the $T = 1$ binding energy is shifted down; in other words the CSB force contributes in a major way with respect to the CIB force to the MDE.

In the code HFODD one can include pairing in a calculation by performing a HFB calculation. It is necessary to de ne a pairing strength in the following zero-range pairing potential

$$V(\vec{r}) = (V_0 + V_1 (\vec{r})) (\vec{r} - \vec{r}^{0}) \tag{4.6}$$

Many studies show that a density dependent delta interaction provides good agreement with experiments [56]. The model used in this work for the pairing force is the two body interaction (4.6) where V_0 and are constants to be adjusted phenomenologically. Note that an attractive interaction requires $V_0 < 0$. In this work a density-independent pairing force (volume pairing) has been considered and then $V_1 = 0$ and $= 1$. The value of V_0 depends on the interaction used in the calculation. The value of V_0 has been adjusted so that ^{120}Sn have a paring gap $_n = 1.4$ MeV for each type of calculation. In this work four values of V_0 have been determined, and they are showed in the following gures.

(a) (b)

Figure 4.2: Trend of the proton ($_p$) and neutron ($_n$) pairing gap as a function of $|V_0|$ for ^{120}Sn. Filled diamonds indicate the value of V_0 for which $_n$=1.4 MeV, that are V_0=-220.778 [MeV fm ^{3}] in the panel (a) and V_0=-218.715 [MeV fm ^{3}] in the panel (b). Calculation performed with 12 shells.

(a) (b)

Figure 4.3: Same of the gure 4.2, but for 14 shells.V_0=-215.327 [MeV fm ^{3}] in the panel (a) and V_0=-214.151 [MeV fm ^{3}] in the panel (b).

The values of V_0 are grouped in this table

# Shells	SAMi-noISB	SAMi-CSB
12	-220.778	-218.715
14	-215.327	-214.151

Table 4.2: Values of V_0 in [MeV fm ^{3}].

In the gures 4.2 and 4.3 and in the table 4.2 SAMi-noISB means that we have used the SAMi-ISB parameters 3.1 without by setting to zero the ISB terms in the calculation; while SAMi-CSB means that the SAMi-ISB parameter set has been used and the only the class III force (CSB terms) have been included. The 12 and 14 are two numbers related to the HO basis size. In particular 12 and 14 indicate the number of HO quanta in either of the Cartesian direction (in [23] this number is indicated with N_0). In order to obtain a more sensible value of the binding energy, the heavier the nucleus considered for the calculation, the greater the value of N_0 must be. Four values of V_0 have been adjusted because those related to 12 shells have been used for the calculation of the $A = 30; 34$ mirror nuclei, while those related to 14 shells have been used for the calculation of the $A = 50; 52$ mirror nuclei.

These preliminary tests pave the way to the calculation on the mirror nuclei that are object of this work. The Skyrme parameter set used in this study is SAMi-ISB (table 3.1). In order to understand the e ect of pairing and CSB force on the binding energies separately, for each pair of mirror nuclei four types of calculations have been made:

a calculation that does not include pairing and does not include CSB interaction (in the next section this calculation is summarized with the notation "0Pair0CSB");

a calculation that does not include pairing and includes CSB interaction ("0Pair1CSB");

a calculation that includes pairing and does not include CSB interaction ("1Pair0CSB");

a calculation that includes both pairing and CSB interaction ("1Pair1CSB").

The following sections are structured as follows: for each pair of mirror nuclei the results on binding energies and charge radii obtained by a calculation without pairing and without CSB interaction, with pairing and without and then those obtained by including both the pairing and CSB interaction will be explicitly shown in some tables. The results of the calculation with pairing and without CSB interaction is not reported explicitly in tables but it is included in the summary figure that compares all the MDEs calculated at the end of each section. The results calculated by HFODD, HFBTHO and experimental values (binding energies taken from [60] and charge radii from [1]) are compared. The tables show the binding energies, the rms proton and neutron radii, the deformation parameters ; separately for protons and neutrons and the rms charge radii. Since the codes HFODD and HFBTHO do not calculate charge radii, but only proton and neutron radii, the charge radii are calculated from the value of the rms proton radius by means of the empirical formula [19]:

$$\langle r_{ch} \rangle^2 = \langle r_p \rangle^2 + (0.8)^2 \quad [\mathrm{fm}^2] \tag{4.7}$$

HFODD does not even calculate the deformation parameters, but the quadrupole moments Q_{20} and Q_{22} are calculated. Thus and have been calculated from the quadrupole moments as [23, 44]

$$= \sqrt{\frac{5}{}}\frac{Q_{20}}{Z\langle r_p \rangle^2} \qquad \tan = \frac{Q_{22}}{Q_{20}} \tag{4.8}$$

HFBTHO calculates the beta and gamma values on its own.

4.1.2 Calculations on ^{30}Si-^{30}S

^{30}Si	HFODD	HFBTHO	Experimental
E_{tot} [MeV]	-256.178	-250.907	-255.619
$\langle r_p \rangle$ [fm]	3.1587	3.0537	-
$_p$	0.1830	0.00	-
$_p$	-68.670	0.00	-
$\langle r_n \rangle$ [fm]	3.1841	3.1126	-
$_n$	0.1044	0.00	-
$_n$	-77.478	0.00	-
$\langle r_{ch} \rangle$ [fm]	3.2584	3.1567	3.1336

Table 4.3: Calculation for ^{30}Si without pairing and without CSB interaction

^{30}S	HFODD	HFBTHO	Experimental
E_{tot} [MeV]	-244.952	-239.714	-243.681
$\langle r_p \rangle$ [fm]	3.2353	3.1593	-
$_p$	0.1068	0.00	-
$_p$	-77.337	0.00	-
$\langle r_n \rangle$ [fm]	3.1344	3.0287	-
$_n$	0.1898	0.00	-
$_n$	-68.2898	0.00	-
$\langle r_{ch} \rangle$ [fm]	3.3327	3.2590	-

Table 4.4: Calculation for ^{30}S without pairing and without CSB interaction

In this calculation HFODD and HFBTHO predicts very different values of binding energies for both the nuclei. The results of HFODD on the radii say us that ^{30}Si and ^{30}S are triaxial nuclei, because the values of and are non-zero. HFBTHO finds out only spherical nuclei. The experimental charge radius of the ^{30}S has not been measured yet. Below we show the calculated values including pairing interaction.

^{30}Si	HFODD	HFBTHO	Experimental
E_{tot} [MeV]	-254.817	-254.835	-255.619
$\langle r_p \rangle$ [fm]	3.0666	3.0665	-
$\langle r_n \rangle$ [fm]	3.0991	3.0991	-
$V_0^p = V_0^n$ [MeV fm ^{3}]	-220.778	-220.778	-
$\langle r_{ch} \rangle$ [fm]	3.1692	3.1691	3.1336

Table 4.5: Calculation ^{30}Si with Pairing and without CSB interaction

^{30}S	HFODD	HFBTHO	Experimental
E_{tot} [MeV]	-243.477	-243.495	-243.681
$\langle r_p \rangle$ [fm]	3.1480	3.1480	-
$\langle r_n \rangle$ [fm]	3.0371	3.0371	-
$V_0^p = V_0^n$ [MeV fm ^{3}]	-220.778	-220.778	-
$\langle r_{ch} \rangle$ [fm]	3.2481	3.2481	-

Table 4.6: Calculation for ^{30}S with Pairing and without CSB interaction

^{30}Si	HFODD	HFBTHO	Experimental
E_{tot} [MeV]	-255.933	-255.950	-255.619
$\langle r_p \rangle$ [fm]	3.0767	3.0765	-
$\langle r_n \rangle$ [fm]	3.0839	3.0834	-
$V_0^p = V_0^n$ [MeV fm ^{3}]	-218.715	-218.715	-
$\langle r_{ch} \rangle$ [fm]	3.1789	3.1788	3.1336

Table 4.7: Calculation for ^{30}Si with Pairing and CSB interaction included

^{30}S	HFODD	HFBTHO	Experimental
E_{tot} [MeV]	-242.525	-242.543	-243.681
$\langle r_p \rangle$ [fm]	3.1636	3.1635	-
$\langle r_n \rangle$ [fm]	3.0266	3.0266	-
$V_0^p = V_0^n$ [MeV fm ^{3}]	-218.715	-218.715	-
$\langle r_{ch} \rangle$ [fm]	3.2631	3.2630	-

Table 4.8: Calculation for ^{30}S with Pairing and CSB interaction included

In these tables the values of and are not reported because the two codes have calculated two nuclei that are perfectly spherical. In this case the results of the codes on the binding energies and charge radii are in very good agreement. The following gure summarizes all the MDE calculated for the mirror nuclei ^{30}Si-^{30}S.

Code	0Pair0CSB	0Pair1CSB	1Pair0CSB	1Pair1CSB
HFODD	11.226	13.341	11.340	13.408
HFBTHO	11.193	13.082	11.340	13.407

Table 4.9: Summary of the calculated MDEs [MeV] by HFODD and HFBTHO for ^{30}Si-^{30}S

Figure 4.4: Comparison of MDE/A between the experimental results (black line), HFODD results (red squares) and HFBTHO results (blue asterisks) for the mirror nuclei ^{30}Si-^{30}S.

4.1.3 Calculations on ^{34}S-^{34}Ar

^{34}S	HFODD	HFBTHO	Experimental	
E_{tot} [MeV]	-296.481	-295.868	-291.840	
$\langle r_p \rangle$ [fm]	3.2317	3.2293	-	
$_p$	3.812510^{-2}	-0.2272	-	
$_p$	84.186	0.00	-	
$\langle r_n \rangle$ [fm]	3.2414	3.2389	-	
$_n$	9.78510^{-2}	0.2052	-	
$_n$	72.813	0.00	-	
$\langle r_{ch} \rangle$ [fm]	3.3292	3.3254	3.3269	3.2847

Table 4.10: Calculation for ^{34}S without pairing and without CSB interaction

^{34}Ar	HFODD	HFBTHO	Experimental
E_{tot} [MeV]	-283.954	-283.083	-278.721
$\langle r_p \rangle$ [fm]	3.2942	3.2926	-
$_p$	-0.3302	-0.2101	-
$_p$	-12.878	0.00	-
$\langle r_n \rangle$ [fm]	3.2024	3.1983	-
$_n$	-0.3542	-0.2145	-
$_n$	-23.477	0.00	-
$\langle r_{ch} \rangle$ [fm]	3.3899	3.3883	3.3654

Table 4.11: Calculation for ^{34}Ar without pairing and without CSB interaction

In this calculation HFODD and HFBTHO predict slightly different values of binding energies for these nuclei. The results of HFODD on the radii say us that ^{34}S and ^{34}Ar are triaxial nuclei, because the values of and are non-zero. HFBTHO finds out axially deformed nuclei. Below we show the calculated values including pairing interaction.

^{34}S	HFODD	HFBTHO	Experimental
E_{tot} [MeV]	-297.033	-297.052	-291.840
$\langle r_p \rangle$ [fm]	3.1820	3.1819	-
$\langle r_n \rangle$ [fm]	3.1955	3.1954	-
$V_0^p = V_0^n$ [MeV fm ^{3}]	-220.778	-220.778	-
$\langle r_{ch} \rangle$ [fm]	3.2810	3.2809	3.2847

Table 4.12: Calculation for ^{34}S with pairing and without CSB interaction

^{34}Ar	HFODD	HFBTHO	Experimental
E_{tot} [MeV]	-284.390	-284.410	-278.721
$\langle r_p \rangle$ [fm]	3.2470	3.2470	-
$\langle r_n \rangle$ [fm]	3.1495	3.1496	-
$V_0^p = V_0^n$ [MeV fm ^{3}]	-220.778	-220.778	-
$\langle r_{ch} \rangle$ [fm]	3.3441	3.3441	3.3654

Table 4.13: Calculation for ^{34}Ar with pairing and without CSB interaction

^{34}S	HFODD	HFBTHO	Experimental
E_{tot} [MeV]	-298.299	-298.318	-291.840
$\langle r_p \rangle$ [fm]	3.1924	3.1922	-
$\langle r_n \rangle$ [fm]	3.1804	3.1799	-
$V_0^p = V_0^n$ [MeV fm ^{3}]	-218.715	-218.715	-
$\langle r_{ch} \rangle$ [fm]	3.2911	3.2910	3.2847

Table 4.14: Calculation for ^{34}S with pairing and CSB interaction included

^{34}Ar	HFODD	HFBTHO	Experimental
E_{tot} [MeV]	-283.435	-283.454	-278.721
$\langle r_p \rangle$ [fm]	3.2624	3.2623	-
$\langle r_n \rangle$ [fm]	3.1392	3.1392	-
$V_0^p = V_0^n$ [MeV fm ^{3}]	-218.715	-218.715	-
$\langle r_{ch} \rangle$ [fm]	3.3590	3.3589	3.3654

Table 4.15: Calculation for ^{34}Ar with pairing and CSB interaction included

In these tables the values of and are not reported because the two codes have calculated two nuclei that are perfectly spherical. In this case the results of the codes on the binding energies and charge radii are in very good agreement. The following gure summarizes all the MDE calculated for the mirror nuclei ^{34}S-^{34}Ar.

Code	0Pair0CSB	0Pair1CSB	1Pair0CSB	1Pair1CSB
HFODD	12.527	14.704	12.643	14.864
HFBTHO	12.785	14.526	12.642	14.864

Table 4.16: Summary of the calculated MDEs [MeV] by HFODD and HFBTHO for ^{34}S-^{34}Ar

Figure 4.5: Comparison of MDE/A between the experimental results (black line), HFODD results (red squares) and HFBTHO results (blue asterisks) for the mirror nuclei ^{34}S-^{34}Ar.

4.1.4 Calculations on ^{50}Ti- ^{50}Ni

^{50}Ti	HFODD	HFBTHO	Experimental
E_{tot} [MeV]	-442.501	-442.530	-437.785
$\langle r_p \rangle$ [fm]	3.5553	3.5552	-
$_p$	-0.2214	0.2783	-
$_p$	60.003	0.00	-
$\langle r_n \rangle$ [fm]	3.6877	3.6876	-
$_n$	-0.2516	0.3162	-
$_n$	60.001	0.00	-
$\langle r_{ch} \rangle$ [fm]	3.6439	3.6440	3.3570

Table 4.17: Calculation for ^{50}Ti without pairing and without CSB interaction

^{50}Ni	HFODD	HFBTHO	Experimental
E_{tot} [MeV]	-394.281	-394.310	-385.800
$\langle r_p \rangle$ [fm]	3.7690	3.7689	-
$_p$	-0.2557	0.3213	-
$_p$	60.000	0.00	-
$\langle r_n \rangle$ [fm]	3.5235	3.6876	-
$_n$	-0.2228	0.2800	-
$_n$	59.992	0.00	-
$\langle r_{ch} \rangle$ [fm]	3.8529	3.8528	-

Table 4.18: Calculation for ^{50}Ni without pairing and without CSB interaction

In this calculation HFODD and HFBTHO give values of binding energies that are in very agreement for both the nuclei (30 keV di erent). The results of HFODD on the radii say us that ^{50}Ti and

^{50}Ni are oblate axially deformed nuclei. HFBTHO finds out that they are prolate axially deformed nuclei. Below we show the calculated values including pairing interaction.

^{50}Ti	HFODD	HFBTHO	Experimental
E_{tot} [MeV]	-443.132	-443.172	-437.785
$\langle r_p \rangle$ [fm]	3.4865	3.4865	-
$\langle r_n \rangle$ [fm]	3.6158	3.6157	-
$V_0^p = V_0^n$ [MeV fm ^{3}]	-215.327	-215.327	-
$\langle r_{ch} \rangle$ [fm]	3.5771	3.5771	3.3570

Table 4.19: Calculation for ^{50}Ti with pairing and without CSB interaction

^{50}Ni	HFODD	HFBTHO	Experimental
E_{tot} [MeV]	-394.352	-394.382	-385.800
$\langle r_p \rangle$ [fm]	3.6932	3.6931	-
$\langle r_n \rangle$ [fm]	3.4528	3.4527	-
$V_0^p = V_0^n$ [MeV fm ^{3}]	-215.327	-215.327	-
$\langle r_{ch} \rangle$ [fm]	3.7788	3.7787	-

Table 4.20: Calculation for ^{50}Ni with pairing and without CSB interaction

^{50}Ti	HFODD	HFBTHO	Experimental
E_{tot} [MeV]	-446.517	-446.547	-437.785
$\langle r_p \rangle$ [fm]	3.4949	3.4946	-
$\langle r_n \rangle$ [fm]	3.5998	3.5991	-
$V_0^p = V_0^n$ [MeV fm ^{3}]	-214.151	-214.151	-
$\langle r_{ch} \rangle$ [fm]	3.5852	3.5850	3.3570

Table 4.21: Calculation for ^{50}Ti with pairing and CSB interaction included

^{50}Ni	HFODD	HFBTHO	Experimental
E_{tot} [MeV]	-391.713	-391.780	-385.800
$\langle r_p \rangle$ [fm]	3.7103	3.7103	-
$\langle r_n \rangle$ [fm]	3.4431	3.4433	-
$V_0^p = V_0^n$ [MeV fm ^{3}]	-214.151	-214.151	-
$\langle r_{ch} \rangle$ [fm]	3.7955	3.7955	-

Table 4.22: Calculation for ^{50}Ni with pairing and CSB interaction included

In these tables the values of and are not reported because the two codes have calculated two nuclei that are perfectly spherical. In this case the results of the codes on the binding energies

and charge radii are in very agreement. The following figure summarizes all the MDE calculated for the mirror nuclei ^{50}Ti-^{50}Ni.

Code	0Pair0CSB	0Pair1CSB	1Pair0CSB	1Pair1CSB
HFODD	48.220	54.383	48.780	54.804
HFBTHO	48.221	54.383	48.750	54.767

Table 4.23: Summary of the calculated MDEs [MeV] by HFODD and HFBTHO for ^{50}Ti-^{50}Ni

Figure 4.6: Comparison of MDE/A between the experimental results (black line), HFODD results (red squares) and HFBTHO results (blue asterisks) for the mirror nuclei ^{50}Ti-^{50}Ni.

4.1.5 Calculations on ^{52}Cr-^{52}Ni

^{52}Cr	HFODD	HFBTHO	Experimental
E_{tot} [MeV]	-462.292	-462.322	-456.351
$\langle r_p \rangle$ [fm]	3.6535	3.6534	-
$_p$	-0.2693	0.3384	-
$_p$	59.999	0.00	-
$\langle r_n \rangle$ [fm]	3.7075	3.7074	-
$_n$	-0.2787	0.3502	-
$_n$	59.999	0.00	-
$\langle r_{ch} \rangle$ [fm]	3.7400	3.7399	3.6452

Table 4.24: Calculation for ^{52}Cr without pairing and without CSB interaction

^{52}Ni	HFODD	HFBTHO	Experimental
E_{tot} [MeV]	-428.835	-423.720	-420.108
$\langle r_p \rangle$ [fm]	3.7802	3.7511	-
$_p$	-0.2826	-0.2333	-
$_p$	59.999	0.00	-
$\langle r_n \rangle$ [fm]	3.6156	3.5709	-
$_n$	-0.2713	-0.2139	-
$_n$	60.001	0.00	-
$\langle r_{ch} \rangle$ [fm]	3.8692	3.8354	-

Table 4.25: Calculation for ^{52}Ni without pairing and without CSB interaction

In this calculation HFODD and HFBTHO give values of binding energies that are in very agreement for both the nuclei for ^{52}Cr, but they are different as regards the binding energies of ^{52}Ni. The results of HFODD on the radii say us that ^{52}Cr and ^{52}Ti are oblate axially deformed nuclei. HFBTHO finds out that ^{52}Ni is an oblate axially deformed nucleus and that ^{52}Cr is a prolate axially deformed nucleus. Below we show the calculated values including pairing interaction.

^{52}Cr	HFODD	HFBTHO	Experimental
E_{tot} [MeV]	-458.689	-458.721	-456.351
$\langle r_p \rangle$ [fm]	3.5626	3.5625	-
$\langle r_n \rangle$ [fm]	3.6214	3.6213	-
$V_0^p = V_0^n$	-215.327	-215.327	-
$\langle r_{ch} \rangle$ [fm]	3.6513	3.6512	3.6452

Table 4.26: Calculation for ^{52}Cr with pairing and without CSB interaction

^{52}Ni	HFODD	HFBTHO	Experimental
E_{tot} [MeV]	-425.005	-425.036	-420.108
$\langle r_p \rangle$ [fm]	3.6906	3.6905	-
$\langle r_n \rangle$ [fm]	3.5216	3.5215	-
$V_0^p = V_0^n$	-215.327	-215.327	-
$\langle r_{ch} \rangle$ [fm]	3.7763	3.7762	-

Table 4.27: Calculation for ^{52}Ni with pairing and without CSB interaction

^{52}Cr	HFODD	HFBTHO	Experimental
E_{tot} [MeV]	-461.127	-461.158	-456.351
$\langle r_p \rangle$ [fm]	3.5720	3.5718	-
$\langle r_n \rangle$ [fm]	3.6068	3.6063	-
$V_0^p = V_0^n$	-214.151	-214.151	-
$\langle r_{ch} \rangle$ [fm]	3.6604	3.6601	3.6452

Table 4.28: Calculation for ^{52}Cr with pairing and CSB interaction included

^{52}Ni	HFODD	HFBTHO	Experimental
E_{tot} [MeV]	-423.336	-423.367	-420.108
$\langle r_p \rangle$ [fm]	3.7057	3.7056	-
$\langle r_n \rangle$ [fm]	3.5112	3.5112	-
$V_0^p = V_0^n$	-214.151	-214.151	-
$\langle r_{ch} \rangle$ [fm]	3.7910	3.7909	-

Table 4.29: Calculation for ^{52}Ni with pairing and CSB interaction included

In these tables the values of and are not reported because the two codes have calculated two nuclei that are perfectly spherical. In this case the results of the codes on the binding energies and charge radii are in good agreement between them. The following gure summarizes all the MDE calculated for the mirror nuclei ^{52}Cr-^{52}Ni.

Code	0Pair0CSB	0Pair1CSB	1Pair0CSB	1Pair1CSB
HFODD	33.457	37.781	33.684	37.791
HFBTHO	38.602	37.781	33.685	37.791

Table 4.30: Summary of the calculated MDEs [MeV] by HFODD and HFBTHO for ^{52}Cr-^{52}Ni

Figure 4.7: Comparison of MDE/A between the experimental results (black line), HFODD results (red squares) and HFBTHO results (blue asterisks) for the mirror nuclei ^{52}Cr-^{52}Ni.

4.1.6 Summary of the Results

In the previous sections we have shown the results of the calculations performed in several ways with two different codes, HFODD and HFBTHO. In this section we summarize all the results of each pair in two tables and figures, one for all the results performed with HFODD and one which shows all the results performed with HFBTHO.

Pairs	Experimental	0Pair0CSB	0Pair1CSB	1Pair0CSB	1Pair1CSB
^{30}Si-^{30}S	11.937	11.126	13.341	11.340	13.408
^{34}S-^{34}Ar	13.118	12.527	14.704	12.643	14.864
^{50}Ti-^{50}Ni	51.985	48.220	54.383	48.780	54.804
^{52}Cr-^{52}Ni	36.243	33.457	37.781	33.684	37.791

Table 4.31: Summary of the experimental and calculated by HFODD MDEs for each pair of mirror nuclei indicated in the first column left on the left. The MDEs are measured in [MeV].

Pairs	Experimental	0Pair0CSB	0Pair1CSB	1Pair0CSB	1Pair1CSB
^{30}Si-^{30}S	11.937	11.193	13.082	11.340	13.407
^{34}S-^{34}Ar	13.118	12.785	14.526	12.642	14.864
^{50}Ti-^{50}Ni	51.985	48.221	54.383	48.750	54.767
^{52}Cr-^{50}Ni	36.243	38.602	37.781	33.685	37.791

Table 4.32: Summary of the experimental and calculated by HFBTHO MDEs for each pair of mirror nuclei indicated in the first column on the left. The MDEs are measured in [MeV].

The figures show the all the MDE calculated and the experimental MDE divided by A and then divided again by $|N - Z|$ for reasons related to the scale of the pictures.

(a) (b)

Figure 4.8: Comparison of $(MDE/A)/|N - Z|$ [MeV] calculated with HFODD in panel (a) and calculated with HFBTHO in panel (b). The black filled diamond indicates the experimental value

In this gure one can observe very well the e ects of pairing and CSB interaction both when they are included separately and when they act together. As we can see on this gure, HFODD and HFBTHO give results in very good agreement except for $A = 52$. The case $A = 52$ gives a di erent result for the "initial" calculated MDE, because the binding energies calculated for ^{52}Ni are very di erent for the two codes. The reason of this fact is unknown. The two codes have been run with the same initial conditions on their inputs. The di erences on the results are discussed in the next section. The rms di erences between the calculated MDEs by HFODD and the experimental MDEs are listed in the following table:

	0Pair0CSB	0Pair1CSB	1Pair0CSB	1Pair1CSB
$\langle MDE_{HFODD} - MDE_{Exp} \rangle$ [MeV]	2.395	1.775	2.086	1.972
$\langle MDE_{HFBTHO} - MDE_{Exp} \rangle$ [MeV]	2.258	1.688	2.097	1.958

Table 4.33: rms of the di erence between the calculated by HFODD, HFBTHO and the experimental MDEs in [MeV]

4.2 Discussion

The purpose of this study is to reproduce the experimental MDEs of some pairs of mirror nuclei. One must rst of all understand the e ect of ISB terms on the binding energies of the mirror nuclei. In the previous sections we have shown the results of the results of the calculations on the mirror nuclei ^{30}Si-^{30}S, ^{34}S-^{34}Ar, ^{50}Ti-^{50}Ni and ^{52}Cr-^{52}Ni. In order to understand the e ects of pairing and CSB interaction, we have performed many calculations, without both pairing and CSB interaction, with only one of them and the other excluded and when they are included at the same time.

Let us consider for example the rst pair of mirror nuclei, that is ^{30}Si-^{30}S. When we compare the results of the calculation without considering the pairing, HFODD nds out that these two nuclei are deformed, in particular they are triaxial because of the non-zero values of and . HFBTHO instead nds out that ^{30}Si and ^{30}S are both spherical. Their values of rms proton radii and charge radii are not in agreement with the experimental values. This can be due to the fact that if a code performs a search on the plane these nuclei do not have a well de ned minimum in the ground-state binding energy and it is possible that HFODD has found a deeper minimum than than the minimum found by HFBTHO that can be a local minimum on the plane. It can be di cult for these nuclei to nd two solutions with similar deformation parameters calculated by the two codes in such a way that the solutions are truly in agreement with each other (in other words that the two codes nd the same minimum on the plane). When pairing is introduced in the calculation the results performed by the two code are in very good agreement with each other. The di erence between the binding energies is 20 keVs and the proton radii almost coincide. This fact is re ected also in the values of the calculated MDEs with the two codes that are almost coincident. The results of these calculations nd that the two nuclei are perfectly spherical, this because the e ect of the pairing favors a spherical shape of the nucleus, as mentioned in chapter 2. When the pairing is included the two nuclei have a deeper ground-state minimum with respect to the case in which it is not included.

A similar discussion can be made also for the mirror nuclei ^{34}S-^{34}Ar. The initial calculation for these nuclei (that means without pairing and without CSB) performed by HFODD nds out that they are triaxial while the calculation performed by HFBTHO nds out that the these nuclei

are axially deformed. Again one can say that these nuclei have di erent local minima in the ground-state binding energies on the plane and the two codes nd two di erent local minima. By including the pairing again one nds out that the two codes give a spherical solution and values of the binding energies are very close for both nuclei (20 keV di erence). Again the radii are almost coincident.

The case of the mirror nuclei ^{50}Ti- ^{50}Ni is slightly di erent. In the initial calculations the two codes provide two solutions in which the binding energies are very close (30 keVs di erence for both nuclei). According to HFODD the two nuclei are axially deformed and oblate, while according to HFBTHO the two nuclei are axially deformed and prolate. Again these nuclei can have two local minima of the binding-energy on the plane. Again, when pairing is included in the calculation the solutions correspond to spherical nuclei with binding-energies and radii in agreement with each other. In a similar way we can justify the result of the mirror nuclei ^{52}Cr-^{52}Ni. In this speci c case, when both pairing and CSB interaction are not included, the two codes nd two very di erent minima on the plane for ^{52}Ni. For this reason the related MDE are 5 Mev di erent.

The general e ect of the CSB interaction on MDEs between the two mirror nuclei is to evidently increase this di erence, as we can see in the gure 4.8. The pairing e ect on MDEs is again to increase the di erence but the e ect is much smaller than the e ect due to CSB interaction. As we can see on the gure 4.8, by including pairing and CSB interaction in the calculation MDE can not always be reproduced better. In the case of the $A = 30$ mass nuclei the di erence between the calculated and the experimental MDE worsens by 10% for both the codes. In the case of the $A = 34$ mass nuclei it worsens by 7% for both the codes. In the $A = 50$ and $A = 52$ mass nuclei instead, one can reproduce better the experimental MDEs. In fact for $A = 50$ the di erence between the calculated and the experimental MDE improves by 2% while for $A = 52$ it improves by 3%. However, given the results of the quadratic mean values of the di erences between calculated and experimental MDEs shown in table 4.33, we can say that in general the e ects of the CSB and pairing interactions improves the agreement of the calculated MDEs with the experimental MDEs.

We can explain why the agreement with the experimental MDEs worsens in the case of the lighter nuclei as follows. These nuclei have a complicated structure that can not be reproduced well with the HFB calculations performed here. This fact is con rmed by the results of HFB calculations performed with the Gogny e ective interaction by other people. They have shown that the energy surface on the plane of these nuclei have a very at minimum; furthermore it is spread in a zone on the plane in which the values of and describe complicated or triaxial shapes. For this reason we can consider the calculations on these nuclei performed with HFB method with a single Slater determinant as unreliable. The real wave function which describes the ground-state of these nuclei has to be a more general wave function that is composed by a superposition of many Slater determinants so that it covers the whole bottom of the energy surface. As regards the heavier nuclei, the Gogny HFB calculations have shown that their energy surface on the plane have a well-de ned minimum and have a quasi-spherical shape. For this reason we can consider our HFB calculations performed with a single Slater determinant as realiable.

The e ect of the CIB interaction has not been studied in this work. So, one can wonder whether a better agreement between the calculated MDE and the experimental MDE can be reached if both the ISB interactions are included in the calculation. However, having seen the preliminary test on the ISB interactions with the isocranking method, the e ect of the CIB

interaction on MDEs should be small. In order to understand this, a further calculation has been made with HFBTHO by including the CIB interaction without pairing. Excluding pairing from the calculation should not lead to a signi cant loss of information because it has little in uence on MDEs. This calculation is slightly di erent because 20 HO quanta have been used instead 12 or 14 for the basis. The results are summarized in the following table:

Interaction	^{30}Si-^{30}S	^{34}S-^{34}Ar	^{50}Ti-^{50}Ni	^{52}Cr-^{52}Ni
no ISB inter.	11.176	12.785	48.192	38.629
CSB	13.061	15.977	54.347	42.801
CIB	11.105	12.397	47.955	27.762
CSB+CIB	12.953	15.972	54.012	37.537
Experimental	11.937	13.118	51.985	36.243

Table 4.34: Comparison the MDEs [MeV] performed with HFBTHO (20 shells) without pairing.

The general e ect of the CIB interaction on the MDE is to decrease the value of this di erence, but it is much smaller than the e ect due to the CSB interaction. So by including both ISB interactions in the calculations one might better reproduce the experimental MDEs, but this probably is not the case for the $A = 30; 34$ mass nuclei. As regards the $A = 50; 52$ mass nuclei, instead, we can say that by including the CIB interaction one obtains a better agreement with the experimental results.

Conclusion

In this work we have brie y introduced the concept of deformation in nuclei. We have reviewed the evidences that allow us to assume that the nucleons move independently in an average potential. Then the Hartree-Fock method is explained in order to microscopically extract such mean- eld potential. Skyrme e ective interaction has been introduced to solve the HFB equations. Then we have discuss about the isospin properties, in particular we have described the forces which break isospin symmetry motivated by some experimental evidences, as the Nolen-Schi er anomaly [41]. In order to do that, we have added to the Skyrme interaction two new terms, which break charge symmetry and charge independence. In this way we have been able to calculate the binding energies of some mirror nuclei with the codes HFODD and HFBTHO by including isospin symmetry breaking e ects coming from the nuclear strong interaction.

We started with a "basic" calculation (in which pairing and ISB interaction are excluded) of the binding energies of the mirror nuclei ^{30}Si-^{30}S, ^{34}S-^{34}Ar, ^{50}Ti-^{50}Ni and ^{52}Cr-^{52}Ni. We have encountered some di culties in nding an agreement between the results of the two codes due to the deformation of these nuclei; in particular HFODD has found that the mirror nuclei ^{30}Si-^{30}S and ^{34}S-^{34}Ar are triaxial, while HFBTHO that they are axially deformed. As regards the mirror nuclei ^{50}Ti-^{50}Ni and ^{52}Cr-^{52}Ni both the codes have found that these nuclei are axially deformed. Starting from these results, we calculated the relative MDEs. Then we complicated the calculations, rstly by adding either pairing or CSB interaction and nally by adding both at the same time. After calculating all the MDEs, we compared them with those obtained from the experimental values of the binding energies of these nuclei. We have obtained that for the mirror nuclei ^{30}Si-^{30}S, ^{34}S-^{34}Ar that the inclusion of the CSB interaction in the calculations has worsened the agreement between the calculated MDEs and the experimental MDEs with respect the result of the calculation without pairing and CSB interactions included. As regards the mirror nuclei ^{50}Ti-^{50}Ni and ^{52}Cr-^{52}Ni, we have instead obtained a better agreement with the experimental MDEs with respect to the calculation without pairing and CSB interactions.

Since we have not included in the calculation the CIB interaction in HFODD, with the help of the code HFBTHO we have tried to reconstruct the e ect of this interaction on the MDEs. In doing this, however, we have not included pairing interaction in the calculation. We concluded that by including CIB interaction, the agreement between the experimental and calculated MDE de nitely improves for the mirror nuclei nuclei ^{50}Ti-^{50}Ni and ^{52}Cr-^{52}Ni but but we can not guarantee that this also applies to the other two pairs of mirror nuclei.

In order to obtain more agreement between the experimental and the calculated one should generalise the model we have described in this thesis. For example one should rst include the CIB interaction (it must depend on both the terms $\tau_1^z \tau_2^z$ and $\vec{\tau}_1 \cdot \vec{\tau}_2$ as shown in chapter 3) in the HFODD code as well as further electromagnetic corrections to the Coulomb potential such as the electromagnetic nite size of neutrons and protons, the electromagnetic spin-orbit and the

vacuum polarization. The ISB interactions depends on free parameters. One can fit them to find the best values that reproduce the MDEs of even-even deformed nuclei. What has been said could be extended to odd (and odd-odd) nuclei, and generalized including corrections that have been neglected here. In this way one could make a more systematic analysis on the ISB effects on the mirror nuclei.

Appendix A

Isospin Symmetry Breaking Energy Densities

In this appendix the calculations for the energy density of the CIB and CSB potentials are reported. In all the calculations one assumes that the subspace of all occupied states in invariant under time-reversal. In other words, if a single-particle state $|i\rangle$ is occupied, its time-reversed single-particle state $|\bar{i}\rangle = \hat{T}|i\rangle$ is occupied too. Moreover it is assumed that there is no charge mixing of the Hartree-Fock states. The CSB and the CIB potentials are de ned as (see Chapter 2):

$$\begin{aligned} v_{CSB}(1;2) &= (\tau_1^z + \tau_2^z)\ (\vec{r}_1 - \vec{r}_2)\ s_0\ (1 + y_0 P^{12}) \\ &+ \frac{1}{2} s_1\ (1 + y_1 P^{12})\ \{\vec{k}^2 + \vec{k}'^2\} + s_2\ (1 + y_2 P^{12})\ (\vec{k} \times \vec{k}')\ = \\ &= v_{CSB}^{(0)}(1;2) + v_{CSB}^{(1)}(1;2) + v_{CSB}^{(2)}(1;2) \end{aligned} \tag{A.1}$$

$$\begin{aligned} v_{CIB}(1;2) &= (\tau_1^z \tau_2^z)\ (\vec{r}_1 - \vec{r}_2)\ u_0\ (1 + z_0 P^{12}) \\ &+ \frac{1}{2} u_1\ (1 + z_1 P^{12})\ \{\vec{k}^2 + \vec{k}'^2\} + u_2\ (1 + z_2 P^{12})\ (\vec{k} \times \vec{k}')\ = \\ &= v_{CIB}^{(0)}(1;2) + v_{CIB}^{(1)}(1;2) + v_{CIB}^{(2)}(1;2) \end{aligned} \tag{A.2}$$

In the equations (A.1) and (A.2) some symbols are here speci ed:

$$P^{12} = \frac{1}{2}(1 + \vec{\sigma}_1 \cdot \vec{\sigma}_2); \qquad \vec{k} = \frac{1}{2i}(\vec{\nabla}_1 - \vec{\nabla}_2)$$

where the vector $\vec{k}'$ is the complex conjugated of $\vec{k}$ and it acts on the left. In order to calculate the contribution of the potentials to the total energy, as already mentioned, we need to calculate the antisymmetrized matrix elements of the two-body potential $v(1;2)$, written as

$$\begin{aligned} V &= \frac{1}{2} \sum_{ij} \langle ij\, |v(1;2)| ij \rangle_{AS} = \\ &= \sum_{ij} \int d^3 r_1 \int d^3 r_2\, \varphi_i^*(\vec{r}_1) \varphi_j^*(\vec{r}_2) v(1;2) [\varphi_i(\vec{r}_1)\varphi_j(\vec{r}_2) - \varphi_i(\vec{r}_2)\varphi_j(\vec{r}_1)] \end{aligned}$$

The interaction can be antisymmetrized by multiplying it by the factor $(1 - P_r^{12}P^{12}P^{12})$. In this one, P_{12}^r is the operator that exchanges the positions $\vec{r}_1$ and $\vec{r}_2$ and it has no effect in this situation because of the presence of the delta force and then one can substitute it with the unity; instead P_{12} and P_{12} are the spin and isospin exchange operators, respectively, and they have the same form defined above. This trick allows to calculate the matrix element directly, because the anti-symmetric part is "discharged" on this operator. Before starting, it is important to control the behaviour of the isospin operators when combined with the isospin exchange operator P_{12} (remember that the squared Pauli matrices are equal to the identity matrix):

$$\begin{aligned}
(\tau_1^z + \tau_2^z)P_{12} &= (\tau_1^z + \tau_2^z)\frac{1}{2}(1 + \vec{\tau}_1 \cdot \vec{\tau}_2) = \\
&= (\tau_1^z + \tau_2^z)\frac{1}{2}\left(1 + \tau_1^z\tau_2^z + \frac{1}{2}\left(\tau_1^+\tau_2^- + \tau_1^-\tau_2^+\right)\right) = \\
&= \frac{1}{2}\left((\tau_1^z + \tau_2^z) + \tau_1^z\tau_2^z(\tau_1^z + \tau_2^z)\right) = \\
&= \frac{1}{2}(\tau_1^z + \tau_2^z + \tau_1^z\tau_2^z\tau_1^z + \tau_1^z\tau_2^z\tau_2^z) = \\
&= \tau_1^z + \tau_2^z
\end{aligned} \tag{A.3}$$

$$\begin{aligned}
\tau_1^z\tau_2^z P_{12} &= \tau_1^z\tau_2^z\frac{1}{2}(1 + \vec{\tau}_1 \cdot \vec{\tau}_2) = \\
&= \tau_1^z\tau_2^z\frac{1}{2}\left(1 + \tau_1^z\tau_2^z + \frac{1}{2}\left(\tau_1^+\tau_2^- + \tau_1^-\tau_2^+\right)\right) = \\
&= \frac{1}{2}(\tau_1^z\tau_2^z + \tau_1^z\tau_2^z\tau_1^z\tau_2^z) = \\
&= \frac{1}{2}\left(1 + \tau_1^z\tau_2^z + \frac{1}{2}\left(\tau_1^+\tau_2^- + \tau_1^-\tau_2^+\right)\right) = P_{12}
\end{aligned} \tag{A.4}$$

Because of the presence of no charge mixing states, in the equations (A.3) and (A.4) the component containing the raising and lowering operators $\tau^+ = \tau^x + i\tau^y$ and $\tau^- = \tau^x - i\tau^y$ have been considered null. When P_{12} is not combined with other isospin operators, it can be substituted with $\delta_{q_i q_j}$, where q_i denotes the charge of the single-particle state $|i\rangle$.

A.1 CSB Energy Density

The CSB contribution to energy density is then calculated as follows:

$$\begin{aligned}
E_{CSB} &= \frac{1}{2}\sum_{ij}\langle ij|v_{CSB}(1;2)|ij\rangle_{AS} = \\
&= \frac{1}{2}\sum_{ij}\langle ij|\left(v_{CSB}^{(0)}(1;2) + v_{CSB}^{(1)}(1;2) + v_{CSB}^{(2)}(1;2)\right)|ij\rangle_{AS} = \\
&= E_{CSB}^{(0)} + E_{CSB}^{(1)} + E_{CSB}^{(2)}
\end{aligned} \tag{A.5}$$

Now all the terms are calculated separately, starting from the central term.

A.1.1 Central CSB term (/ s_0)

$$E^{(0)}_{CSB} = \frac{1}{2}\sum_{ij} \langle ij\,|\,(\tau^z_1 + \tau^z_2)\ (r_1 - r_2)\, s_0\ 1 + y_0 P^{12}\ |\,ij\rangle_{AS} =$$

$$= \frac{1}{2}\sum_{ij} \langle ij\,|\,(\tau^z_1 + \tau^z_2)\ (r_1 - r_2)\, s_0\ 1 + y_0 P^{12}\ (1 - P^{12}_r P^{12} P^{12})\,|\,ij\rangle$$

Because of the combination of $(\tau^z_1 + \tau^z_2)$ with P_{12}, for the equation (A.3) and for the easly demonstrable condition

$$\sum_i \phi_i(r,\sigma)\tilde{\phi}_i(r,\sigma) = 0 \qquad (A.6)$$

for which the terms containing Pauli matrices do not contribute, one finally obtains:

$$E^{(0)}_{CSB} = \frac{1}{2}\sum_{ij} \langle ij\,|\,(\tau^z_1 + \tau^z_2)\ (r_1 - r_2)\, s_0\ 1 + y_0 P^{12} - P^{12}(y_0 + P^{12})\,|\,ij\rangle =$$

$$= \frac{1}{2}\sum_{ij} \langle ij\,|\,(\tau^z_1 + \tau^z_2)\ (r_1 - r_2)\, s_0\ \frac{1 - y_0}{2}\,|\,ij\rangle$$

Because of the symmetry of the indices 1 and 2 in the isospin operator, two identical contributions are obtained, one for τ^z_1 and one for τ^z_2; so the substitution $\tau^z_1 + \tau^z_2 = 2\,\tau^z_1$ is allowed. Therefore:

$$E^{(0)}_{CSB} = \sum_{ij} \langle ij\,|\,(r_1 - r_2)\ \tau^z_1 s_0\ \frac{1 - y_0}{2}\,|\,ij\rangle =$$

$$= s_0 \int d^3r_1 \int d^3r_2\ (r_1 - r_2) \sum_{ij} (\phi^*_i(r_1)\,\tau^z_1\,\phi_i(r_1))(\phi^*_j(r_2)\phi_j(r_2))\ \frac{1 - y_0}{2}$$

And finally, after removing the delta on the positions as well,

$$E^{(0)}_{CSB} = \int d^3r\, \frac{s_0(1 - y_0)}{2}\ \rho^2_n(r) - \rho^2_p(r) \qquad (A.7)$$

where the definition of density

$$\rho_q(r) = \sum_i |\phi_i(r,\sigma,q)|^2$$

has been used. In the last step $\rho^2_n(r)$ and $\rho^2_p(r)$ are defined as the neutron and proton densities, respectively.

A.1.2 First Momentum-Dependent CSB term (/ s_1)

$$E^{(1)}_{CSB} = \frac{1}{2}\sum_{ij} \langle ij\,|\,(\tau^z_1 + \tau^z_2)\ (r_1 - r_2)\,\frac{s_1}{2}\ 1 + y_1 P^{12}\ k^2 + k'^2\ (1 - P^{12}_r P^{12} P^{12})\,|\,ij\rangle =$$

$$= \frac{s_1}{16}\sum_{ij} \langle ij\,|\,(\tau^z_1 + \tau^z_2)\ (r_1 - r_2)(r^2_1 + r^2_2 - 2\vec{r}_1\vec{r}_2)\ 1 + y_1 P^{12}\ (1 - P^{12} P^{12})\,|\,ij\rangle + \text{H.c.} \qquad (A.8)$$

Where H.c. in Eq. (A.8) denotes the Hermitian conjugate of the rst term and it contributes in the same way. Here again, the terms containing Pauli matrices does not contribute when combined with r_1^2 and r_2^2 because of (A.6); so, one can divide $E_{CSB}^{(1)}$ into two components:

$$\frac{s_1}{16}\sum_{ij} \langle ij|(\tau_{z1}+\tau_{z2})(\delta_1-\delta_2)(r_1^2+r_2^2-2\vec{r}_1\cdot\vec{r}_2)\left(1+\frac{y_1}{2}-P^{12}\left(y_1+\frac{1}{2}\right)\right)|ij\rangle$$

$$+\frac{s_1}{16}\sum_{ij}\langle ij|(\tau_{z1}+\tau_{z2})(\delta_1-\delta_2)(\vec{r}_1-\vec{r}_2)\cdot(\vec{\sigma}_1-\vec{\sigma}_2)\left(y_1-P^{12}\right)|ij\rangle \qquad (A.9)$$

In order to calculate the rst term of (A.9), the following properties must be used:

$\sum_i \psi_i(\vec{r})r^2\psi_i(\vec{r}) = \frac{1}{2}r^2\rho(\vec{r}) - K(\vec{r})$, where $K_q(\vec{r}) = \sum_{i,\sigma}|\vec{\nabla}\psi_i(\vec{r},\sigma,q)|^2$ is the kinetic energy density density;

Owing to time-reversal invariance, $\sum_i \psi_i(\vec{r})\vec{\nabla}\psi_i(\vec{r}) = \frac{1}{2}\vec{\nabla}\rho(\vec{r})$;

Equation (A.3);

The Green formula for integration by parts: $\int(\vec{\nabla}v\cdot\vec{\nabla}u)\,d^3x = \int_{@}v\vec{\nabla}u\,d\vec{S} - \int(v\nabla^2u)\,d^3x$ where the border term is null.

For the rst term, it is useful to divide it again into two parts. It is important to notice that the contribution of τ_{z1} is equal to the contribution of τ_{z2} and that the contribution r_1^2 is equal to r_2^2, namely

$$(r_1^2+r_2^2)(\tau_{z1}+\tau_{z2}) = r_1^2\tau_{z1}+r_1^2\tau_{z2}+r_2^2\tau_{z1}+r_2^2\tau_{z2} = 2(r_1^2\tau_{z1}+r_1^2\tau_{z2})$$

that is, in the last step we have that the contributions of the rst with the fourth term and the second with the third are equal. Then, the rst part is given by

$$\frac{s_1}{8}\int d^3r_1\int d^3r_2\,(\delta_1-\delta_2)\sum_{ij}\psi_i(\vec{r}_1)r_1^2\tau_{z1}\psi_i(\vec{r}_1)\psi_j(\vec{r}_2)\psi_j(\vec{r}_2)\left(\frac{1-y_1}{2}\right)$$

$$\frac{s_1}{8}\int d^3r_1\int d^3r_2\,(\delta_1-\delta_2)\sum_{ij}\psi_i(\vec{r}_1)r_1^2\psi_i(\vec{r}_1)\psi_j(\vec{r}_2)\tau_{z2}\psi_j(\vec{r}_2)\left(\frac{1-y_1}{2}\right) =$$

Then

$$= \frac{s_1}{8}\int d^3r\left(\frac{1-y_1}{2}\right)\left(\frac{1}{2}r^2\rho_n(\vec{r})-K_n(\vec{r})-\frac{1}{2}r^2\rho_p(\vec{r})+K_p(\vec{r})\right)(\rho_n(\vec{r})+\rho_p(\vec{r}))$$

$$\frac{s_1}{8}\int d^3r\left(\frac{1-y_1}{2}\right)\left(\frac{1}{2}r^2\rho_n(\vec{r})-K_n(\vec{r})+\frac{1}{2}r^2\rho_p(\vec{r})-K_p(\vec{r})\right)(\rho_n(\vec{r})-\rho_p(\vec{r})) =$$

The rst part of this term is given by

$$= \int d^3r\,\frac{s_1(1-y_1)}{16}\left(\rho_n(\vec{r})r^2\rho_n(\vec{r})-\rho_p(\vec{r})r^2\rho_p(\vec{r})-2\rho_n(\vec{r})K_n(\vec{r})+2\rho_p(\vec{r})K_p(\vec{r})\right)$$

Secondly, the part containing the product of the nablas gives the following contribution:

$$\frac{s_1}{8}\sum_{ij}\langle ij|(\hat{\tau}_1+\hat{\tau}_2)\,(\hat{r}_1-\hat{r}_2)\,\vec{\nabla}_1\,\vec{\nabla}_2\,\frac{1-y_1}{2}|ij\rangle =$$

$$\frac{s_1}{4}\int d^3r_1\int d^3r_2\,(\hat{r}_1-\hat{r}_2)\sum_{ij}\varphi_i(\hat{r}_1)\vec{\nabla}_1\frac{\vec{\nabla}_1}{1}\varphi_i(\hat{r}_1)\;\;\varphi_j(\hat{r}_2)\vec{\nabla}_2\varphi_j(\hat{r}_2)\;\;\frac{1-y_1}{2}=$$

$$\frac{s_1}{4}\int d^3r\;\;\frac{1-y_1}{2}\;\;\frac{1}{4}\Big[\vec{\nabla}\rho_n(\hat{r})\;\;\vec{\nabla}\rho_p(\hat{r})\Big]\Big[\vec{\nabla}\rho_n(\hat{r})+\vec{\nabla}\rho_p(\hat{r})\Big]=$$

$$\frac{s_1}{16}\int d^3r\;\;\frac{1-y_1}{2}\;\;\Big[(\vec{\nabla}\rho_n(\hat{r}))^2\;\;(\vec{\nabla}\rho_p(\hat{r}))^2\Big]$$

which, to be added to the previous one, must be integrated by parts with the Green formula, obtaining

$$\frac{s_1}{16}\int d^3r\;\;\frac{1-y_1}{2}\;\;\frac{1}{2}\rho_n(\hat{r})\nabla^2\rho_n(\hat{r})\;\;\frac{1}{2}\rho_p(\hat{r})\nabla^2\rho_p(\hat{r})$$

Then, the first term becomes

$$\int d^3r\;\;\frac{s_1(1-y_1)}{16}\;\;\frac{3}{2}\rho_n(\hat{r})\nabla^2\rho_n(\hat{r})\;\;\frac{3}{2}\rho_p(\hat{r})\nabla^2\rho_p(\hat{r})\;\;2\rho_n(\hat{r})K_n(\hat{r})+2\rho_p(\hat{r})K_p(\hat{r}) \tag{A.10}$$

The second term in (A.9) is evaluated by using the identity

$$(\hat{r}_1-\hat{r}_2)(\vec{\sigma}_1-\vec{\sigma}_2)=\frac{1}{3}(\hat{r}_1-\vec{\sigma}_1)(\hat{r}_2-\vec{\sigma}_2)+\frac{1}{2}(\hat{r}_1-\vec{\sigma}_1)\;\;(\hat{r}_2-\vec{\sigma}_2)+(\hat{r}_1-\vec{\sigma}_1)^{(2)}\;\;(\hat{r}_2-\vec{\sigma}_2)^{(2)}$$

One can find out that the quantities $\sum_i\varphi_i(\hat{r})(\hat{r}-\vec{\sigma})\vec{\nabla}\varphi_i(\hat{r})$ and $\sum_i\varphi_i(\hat{r})(\hat{r}-\vec{\sigma})^{(2)}\vec{\nabla}\varphi_i(\hat{r})$ vanish identically, because of the assumptions made so far and (A.6). Remebering the definition of spin density:

$$\vec{J}_q=(-i)\sum_{i;\sigma;\sigma'}\varphi_i(\hat{r};\sigma;q)\,\vec{\nabla}\varphi_i(\hat{r};\sigma',q)\,\langle\sigma'|\vec{\sigma}|\sigma\rangle$$

the second term is calculated as follows:

$$\frac{s_1}{16}\langle ij|(\hat{\tau}_1+\hat{\tau}_2)\,(\hat{r}_1-\hat{r}_2)(\vec{\sigma}_1-\vec{\sigma}_2)\;\;y_1\;\;P^{12}|ij\rangle =$$

$$=\frac{s_1}{16}\langle ij|\hat{\tau}_1\frac{\vec{\sigma}_1}{1}\,(\hat{r}_1-\hat{r}_2)(\vec{\sigma}_1-\vec{\sigma}_2)\,(\hat{r}_2-\vec{\sigma}_2)(y_1-1)|ij\rangle =$$

$$=\frac{s_1}{16}\int d^3r_1\,d^3r_2\,(\hat{r}_1-\hat{r}_2)\sum_{ij}\varphi_i(\hat{r}_1)(\vec{\sigma}_1-\vec{\sigma}_1)\frac{\vec{\sigma}_1}{1}\varphi_i(\hat{r}_1)\;\;\varphi_j(\hat{r}_2)(\vec{\sigma}_2-\vec{\sigma}_2)\varphi_j(\hat{r}_2)\;\;(y_1-1)=$$

$$=\frac{s_1}{16}\int d^3r(1-y_1)\;\vec{J}_n(\hat{r})\;\;\vec{J}_p(\hat{r})\;\;\vec{J}_n(\hat{r})+\vec{J}_p(\hat{r})\;=$$

$$=\int d^3r\,\frac{s_1(1-y_1)}{16}\;\;J_n^2(\hat{r})\;\;J_p^2(\hat{r})$$

Collecting all the previous terms and adding their Hermitian conjugates, one obtain the result for the equation (A.8):

$$E^{(1)}_{CSB} = \int d^3r \frac{s_1(1 \quad y_1)}{8} \quad \frac{3}{2} \ _n(\mathbf{r}) r^{\ 2} \ _n(\mathbf{r}) + \frac{3}{2} \ _p(\mathbf{r}) r^{\ 2} \ _p(\mathbf{r}) + 2 \ _n(\mathbf{r}) K_n(\mathbf{r}) \quad 2 \ _p(\mathbf{r}) K_p(\mathbf{r}) + \quad J_n^2(\mathbf{r}) \quad J_p^2(\mathbf{r}) \tag{A.11}$$

A.1.3 Second Momentum-Dependent CSB term (/ s_2)

$$E^{(2)}_{CSB} = \frac{1}{2} \sum_{ij} \ hij \ j(\ ^z_1 + \ ^z_2) \ (\mathbf{r}_1 \quad \mathbf{r}_2) s_2 \ 1 + y_2 P^{12} \quad k^2 \ k^{y2} \ (1 \quad P_r^{12} P^{12} P^{12}) jij \ i$$

In this case is important to notice that the operator $k^2 \ k^{y2}$ is antisymmetric under exchange of the spatial coordinates, so it is necessary to substitute P^{12} with -1. In this way, using the symmetry between the indices 1 and 2, one obtains:

$$E^{(2)}_{CSB} = \frac{s_2}{4} \sum_{ij} \ hij \ j(\ ^z_1 + \ ^z_2) \ (\mathbf{r}_1 \quad \mathbf{r}_2)(\tilde{r}^y_1 \ \tilde{r}_1 \quad \tilde{r}^y_2 \ \tilde{r}_1) \ 1 + y_2 P^{12} \ (1 \quad P_r^{12} P^{12} P^{12}) jij \ i \tag{A.12}$$

where in this equation, one can write the following product as:

$$1 + y_2 P^{12} \ (1 \quad P_r^{12} P^{12} P^{12}) = \ 1 + \frac{y_2}{2} + P^{12} \ y_2 + \frac{1}{2} \ + \frac{1}{2}(\sigma_1 \ \sigma_2)(y_2 + P^{12})$$

Keeping in mind again that the terms containing Pauli matrices contribute only when combined with $\tilde{r}_1 \ \tilde{r}_2$, it is useful to divide (A.12) into two parts:

$$E^{(2)}_{CSB} = \frac{s_2}{4} \sum_{ij} \ hij \ j(\ ^z_1 + \ ^z_2) \ (\mathbf{r}_1 \quad \mathbf{r}_2)(\tilde{r}^y_1 \ \tilde{r}_1 \quad \tilde{r}^y_2 \ \tilde{r}_1) \ 1 + \frac{y_2}{2} + P^{12} \ y_2 + \frac{1}{2} \quad jij \ i$$

$$\frac{s_2}{8} \sum_{ij} \ hij \ j(\ ^z_1 + \ ^z_2) \ (\mathbf{r}_1 \quad \mathbf{r}_2)(\tilde{r}^y_2 \ \tilde{r}_1)(\sigma_1 \ \sigma_2)(y_2 + P^{12}) jij \ i \tag{A.13}$$

In this way, the evaluation of the two terms in (A.13) is easy because is very similar to the calculation of the preceding energy density /(s_1). Infact, the rst term is equal to

$$\int d^3r \frac{3s_2(1 + y_2)}{8} \ (K_n(\mathbf{r}) \quad K_p(\mathbf{r})) \ (\mathbf{r}) + K(\mathbf{r})(\ _n(\mathbf{r}) \quad \ _p(\mathbf{r})) \quad \frac{1}{2}\tilde{r} \ (\mathbf{r}) \ (\tilde{r} \ _n(\mathbf{r}) \quad \tilde{r} \ _p(\mathbf{r}))$$

where $(\mathbf{r})$, $K(\mathbf{r})$ and $\tilde{r} \ (\mathbf{r})$ represent the total quantities, namely, the sum of the same contributions from neutrons and protons. Carrying out an integration by parts, the rst term in (A.13) is given by:

$$\int d^3r \frac{3s_2(1 + y_2)}{8} \ 2K_n(\mathbf{r}) \ _n(\mathbf{r}) \quad 2K_p(\mathbf{r}) \ _p(\mathbf{r}) + \frac{1}{2} \ _n(\mathbf{r}) r^{\ 2} \ _n(\mathbf{r}) \quad \frac{1}{2} \ _p(\mathbf{r}) r^{\ 2} \ _p(\mathbf{r})$$

As was done previously, in order to calculate the second term in (A.13), one must develop again the operator $(\vec{r}_2^{\,y} - \vec{r}_1)(\vec{\sigma}_1 \cdot \vec{\sigma}_2)$, obtaining

$$\frac{s_2}{16}\sum_{ij} \langle i|\tau_j|(\tau_1^z + \tau_2^z)\,(\vec{r}_1 - \vec{r}_2)(\vec{r}_1 - \vec{\sigma}_1)\,(\vec{r}_2 - \vec{\sigma}_2)(y_2 + 1)|j\rangle|i\rangle =$$

$$\frac{s_2}{8}\int d^3r\,(1 + y_2)\,J_n^2(\vec{r}) - J_p^2(\vec{r})$$

In the end the equation (A.12) becomes

$$\begin{aligned} E_{CSB}^{(2)} = \int d^3r\, & \frac{s_2(1 + y_2)}{8}\,\big[6K_n(\vec{r})\,\rho_n(\vec{r}) - 6K_p(\vec{r})\,\rho_p(\vec{r}) \\ & + \frac{3}{2}\rho_n(\vec{r})\nabla^2\rho_n(\vec{r}) - \frac{3}{2}\rho_p(\vec{r})\nabla^2\rho_p(\vec{r}) - J_n^2(\vec{r}) + J_p^2(\vec{r})\big] \end{aligned} \tag{A.14}$$

A.1.4 Summary

Adding all the contributions of the equations (A.7), (A.11) and (A.14), one obtains the total CSB energy density:

$$\begin{aligned} E_{CSB} = \int d^3r\, & \Big[\frac{s_0(1 - y_0)}{2}\,\rho_n^2(\vec{r}) - \rho_p^2(\vec{r}) \\ & + \frac{s_1(1 - y_1)}{8}\Big[\frac{3}{2}\rho_n(\vec{r})\nabla^2\rho_n(\vec{r}) + \frac{3}{2}\rho_p(\vec{r})\nabla^2\rho_p(\vec{r}) \\ & + 2\rho_n(\vec{r})K_n(\vec{r}) - 2\rho_p(\vec{r})K_p(\vec{r}) + J_n^2(\vec{r}) - J_p^2(\vec{r})\Big] \\ & + \frac{s_2(1 + y_2)}{8}\,\big[6K_n(\vec{r})\,\rho_n(\vec{r}) - 6K_p(\vec{r})\,\rho_p(\vec{r}) \\ & + \frac{3}{2}\rho_n(\vec{r})\nabla^2\rho_n(\vec{r}) - \frac{3}{2}\rho_p(\vec{r})\nabla^2\rho_p(\vec{r}) - J_n^2(\vec{r}) + J_p^2(\vec{r})\big]\Big] \end{aligned} \tag{A.15}$$

A.2 CIB Energy Density

The CIB contribution to energy density is then calculated as follows:

$$\begin{aligned} E_{CIB} &= \frac{1}{2}\sum_{ij} \langle ij|v_{CIB}(1;2)|ij\rangle_{AS} = \\ &= \frac{1}{2}\sum_{ij} \langle ij|\left(v^{(0)}_{CIB}(1;2) + v^{(1)}_{CIB}(1;2) + v^{(2)}_{CIB}(1;2)\right)|ij\rangle_{AS} = \\ &= E^{(0)}_{CIB} + E^{(1)}_{CIB} + E^{(2)}_{CIB} \end{aligned} \tag{A.16}$$

Now, as the case of the CSB, all the terms are calculated separately. Each consideration previously made about the operators, holds on.

A.2.1 Central CIB term (/ u_0)

$$E^{(0)}_{CIB} = \frac{1}{2}\sum_{ij} \langle ij|(\tau_{z1}\tau_{z2})\,(r_1 - r_2)\,u_0\,[1 + z_0 P^{12}]\,|ij\rangle_{AS} =$$

$$= \frac{1}{2}\sum_{ij} \langle ij|(\tau_{z1}\tau_{z2})\,(r_1 - r_2)\,u_0\,[1 + z_0 P^{12} - P^{12}(z_0 + P^{12})]\,|ij\rangle$$

In this case again, all the terms containing the Pauli matrices do not contribute to energy. For all the CIB term it is important remember the property (A.4). Then it is convenient to divide $E^{(0)}_{CIB}$ into two components:

$$E^{(0)}_{CIB} = \frac{u_0}{2}\sum_{ij} \langle ij|(\tau_{z1}\tau_{z2})\,(r_1 - r_2)\,\left[1 + \frac{z_0}{2}\right]|ij\rangle - \frac{u_0}{2}\sum_{ij} \langle ij|\,(r_1 - r_2)P^{12}\,\left[z_0 + \frac{1}{2}\right]|ij\rangle =$$

$$= \frac{u_0}{2}\int d^3r_1 \int d^3r_2\,(r_1 - r_2)\sum_{ij}(\psi_i(r_1)\,\tau_{z1}\psi_i(r_1))(\psi_j(r_2)\,\tau_{z2}\psi_j(r_2))\left[1 + \frac{z_0}{2}\right]$$

$$\frac{u_0}{2}\int d^3r_1 \int d^3r_2\,(r_1 - r_2)\sum_{ij}(\psi_i(r_1)\psi_i(r_1))(\psi_j(r_2)\psi_j(r_2))\,q_i q_j\,\left[z_0 + \frac{1}{2}\right] =$$

By using the de nition of density, (see above):

$$= \frac{u_0}{2}\int d^3r\,\left[1 + \frac{z_0}{2}\right](\rho_n(r) - \rho_p(r))(\rho_n(r) - \rho_p(r))\left[z_0 + \frac{1}{2}\right] - \rho^2_n(r) + \rho^2_p(r)$$

Then nally

$$E^{(0)}_{CIB} = \int d^3r\,\frac{u_0(1 - z_0)}{4}\,\rho^2_n(r) + \rho^2_p(r) - u_0\left[1 + \frac{z_0}{2}\right]\rho_n(r)\,\rho_p(r) \tag{A.17}$$

A.2.2 First Momentum-Dependent CIB term (/ u_1)

$$E^{(1)}_{CIB} = \frac{1}{2}\sum_{ij} \hbar ij\, j(\ ^{z}_{1}\ ^{z}_{2})\ \ (\text{ŕ}_1 \quad \text{ŕ}_2)\,\frac{u_1}{2}\ 1 + z_1 P^{12} \quad k^2 + k^{y2}\ \ (1 \quad P_r^{12}P^{12})jij\, i \qquad (A.18)$$

The calculation of this term is very similar to the one made for $E^{(1)}_{CSB}$.

$$E^{(1)}_{CIB} = \frac{u_1}{4}\sum_{ij} \hbar ij\, j(\ ^{z}_{1}\ ^{z}_{2})\ \ (\text{ŕ}_1 \quad \text{ŕ}_2)\, k^2\ 1 + z_1 P^{12} \quad P^{12}\ z_1 P_r + P^{12} P_r \quad jij\, i + H.c. \qquad (A.19)$$

Then it is convenient to write (A.19) into two parts,taking into account (A.4), i.e. one depending on the operator $(\ ^{z}_{1}\ ^{z}_{2})$ and one on the exchange isospin operator:

$$E^{(1)}_{CIB} = \frac{u_1}{4}\sum_{ij} \hbar ij\, j(\ ^{z}_{1}\ ^{z}_{2})\ \ (\text{ŕ}_1 \quad \text{ŕ}_2)\, k^2 \overset{h}{1} + \frac{z_1}{2} + \frac{z_1}{2}(\tilde{}_1 \quad \tilde{}_2) \overset{i}{} jij\, i + H.c.$$

$$\frac{u_1}{4}\sum_{ij} \hbar ij P^{12}\ \ (\text{ŕ}_1 \quad \text{ŕ}_2)\, k^2\ z_1 + \frac{1}{2} + \frac{1}{2}(\tilde{}_1 \quad \tilde{}_2)\ \ jij\, i + H.c.$$

Now it is useful divide again into the part which does not contain the Pauli matrices and one which does:

$$\frac{u_1}{4}\sum_{ij} \hbar ij\ \ (\text{ŕ}_1 \quad \text{ŕ}_2)\, k^2\ \ (\ ^{z}_{1}\ ^{z}_{2})\ \ 1 + \frac{z_1}{2} \quad P^{12}\ \ z_1 + \frac{1}{2} \quad jij\, i + H.c. =$$

$$+ \frac{u_1}{4}\sum_{ij} \hbar ij\ \ (\text{ŕ}_1 \quad \text{ŕ}_2) k^2 \frac{1}{2}(\tilde{}_1 \quad \tilde{}_2)\ \ ^{z}_{1}\ ^{z}_{2} z_1 \quad P^{12}\ jij\, i + H.c. \qquad (A.20)$$

Now, in the equation (A.20), one can substitute the isospin exchange operator with $\sigma_i \sigma_j$. In this way the rst term in (A.20) becomes (without considering the Hermitian conjugate for now):

$$\frac{u_1}{16}\sum_{ij} \hbar ij\ \ (\text{ŕ}_1 \quad \text{ŕ}_2)(r\ ^{2}_{1} + r\ ^{2}_{2} \quad 2\tilde{r}_1\ \tilde{r}_2)\ \ (\ ^{z}_{1}\ ^{z}_{2})\ \ 1 + \frac{z_1}{2} \quad P^{12}\ \ z_1 + \frac{1}{2} \quad jij\, i$$

It can be noted that there is a symmetry between the indices 1 and 2, so one can substitute $r\ ^{2}_{1} + r\ ^{2}_{2} = 2r\ ^{2}_{1}$:

$$\frac{u_1}{8}\sum_{ij} \hbar ij\ \ (\text{ŕ}_1 \quad \text{ŕ}_2) r\ ^{2}_{1}\ \ (\ ^{z}_{1}\ ^{z}_{2})\ \ 1 + \frac{z_1}{2} \quad P^{12}\ \ z_1 + \frac{1}{2} \quad jij\, i$$

$$+ \frac{u_1}{8}\sum_{ij} \hbar ij\ \ (\text{ŕ}_1 \quad \text{ŕ}_2)(\tilde{r}_1\ \tilde{r}_2)\ \ (\ ^{z}_{1}\ ^{z}_{2})\ \ 1 + \frac{z_1}{2} \quad P^{12}\ \ z_1 + \frac{1}{2} \quad jij\, i =$$

So, four terms are obtained:

$$\frac{u_1}{8}\int d^3r_1 \int d^3r_2\ (\text{ŕ}_1 \quad \text{ŕ}_2)\sum_{ij}\ '_i(\text{ŕ}_1) r\ ^{2}_{1}\ ^{z}_{1}\, '_i(\text{ŕ}_1) \quad '_j(\text{ŕ}_2)\ ^{z}_{2}\, '_j(\text{ŕ}_2) \quad 1 + \frac{z_1}{2}$$

$$+\frac{u_1}{8}\int d^3r_1\int d^3r_2\ (\mathbf{r}_1-\mathbf{r}_2)\sum_{ij}\ '_i(\mathbf{r}_1)r_1^2\,'_i(\mathbf{r}_1)\ \ '_j(\mathbf{r}_2)'_j(\mathbf{r}_2)\quad q_iq_j\quad z_1+\frac{1}{2}$$

$$+\frac{u_1}{8}\int d^3r_1\int d^3r_2\ (\mathbf{r}_1-\mathbf{r}_2)\sum_{ij}\ '_i(\mathbf{r}_1)\tilde{r}_1\tfrac{z}{1}'_i(\mathbf{r}_1)\quad '_j(\mathbf{r}_2)\tilde{r}_2\tfrac{z}{2}'_j(\mathbf{r}_2)\quad 1+\frac{z_1}{2}$$

$$\frac{u_1}{8}\int d^3r_1\int d^3r_2\ (\mathbf{r}_1-\mathbf{r}_2)\sum_{ij}\ '_i(\mathbf{r}_1)\tilde{r}_1'_i(\mathbf{r}_1)\quad '_j(\mathbf{r}_2)\tilde{r}_2'_j(\mathbf{r}_2)\quad q_iq_j\quad z_1+\frac{1}{2}\ =$$

So,

$$\frac{u_1}{8}\int d^3r\ \ 1+\frac{z_1}{2}\quad\frac{1}{2}r^2{}_n(\mathbf{r})\quad K_n(\mathbf{r})\quad\frac{1}{2}r^2{}_p(\mathbf{r})+K_p(\mathbf{r})\quad(\ {}_n(\mathbf{r})\quad{}_p(\mathbf{r}))$$

$$+\frac{u_1}{8}\int d^3r\ \ z_1+\frac{1}{2}\quad\frac{1}{2}\,{}_n(\mathbf{r})r^2{}_n(\mathbf{r})+\frac{1}{2}\,{}_p(\mathbf{r})r^2{}_p(\mathbf{r})\quad K_n(\mathbf{r})\,{}_n(\mathbf{r})\quad K_p(\mathbf{r})\,{}_p(\mathbf{r})$$

$$+\frac{u_1}{8}\int d^3r\ \ 1+\frac{z_1}{2}\quad\frac{1}{4}\quad\tilde{r}\,{}_n(\mathbf{r})\quad\tilde{r}\,{}_p(\mathbf{r})\quad\tilde{r}\,{}_n(\mathbf{r})\quad\tilde{r}\,{}_p(\mathbf{r})$$

$$+\frac{u_1}{8}\int d^3r\ \ z_1+\frac{1}{2}\quad\frac{1}{4}\quad(\tilde{r}\,{}_n(\mathbf{r}))^2\quad(\tilde{r}\,{}_p(\mathbf{r}))^2$$

Then, adding all the term and after an integration by parts, the first term in (A.20) (without the Hermitian conjugate)

$$\int d^3r\,\frac{u_1}{16}\quad\frac{1\quad z_1}{2}\qquad\frac{3}{2}\,{}_n(\mathbf{r})r^2{}_n(\mathbf{r})\quad\frac{3}{2}\,{}_p(\mathbf{r})r^2{}_p(\mathbf{r})+2\,K_n(\mathbf{r})\,{}_n(\mathbf{r})+2\,K_p(\mathbf{r})\,{}_p(\mathbf{r})$$
$$+\quad 1+\frac{z_1}{2}\quad\frac{3}{2}\,{}_n(\mathbf{r})r^2{}_p(\mathbf{r})+\frac{3}{2}\,{}_p(\mathbf{r})r^2{}_n(\mathbf{r})\quad 2K_p(\mathbf{r})\,{}_n(\mathbf{r})\quad 2K_p(\mathbf{r})\,{}_n(\mathbf{r})$$

While the term containing the product $(\tilde{r}_1\quad\tilde{r}_2)(\sim_1\quad\sim_2)$ becomes:

$$\frac{u_1}{32}\sum_{ij}\ \hbar ij\ j\ \ (\mathbf{r}_1\quad\mathbf{r}_2)(\tilde{r}_1\quad\sim_1)\ \ (\tilde{r}_2\quad\sim_2)\ \ z_1(\ \tfrac{z}{1}\ \tfrac{z}{2})\quad q_iq_j\quad jij\ i\ =$$

$$\frac{u_1}{32}\int d^3r_1\int d^3r_2\ (\mathbf{r}_1-\mathbf{r}_2)\sum_{ij}\ z_1\ '_i(\mathbf{r}_1)(\tilde{r}_1\quad\sim_1)\ \tfrac{z}{1}'_i(\mathbf{r}_1)\quad '_j(\mathbf{r}_2)(\tilde{r}_2\quad\sim_2)\ \tfrac{z}{2}'_j(\mathbf{r}_2)$$

$$\frac{u_1}{32}\int d^3r_1\int d^3r_2\ (\mathbf{r}_1-\mathbf{r}_2)\sum_{ij}\ '_i(\mathbf{r}_1)(\tilde{r}_1\quad\sim_1)'_i(\mathbf{r}_1)\quad '_j(\mathbf{r}_2)(\tilde{r}_2\quad\sim_2)'_j(\mathbf{r}_2)\quad q_iq_j\ =$$

$$=\frac{u_1}{32}\int d^3r\ \ (1\quad z_1)(J_n^2(\mathbf{r})+J_p^2(\mathbf{r}))+2\,z_1\mathfrak{J}_n(\mathbf{r})\quad\mathfrak{J}_p(\mathbf{r})$$

In conclusion, taking into account the H.c. part, $E^{(1)}_{CIB}$ is given by:

$$E^{(1)}_{CIB} = \int d^3r \frac{u_1}{16}\,(1 - z_1)\left(\frac{3}{2}\,\rho_n(\vec{r})\,\vec{r}^{\,2}\,\rho_n(\vec{r}) - \frac{3}{2}\,\rho_p(\vec{r})\,\vec{r}^{\,2}\,\rho_p(\vec{r}) + 2K_n(\vec{r})\,\rho_n(\vec{r}) + 2K_p(\vec{r})\,\rho_p(\vec{r})\right)$$
$$(2 + z_1)\left(\frac{3}{2}\,\rho_n(\vec{r})\,\vec{r}^{\,2}\,\rho_p(\vec{r}) + \frac{3}{2}\,\rho_p(\vec{r})\,\vec{r}^{\,2}\,\rho_n(\vec{r}) - 2K_p(\vec{r})\,\rho_n(\vec{r}) - 2K_p(\vec{r})\,\rho_n(\vec{r})\right)$$
$$+ (1 - z_1)(J_n^2(\vec{r}) + J_p^2(\vec{r})) + 2\,z_1 J_n(\vec{r})\,J_p(\vec{r}) \qquad \text{(A.21)}$$

A.2.3 Second Momentum-Dependent CIB term (/ u_2)

Now the calculation of the last term starts here:

$$E^{(2)}_{CIB} = \frac{1}{2}\sum_{ij} \langle ij\,|\,\tau_1^z\,\tau_2^z\,\frac{1}{3}\vec{\sigma}_1\cdot\vec{\sigma}_2\,(\vec{r}_1 - \vec{r}_2)\,u_2\,[1 + z_2 P^{12}]\,k^2\,k'^2\,(1 - P_r^{12}P^{12}P^{12})|ij\rangle$$

In this case is important to notice that the operator $k^2\,k'^2$ is antisymmetric under exchange of the spatial coordinates, so it is necessary to substitute $\vec{P}^2$ with -1. Using the symmetry between the indices 1 and 2, one obtains:

$$E^{(2)}_{CIB} = \frac{u_2}{4}\sum_{ij} \langle ij\,|\,(\tau_1^z\,\tau_2^z)\,(\vec{r}_1 - \vec{r}_2)\,(\vec{r}'^{\,y}_1\,\vec{r}'_1 - \vec{r}'^{\,y}_2\,\vec{r}'_1)\,[1 + z_2 P^{12}]\,(1 - P_r^{12}P^{12}P^{12})|ij\rangle \qquad \text{(A.22)}$$

Keeping in mind again that the terms containing Pauli matrices contribute only when combined with $\vec{r}'^{\,y}_2\,\vec{r}'_1$, it is useful to divide (A.22) into two parts:

$$E^{(2)}_{CIB} = \frac{u_2}{4}\sum_{ij} \langle ij\,|\,(\tau_1^z\,\tau_2^z)\,(\vec{r}_1 - \vec{r}_2)\,(\vec{r}'^{\,y}_1\,\vec{r}'_1 - \vec{r}'^{\,y}_2\,\vec{r}'_1)\,\left[1 + \frac{z_2}{2} + P^{12}\left(z_2 + \frac{1}{2}\right)\right]|ij\rangle$$
$$- \frac{u_2}{8}\sum_{ij} \langle ij\,|\,(\tau_1^z\,\tau_2^z)\,(\vec{r}_1 - \vec{r}_2)\,(\vec{r}'^{\,y}_2\,\vec{r}'_1)(\vec{\sigma}_1\cdot\vec{\sigma}_2)(z_2 + P^{12})|ij\rangle \qquad \text{(A.23)}$$

In this way, the evaluation of the two terms in (A.23) is easy because is very similar to the calculation of the preceding energy density /(u_1). Infact, the rst term is equal to

$$\int d^3r\,\frac{3u_2(1 + z_2)}{8}\,K_n(\vec{r})\,\rho_n(\vec{r}) + K_p(\vec{r})\,\rho_p(\vec{r})\,\frac{1}{4}\,(\vec{\nabla}\rho_n(\vec{r}))^2 + (\vec{\nabla}\rho_p(\vec{r}))^2$$
$$+ \frac{u_2(2 + z_2)}{8}\,\frac{1}{4}\,\vec{\nabla}\rho_n(\vec{r})\,\vec{\nabla}\rho_p(\vec{r}) + \vec{\nabla}\rho_p(\vec{r})\,\vec{\nabla}\rho_n(\vec{r})\,(K_n(\vec{r})\,\rho_p(\vec{r}) + K_p(\vec{r})\,\rho_n(\vec{r}))$$

Carrying out an integration by parts, the rst term in (A.13) is given by:

$$\int d^3r\,\frac{3u_2(1 + y_2)}{8}\,K_n(\vec{r})\,\rho_n(\vec{r}) + K_p(\vec{r})\,\rho_p(\vec{r}) + \frac{1}{4}\,\rho_n(\vec{r})\,\vec{r}^{\,2}\,\rho_n(\vec{r}) + \rho_n(\vec{r})\,\vec{r}^{\,2}\,\rho_n(\vec{r})$$
$$\frac{u_2(2 + z_2)}{8}\,\frac{1}{4}\,\rho_n(\vec{r})\,\vec{r}^{\,2}\,\rho_p(\vec{r}) + \rho_p(\vec{r})\,\vec{r}^{\,2}\,\rho_n(\vec{r}) + (K_n(\vec{r})\,\rho_p(\vec{r}) + K_p(\vec{r})\,\rho_n(\vec{r}))$$

As was done previously, in order to calculate the second term in (A.23), one must develop again the operator $(\vec{r}_2^{\,y} - \vec{r}_1)(\vec{\tau}_1 \cdot \vec{\tau}_2)$, obtaining

$$\frac{u_2}{16}\sum_{ij}\langle ij|(\vec{\sigma}_1\cdot\vec{\sigma}_2)(\vec{\tau}_1\cdot\vec{\tau}_2)(\vec{r}_1-\vec{r}_2)(\vec{r}_1-\vec{r}_2)(z_2+P^{12})|ij\rangle =$$

$$\frac{u_2}{16}\int d^3r\,\Big[(1+z_2)\,J_n^2(\vec{r})+J_p^2(\vec{r})-2z_2\vec{J}_n(\vec{r})\cdot\vec{J}_p(\vec{r})\Big]$$

In the end the equation (A.22) becomes

$$\begin{aligned}E^{(2)}_{CIB} = \int d^3r\;&\frac{3u_2(1+y_2)}{8}\,K_n(\vec{r})\,\rho_n(\vec{r})+K_p(\vec{r})\,\rho_p(\vec{r})+\frac{1}{4}\,\rho_n(\vec{r})\nabla^2\rho_n(\vec{r})+\rho_n(\vec{r})\nabla^2\rho_n(\vec{r})\\&-\frac{u_2(2+z_2)}{8}\,\frac{1}{4}\,\rho_n(\vec{r})\nabla^2\rho_p(\vec{r})+\rho_p(\vec{r})\nabla^2\rho_n(\vec{r})+(K_n(\vec{r})\,\rho_p(\vec{r})+K_p(\vec{r})\,\rho_n(\vec{r}))\\&-\frac{u_2}{16}\Big[(1+z_2)\,J_n^2(\vec{r})+J_p^2(\vec{r})-2z_2\vec{J}_n(\vec{r})\cdot\vec{J}_p(\vec{r})\Big]\end{aligned} \tag{A.24}$$

A.2.4 Summary

Adding the contributions of the equations (A.17), (A.21) and (A.24) ,one obtains the total CIB energy density:

$$\begin{aligned}E_{CIB} = \int d^3r\;&\frac{u_0(1-z_0)}{4}\,\rho_n^2(\vec{r})+\rho_p^2(\vec{r})-u_0\Big(1+\frac{z_0}{2}\Big)\,\rho_n(\vec{r})\,\rho_p(\vec{r})\\&+\frac{u_1}{16}\,2(1-z_1)\,\frac{3}{2}\,\rho_n(\vec{r})\nabla^2\rho_n(\vec{r})-\frac{3}{2}\,\rho_p(\vec{r})\nabla^2\rho_p(\vec{r})+K_n(\vec{r})\,\rho_n(\vec{r})+K_p(\vec{r})\,\rho_p(\vec{r})\\&+2(2+z_1)\,\frac{3}{2}\,\rho_n(\vec{r})\nabla^2\rho_p(\vec{r})+\frac{3}{2}\,\rho_p(\vec{r})\nabla^2\rho_n(\vec{r})-K_p(\vec{r})\,\rho_n(\vec{r})-K_p(\vec{r})\,\rho_n(\vec{r})\\&+(z_1-1)(J_n^2(\vec{r})+J_p^2(\vec{r}))-2z_1\vec{J}_n(\vec{r})\cdot\vec{J}_p(\vec{r})\\&+\frac{3u_2(1+y_2)}{8}\,K_n(\vec{r})\,\rho_n(\vec{r})+K_p(\vec{r})\,\rho_p(\vec{r})+\frac{1}{4}\,\rho_n(\vec{r})\nabla^2\rho_n(\vec{r})+\rho_n(\vec{r})\nabla^2\rho_n(\vec{r})\\&-\frac{u_2(2+z_2)}{8}\,\frac{1}{4}\,\rho_n(\vec{r})\nabla^2\rho_p(\vec{r})+\rho_p(\vec{r})\nabla^2\rho_n(\vec{r})+(K_n(\vec{r})\,\rho_p(\vec{r})+K_p(\vec{r})\,\rho_n(\vec{r}))\\&-\frac{u_2}{16}\Big[(1+z_2)\,J_n^2(\vec{r})+J_p^2(\vec{r})-2z_2\vec{J}_n(\vec{r})\cdot\vec{J}_p(\vec{r})\Big]\end{aligned} \tag{A.25}$$

Appendix B

Numerical Tests for HFODD

Accurancy of the solution of the Hartree-Fock equations with the wave functions expanded onto the cartesian harmonic oscillator, depends on the three parameters $\hbar\omega_x; \hbar\omega_y; \hbar\omega_z$ defining the harmonic oscillator frequencies in the standard cartesian directions, and on the number M of harmonic oscillator states included in the basis, like showed in [23]. In the HFODD code [24], it was used the standard prescription to choose the HO states included in the basis [27], namely the M states with the lowest HO single-particle energies,

$$\varepsilon_{n_x n_y n_z} = \hbar\omega_x \left(n_x + \frac{1}{2}\right) + \hbar\omega_y \left(n_y + \frac{1}{2}\right) + \hbar\omega_z \left(n_z + \frac{1}{2}\right) \tag{B.1}$$

are selected among those which have $n_x \leq N_0$, $n_y \leq N_0$ and $n_z \leq N_0$, where N_0 is the fixed maximum number of HO quanta [23]. It should be noted that both M and N_0 have to be specified to define the basis, for the details see [24]. Usually N_0 is chosen large enough so that all the states allowed by the energy cutoff are included in the basis.
In what follows the results obtained with an axially deformed bases for $\omega_\perp = \omega_x = \omega_y$ are discussed and they are presented in terms of the standard parameters

$$\omega_0^3 = \omega_\perp^2 \omega_0 \qquad \text{and} \qquad q = \frac{\omega_\perp}{\omega_z} \tag{B.2}$$

In the present study tests up to $N_0 = 16$, compatibly with the performances of the available computer.
In the code HFODD the basis parameters are determined as follows. Firstly, ω_0 is defined by the standard value [44] multiplied by a phenomenological factor f quite close to unity:

$$\hbar\omega_0 = f \cdot 41 A^{-\frac{1}{3}} \tag{B.3}$$

where A is the mass-number of the considered nucleus. Then, the code is able to perform Hartree-Fock calculations for a given set of multiple deformations β_{lm}, i.e., for a nuclear shape defined by the radius [44]:

$$R(\theta, \varphi) = R_0 \left[1 + \sum_{l=0}^{l_{max}} \sum_{m=-l}^{+l} \beta_{lm} Y_l^m(\theta, \varphi)\right] \tag{B.4}$$

where $R_0 = r_0 A^{\frac{1}{3}}$ is the standard nuclear spherical radius and $Y_l^m(\theta, \varphi)$ represents the spherical harmonics. Due to the assumed yz-simplex symmetry conserved, see [23], all multipole deformation

parameters $_{lm}$ are real, and only those with $m \quad 0$ are taken into account in the code because then $_{lm} = \ _{lm} = (\ 1)^m \ _{l\ m}$. The lenghts of the volume de ned by the radius (B.4) (which does not depend on the parameter $_{lm}$) can be de ned as $R_x = R(\frac{}{2}; 0)$, $R_y = R(\frac{}{2}; \frac{}{2})$ and $R_z = R(0; 0)$ [44]. The relative values of the HO frequencies are then de ned by the condition

$$! _x R_x = ! _y R_y = ! _z R_z \tag{B.5}$$

together with the common proportionality constant is given by the condition $! _0^3 = ! _x ! _y ! _z$. Here the results of tests performed for di erent basis parameters are presented and compared with those performed with the code skyrme-rpa, see [21] or the code HFBTHO, see [54]. All the calculations have been performed for the Skyrme parametrisation SkM* with the coupling constants $C_t^J = C_t^T = C_t^{\ s} = 0$ in the energy functional [23].

B.1 Numerical test for ^{208}Pb

In this section the results obtained for the spherical nucleus ^{208}Pb are presented, for which the spherical basis is used (q=1). The binding energies are studied in function of $! _0$, by varying the value of the factor f around the unity and without considering the pairing force, as doubly magic nucleus.

(a) (b)

Figure B.1: Ground-state energies of ^{208}Pb calculated as functions of $! _0$ for several values of the number N_0 of HO shells included in the basis. Dots denote the minima. The horizontal dashed line represents the exact result. In the (b) panel the same calculation made by Dobaczewski et al. [23, 24] is reported.

In the gure B.1 panel (a) the horizontal dashed line represents a solution obtained with the code skyrme-rpa performed with the Skyrme parameter set SkM* [19], see [21], and it is considered as the exact value. The solid lines represent the results calculated by the code HFODD with N_0 from 10 to 16. No more value grater than 16 for N_0 is allowed by the performances of the computer supplied. As regards the spherical basis the number of the HO states is given by

$$M = \frac{(N_0 + 1)(N_0 + 2)(N_0 + 3)}{6} \tag{B.6}$$

In figure B.1 for each value of N_0, dots denote the minimum energy which define the optimal value of $\hbar\omega_0$; for example, when $N_0 = 12$ two minima appear. The energies of ^{208}Pb, shown in figure B.1 panel (a), converge rather slowly to the exact value of -1636.545 MeV. For $N_0 = 10$ the difference respect to the exact value is about 6 MeVs; meanwhile for $N_0 = 12$ the difference is about 2 MeVs and for $N_0 = 16$ is less then 100 keVs. As N_0 increases, the value of $\hbar\omega_0$ also increases and then deviates a lot from the unity. Since it was not possible to carry out tests with N_0 greater than 16, it is not possible to establish whether for higher N_0 HFODD calculates a binding energy for ^{208}Pb that converges to the exact value or overestimates it. In any case we can say that with $N_0 = 16$ the result is satisfactory.

In order to have a comparison, figure B.1 panel (b) represents the plot of the same calculation made by the authors Dobaczewski et al. [23, 24]. In this case, the exact value represent a very precise solution obtained by a one-dimensional spherical code in spatial coordinates and it corresponds to -1635.956 MeV; for details see [24]. The two panel of the figure are very similar, and both converge rather slowly to the exact value as N_0 increases.

B.2 Numerical test for ^{24}Mg

In this section the results obtained for the deformed nucleus ^{24}Mg are presented, for which a deformed basis of HO is used. Although ^{24}Mg is not a closed-shell nucleus both for protons and neutrons, the pairing energy is zero. For this reason the calculation performed by HFODD has been performed without tanking into account pairing interaction. If the test were repeated by including also the pairing interaction, the same result would be obtained.

In order to study the optimisation of the deformation of the basis, the calculations are performed with $\hbar\omega_0$ fixed at the value at the value of 14.214 MeV ($f = 1$) with the SkM* parameter set and for several values of q and M. These results results are compared with the result obtained with the code HFBTHO, which is considered as the exact value. The nuclear shape taken into account for these calculations are based on the radius (B.4). Since by default this code imposes a combination of quadrupole and hexadecapolar deformation, the only quadrupole deformation was considered for this test on ^{24}Mg, i.e. in (B.4) only the $l = 2$ term of the multipole expansion has been set. When the only quadrupolar deformation is considered, one can rewrite equation (B.4) in the intrinsic frame [44]:

$$R(\theta, \varphi) = R_0 \left[1 + \sqrt{\frac{5}{16\pi}} \cos\gamma \left(3\cos^2\theta - 1\right) + \sqrt{3}\sin\gamma \sin^2\theta \cos 2\varphi \right] \qquad \text{(B.7)}$$

and the increments of the three semi-axes in the intrinsic frame as function of and [44]:

$$R_k = R_0 \sqrt{\frac{5}{4\pi}} \cos\left(\gamma - \frac{2k\pi}{3}\right), \qquad k = 1, 2, 3$$

The parameters and together with (B.7) describe the ellipsoidal shapes in the limit of small -values.

Figure B.2: Energies of ^{24}Mg (solid lines) calculated as functions of the basis deformation parameter q, $\hbar\omega_0 = 14{:}214$ MeV fixed and for several values of the number M states included in the HO basis. Dots denote the minima. The horizontal dashed line represents the exact result.

Figure B.2 shows the binding energies of ^{24}Mg calculated by HFODD for M=50, 150, 250 and 450. The exact value is -197.134 MeV, which is represented with the vertical dashed line and corresponds to $= 0{:}3961$. The diamond represents the value of -197.159, which is calculated with HFODD for q=1.33 as well. Dots denote the minima for each number of M states included in the basis. The parameter q varies between 1 and 1.9. For the M=50 curve the difference between the exact value and the minimum is more than 1 MeV and the energy trend remains quite constant for the interval of q considered. For M=150 the minimum of the binding energy is found only when ^{24}Mg is considered as a pure spherical nucleus (q=1) and it differs by the exact value about slightly less than 1 MeV. As regards the M=250 curve, its minimum differs by the exact value only about less then 500 keV. The minimum of the curve M=450 is very close to the exact value, it differs about less than 100 keV. The diamond point is very close to the exact value as well, it overestimates the exact value only about less than 50 keV. These last two results are in very good agreement with the exact result.

The convergence of energy in function of M is rather slow; only for M>250 the error respect to the exact value decreases below 500 keV, as previously described. Only for M=150 the optimal basis deformation is rather different from q=1.33. However, for all the other curves, the energy gain from optimizing the value of q is small. The closest minimum to the vertical dashed line is that related to the M=50 curve, but for all the curves (M=450 included) the minimum of energy is rather hardly visible. Figure B.3 shows the values of proton quadrupole moments (Q^p_{20}) calculated with HFODD and compared with that calculated with HFBTHO when q=1.33, the vertical dashed line. In this figure, the dots denote the proton quadrupole moments corresponding to the minima of the energies in figure B.2 for each value of M.

The diamond represents the value of 0.5427(10fm)^2 calculated for q=1.33. It corresponds in energy to the diamond point in figure B.2. The exact value is 0.5560(10fm)^2, the horizontal dashed line. As regards the curves M=150, 250 and 450 in figure B.3 the dependence of the Q^p_{20} on q is the same: it tends to increase as q increases, but the optimal value of q is different from 1.33. The closest q-value is that of =450 curve, but the value of Q^p_{20} is quite different from the

exact value. For M=50 one obtains a much better value of Q^p_{20} for a very close to 1.33 value of q.

Figure B.3: Same as in gure B.2 but for proton quadrupole moments of ^{24}Mg. The horizontal dashed line represents the exact result.

Bibliography

[1] István Angeli and Krassimira Petrova Marinova. Table of experimental nuclear ground state charge radii: An update. Atomic Data and Nuclear Data Tables, 99(1):69 95, 2013.

[2] P Baczyk, Jacek Dobaczewski, Maciej Konieczka, W Satula, Takashi Nakatsukasa, and Koichi Sato. Isospin-symmetry breaking in masses of n=z nuclei. Physics Letters B, 778:178 183, 2018.

[3] Pawel Baczyk, Jacek Dobaczewski, Maciej Konieczka, Takashi Nakatsukasa, Koichi Sato, and Wojciech Satula. Mirror and triplet displacement energies within nuclear dft: numerical stability. arXiv preprint arXiv:1611.01392, 2016.

[4] Pawel Baczyk, Jacek Dobaczewski, Maciej Konieczka, and Wojciech Satula. Strong-interaction isospin-symmetry breaking within the density functional theory. Acta Phys. Pol. B Proc. Supp. 8,539-544, 2015.

[5] B Banerjee, HJ Mang, and P Ring. Variational calculation of energy spectra of rotational nuclei at high spins. Nuclear Physics A, 215(2):366 382, 1973.

[6] M Baranger. Cargese lectures in theoretical physics. Benjamin, New York, 1963.

[7] Michel Baranger. Self-consistent eld theory of nuclear shapes. Physical Review, 122(3):992, 1961.

[8] J Bartel, Ph Quentin, Matthias Brack, C Guet, and H-B Håkansson. Towards a better parametrisation of skyrme-like e ective forces: A critical study of the skm force. Nuclear Physics A, 386:79 100, 1982.

[9] M Beiner, H Flocard, Nguyen Van Giai, and Ph Quentin. Nuclear ground-state properties and self-consistent calculations with the skyrme interaction:(i). spherical description. Nuclear Physics A, 238(1):29 69, 1975.

[10] ST Belyaev. Mat. fys. medd. dan. vid. selsk. 31 (11). Mat. Fys. Medd. Dan. Vid. Selsk, 1959.

[11] Michael Bender, Paul-Henri Heenen, and Paul-Gerhard Reinhard. Self-consistent mean- eld models for nuclear structure. Reviews of Modern Physics, 75(1):121, 2003.

[12] Carlos A Bertulani. Nuclear physics in a nutshell, volume 2. Princeton University Press, 2007.

[13] Claude Bloch and Albert Messiah. The canonical form of an antisymmetric tensor and its application to the theory of superconductivity. Nuclear Physics, 39:95 106, 1962.

[14] A Bohr. Br mottelson," nuclear structure" vol. 1, 1969.

[15] A Bohr, BR Mottelson, Gregory Breit, and Gerald E Brown. Nuclear structure, vol. 2: Nuclear deformations. Physics Today, 30:59, 1975.

[16] David Maurice Brink and George Raymond Satchler. Angular momentum. Clarendon Press, 1968.

[17] BA Brown, WA Richter, and R Lindsay. Displacement energies with the skyrme hartree fock method. Physics Letters B, 483(1-3):49 54, 2000.

[18] E Chabanat, P Bonche, P Haensel, J Meyer, and R Schae er. A skyrme parametrization from subnuclear to neutron star densities. Nuclear Physics A, 627(4):710 746, 1997.

[19] E Chabanat, P Bonche, P Haensel, J Meyer, and R Schae er. A skyrme parametrization from subnuclear to neutron star densities part ii. nuclei far from stabilities. Nuclear Physics A, 635(1-2):231 256, 1998.

[20] Donald D Clayton. Principles of stellar evolution and nucleosynthesis. University of Chicago press, 1983.

[21] Gianluca Colò, Ligang Cao, Nguyen Van Giai, and Luigi Capelli. Self-consistent rpa calculations with skyrme-type interactions: The skyrme_rpa program. Computer Physics Communications, 184(1):142 161, 2013.

[22] Amos De-Shalit and Hermann Feshbach. Theoretical nuclear physics. Wiley, 1974.

[23] J Dobaczewski and J Dudek. Solution of the skyrme-hartree-fock equations in the cartesian deformed harmonic oscillator basis i. the method. Computer physics communications, 102(1-3):166 182, 1997.

[24] J Dobaczewski and J Dudek. Solution of the skyrme hartree fock equations in the cartesian deformed harmonic oscillator basis ii. the program hfodd. Computer physics communications, 102(1-3):183 209, 1997.

[25] J Dobaczewski and P Olbratowski. Solution of the skyrme hartree fock bogolyubov equations in the cartesian deformed harmonic-oscillator basis.(iv) hfodd (v2. 08i): a new version of the program. Computer physics communications, 158(3):158 191, 2004.

[26] J Dobaczewski, MV Stoitsov, and W Nazarewicz. Skyrme-hfb deformed nuclear mass table. In AIP Conference Proceedings, volume 726, pages 51 56. American Institute of Physics, 2004.

[27] H Flocard, Ph Quentin, AK Kerman, and D Vautherin. Nuclear deformation energy curves with the constrained hartree-fock method. Nuclear Physics A, 203(3):433 472, 1973.

[28] Siegfried Flügge. Practical quantum mechanics. Springer Science & Business Media, 1971.

[29] Martin Freer. The clustered nucleus cluster structures in stable and unstable nuclei. Reports on Progress in Physics, 70(12):2149, 2007.

[30] Ernest M Henley and Alejandro Garcia. Subatomic physics World Scienti c Publishing Company, 2007.

[31] Kris LG Heyde. The nuclear shell model Springer, 1994.

[32] S Hilaire and M Girod. The amedee nuclear structure database. In International Conference on Nuclear Data for Science and Technology, pages 107 110. EDP Sciences, 2007.

[33] William Hornyak. Nuclear structure. Elsevier, 1975.

[34] H Krivine, J Treiner, and O Bohigas. Derivation of a uid-dynamical lagrangian and electric giant resonances. Nuclear Physics A, 366(2):155 184, 1980.

[35] LD Landau. On the theory of the fermi liquid. Sov. Phys. JETP, 8(1):70, 1959.

[36] Silvia M Lenzi and MA Bentley. Isospin symmetry breaking in mirror nuclei. Lectures given at Ecole Internationale Joliot Curie 2010, 2010.

[37] R Machleidt. High-precision, charge-dependent bonn nucleon-nucleon potential. Physical Review C, 63(2):024001, 2001.

[38] Maria Goeppert Mayer. Nuclear con gurations in the spin-orbit coupling model. i. empirical evidence. Physical Review, 78(1):16, 1950.

[39] GA Miller and WTH Van Oers. Symmetries and fundamental interactions in nuclei. edited by WC Haxton and EM Henley, World Scienti c, page 127, 1995.

[40] Gerald A Miller and Willem TH Van Oers. Charge independence and charge symmetry. Symmetries and Fundamental Interactions in Nuclei, S, pages 127 167, 1995.

[41] JA Nolen Jr and JP Schi er. Coulomb energies. Annual Review of Nuclear Science, 19(1):471 526, 1969.

[42] R Navarro Perez, Nicolas Schunck, R-D Lasseri, C Zhang, and Jason Sarich. Axially deformed solution of the skyrme hartree-fock bogolyubov equations using the transformed harmonic oscillator basis (iii) hfbtho (v3. 00): A new version of the program. Computer Physics Communications, 220:363 375, 2017.

[43] E Perli«ska, SG Rohozi«ski, J Dobaczewski, and W Nazarewicz. Local density approximation for proton-neutron pairing correlations: Formalism. Physical Review C, 69(1):014316, 2004.

[44] Peter Ring and Peter Schuck. The nuclear many-body problem. Springer Science & Business Media, 2004.

[45] X Roca-Maza, G Colò, and H Sagawa. New skyrme interaction with improved spin-isospin properties. Physical Review C, 86(3):031306, 2012.

[46] Xavier Roca-Maza, Gianluca Colò, and Hiroyuki Sagawa. Nuclear symmetry energy and the breaking of the isospin symmetry: How do they reconcile with each other? Physical review letters, 120(20):202501, 2018.

[47] David J Rowe. Nuclear collective motion: models and theory. World Scienti c, 2010.

[48] Koichi Sato, Jacek Dobaczewski, Takashi Nakatsukasa, and Wojciech Satuªa. Energy-density-functional calculations including proton-neutron mixing. Physical Review Ç, 88(6):061301, 2013.

[49] Wojciech Satuªa and Ramon Wyss. Microscopic structure of fundamental excitations in n= z nuclei. Physical review letters, 87(5):052504, 2001.

[50] Nicolas Schunck, Jacek Dobaczewski, W Satula, P Baczyk, J Dudek, Yuan Gao, M Konieczka, K Sato, Yue Shi, XB Wang, et al. Solution of the skyrme-hartree fock bogolyubovequations in the cartesian deformed harmonic-oscillator basis.(viii) hfodd (v2. 73y): A new version of the program. Computer Physics Communications, 216:145 174, 2017.

[51] Emilio Segre. Nuclei and particles: an introduction to nuclear and subnuclear physics Benjamin, 1964.

[52] THR Skyrme. The e ective nuclear potential. Nuclear Physics, 9(4):615 634, 1958.

[53] John C Slater. A simpli cation of the hartree-fock method. Physical review, 81(3):385, 1951.

[54] MV Stoitsov, Nicolas Schunck, Markus Kortelainen, N Michel, H Nam, E Olsen, Jason Sarich, and S Wild. Axially deformed solution of the skyrme-hartree fock bogoliubov equations using the transformed harmonic oscillator basis (ii) hfbtho v2. 00d: A new version of the program. Computer Physics Communications, 184(6):1592 1604, 2013.

[55] Toshio Suzuki, H Sagawa, and Nguyen Van Giai. Charge independence and charge symmetry breaking interactions and the coulomb energy anomaly in isobaric analog states. Physical Review Ç, 47(4):R1360, 1993.

[56] Naoki Tajima, Paul Bonche, Hubert Flocard, P-H Heenen, and MS Weiss. Self-consistent calculation of charge radii of pb isotopes.Nuclear Physics A, 551(3):434 450, 1993.

[57] DJ Thouless. Stability conditions and nuclear rotations in the hartree-fock theory. Nuclear Physics, 21:225 232, 1960.

[58] D Vautherin and DM t Brink. Hartree-fock calculations with skyrme's interaction. i. spherical nuclei. Physical Review Ç, 5(3):626, 1972.

[59] Markus Walzl, Ulf-G Meiÿner, and Evgeny Epelbaum. Charge-dependent nucleon nucleon potential from chiral e ective eld theory. Nuclear Physics A, 693(3-4):663 692, 2001.

[60] Meng Wang, G Audi, FG Kondev, WJ Huang, S Naimi, and Xing Xu. The ame2016 atomic mass evaluation (ii). tables, graphs and references. Chinese Physics Ç, 41(3):030003, 2017.

[61] Eugene Wigner. On the consequences of the symmetry of the nuclear hamiltonian on the spectroscopy of nuclei.Physical Review, 51(2):106, 1937.

[62] Denys Haigh Wilkinson. ISOSPIN IN NUCLEAR PHYSICS. 1969, 1969.

[63] RB Wiringa, S Pastore, Steven C Pieper, and Gerald A Miller. Charge-symmetry breaking forces and isospin mixing in 8 be.Physical Review Ç, 88(4):044333, 2013.